

Aus dem Zentrum für Medizinische Forschung
der Medizinischen Fakultät Mannheim
Direktor: Prof. Dr. med. Norbert Gretz

Influence of photobiomodulation with blue light on the metabolism,
proliferation and gene expression of human fibroblasts

Inauguraldissertation
zur Erlangung des akademischen Grades
Doctor scientiarum humanarum (Dr. sc. hum.) der
Medizinischen Fakultät Mannheim
der Ruprecht-Karls-Universität
zu
Heidelberg

vorgelegt von
Anna Sophie Klapczynski

aus
Speyer, Deutschland
2019

Dekan: Prof. Dr. med. Sergij Goerd
Referent: Prof. Dr. med. Norbert Gretz

TABLE OF CONTENTS

Page

ABBREVIATIONS

1 INTRODUCTION	1
1.1 Photobiomodulation	1
1.1.1 Irradiation parameters.....	2
1.1.2 Mechanisms of action	3
1.1.3 Medical applications	3
1.2 Human skin	5
1.2.1 Physiology of human skin	5
1.2.2 Fibroblasts in human skin	6
1.2.3 Optical properties of human skin	7
1.3 Blue light.....	8
1.4 MEDILIGHT – Light treatment of chronic wounds	12
1.5 Aim of the study.....	13
2 MATERIAL AND METHODS	14
2.1 Material.....	14
2.1.1 Cell line.....	14
2.1.2 Laboratory equipment.....	15
2.1.3 Light sources	17
2.2 Methods.....	21
2.2.1 Cell culture.....	21
2.2.2 Light treatment.....	21
2.2.3 Temperature measurements	24
2.2.4 Cell metabolism and proliferation assays	25
2.2.5 Functional assays	29
2.2.6 Gene expression analysis.....	31
2.2.7 Statistical analysis	33

3 RESULTS.....	34
3.1 BioLight LED Lamp.....	34
3.1.1 Temperature measurements	34
3.1.2 Cell metabolism assays	35
3.1.3 Cell proliferation assays.....	42
3.1.4 Functional assays	48
3.1.5 Gene expression analysis.....	61
3.2 MEDILIGHT system.....	75
3.2.1 Temperature measurements	75
3.2.2 <i>In vitro</i> validation of prototypes	78
3.2.3 Light distribution studies	80
4 DISCUSSION	82
5 SUMMARY	98
6 REFERENCES	100
7 APPENDIX	110
8 CURRICULUM VITAE AND PUBLICATIONS.....	115
9 ACKNOWLEDGEMENTS.....	117

ABBREVIATIONS

AMPK	AMP-activated protein kinase
AhR	Aryl hydrocarbon receptor
AKT(1)	Serine/threonine kinase 1
ALDH3A1	Aldehyde dehydrogenase 3 family member A1
ANOVA	Analysis of variance
AUR	Amplex® UltraRed Reagent
AV-APC	Annexin V, conjugated to Allophycocyanin
BrdU	5-Bromo-2'-deoxyuridine
CCCP	Carbonyl cyanide 3-chlorophenylhydrazone
CDK	Cyclin-dependent kinase
CYP	Cytochrome P450
DC	Duty cycle
DFU	Diabetic foot ulcer
E2723	Wound dressing URGOSTART
EDTA	Ethylenediamine tetraacetic acid
ELISA	Enzyme-linked immunosorbent assay
FACS	Fluorescence-activated cell sorting
FCS	Fetal calf serum
FDR	False discovery rate
FITC	Fluorescein isothiocyanate
FOXO	Forkhead box protein O
GSEA	Gene Set Enrichment Analysis
GST	Glutathione S-transferase
H ₂ O ₂	Hydrogen peroxide
HRP	Horseradish peroxidase
IQR	Interquartile range
IR	Infrared
KEGG	Kyoto Encyclopedia of Genes and Genomes
LED	Light-emitting diode
LLLT	Low-level laser (light) therapy
MC	Mitotic catastrophe

mTOR	Mechanistic target of rapamycin
NAALT	North American Association for Light Therapy
NES	Normalized Enrichment Score
NF- κ B	Nuclear factor kappa B
NHDF-c	Normal human dermal fibroblasts – cryopreserved
NIR	Near-infrared
NQO1	NAD(P)H quinone dehydrogenase 1
Nrf2	Nuclear factor erythroid 2-related factor 2
OLED	Organic light-emitting diode
PBM	Photobiomodulation
PBS	Phosphate buffered saline
PDT	Photodynamic therapy
PI	Propidium Iodide
PMS	N-methyl dibenzopyrazine methyl sulfate
QTH	Quartz-tungsten halogen
RIN	RNA integrity number
ROS	Reactive oxygen species
RT	Room temperature
SB	Staining buffer
SD	Standard deviation
TGF- β	Transforming growth factor beta
TMRE	Tetramethylrhodamine ethyl ester perchlorate
TNF	Tumor necrosis factor
UGT	UDP-glucuronosyltransferase
UV	Ultraviolet
VIS	Visible
VLU	Venous leg ulcer
WALT	World Association for Laser Therapy
XMEs	Xenobiotic-metabolizing enzymes
XTT	Sodium 3'-[1-(phenylaminocarbonyl)-3, 4-tetrazolium] bis (4-methoxy-6-nitro) benzene sulfonic acid hydrate
7-AAD	7-Aminoactinomycin D
$\Delta\Psi_m$	Mitochondrial membrane potential

1 INTRODUCTION

1.1 Photobiomodulation

The use of light for therapeutic purposes dates back to ancient times. However, the first major milestone in the field of clinical phototherapy was reached by N. R. Finsen in the late 18th century, who succeeded in treating *Lupus vulgaris* with concentrated light radiation¹. However, the therapeutic use of visible (VIS) and infrared (IR) light was pioneered and became widely recognized as a new treatment modality since the invention of lasers in the early 1960s². Shortly afterwards, in 1967, Endre Mester published the first results using low-level laser light. Accompanied by accelerated hair growth³, he had proven beneficial effects of red light on wound healing in both, preclinical and clinical settings^{4, 5}, introducing the term 'laser biostimulation'.

Since then, numerous studies and the development of various artificial light sources paved the way for the use of low-level phototherapy in modern medicine. As a result, new terms were defined in literature involving low-level laser (or light) therapy (LLLT), low-intensity laser therapy, low-power laser therapy, cold laser, soft laser as well as photobiostimulation complicating a consistent nomenclature⁶. Although LLLT is the most frequently used term, its broad definition is not accurate and outdated due to the advanced development of light sources including light-emitting diodes (LEDs), introduced in 1962, organic LEDs (OLEDs) or broadband light devices^{7, 8}. Moreover, the term impedes an unambiguous differentiation from photodynamic therapy (PDT), optogenetics or thermal applications, which are mainly realized with near-infrared (NIR) lasers⁶. Thus, at the joint NAALT and WALT conference in September 2014, 'photobiomodulation' was approved as the term of choice and defined as follows: "A form of light therapy that utilizes non-ionizing forms of light sources, including lasers, LEDs, and broadband light, in the VIS and IR spectrum. It is a non-thermal process involving endogenous chromophores eliciting photophysical (i.e. linear and nonlinear) and photochemical events at various biological scales. This process results in beneficial therapeutic outcomes including but not limited to the alleviation of pain or inflammation, immunomodulation, and promotion of wound healing and tissue regeneration"⁶ (Figure 1).

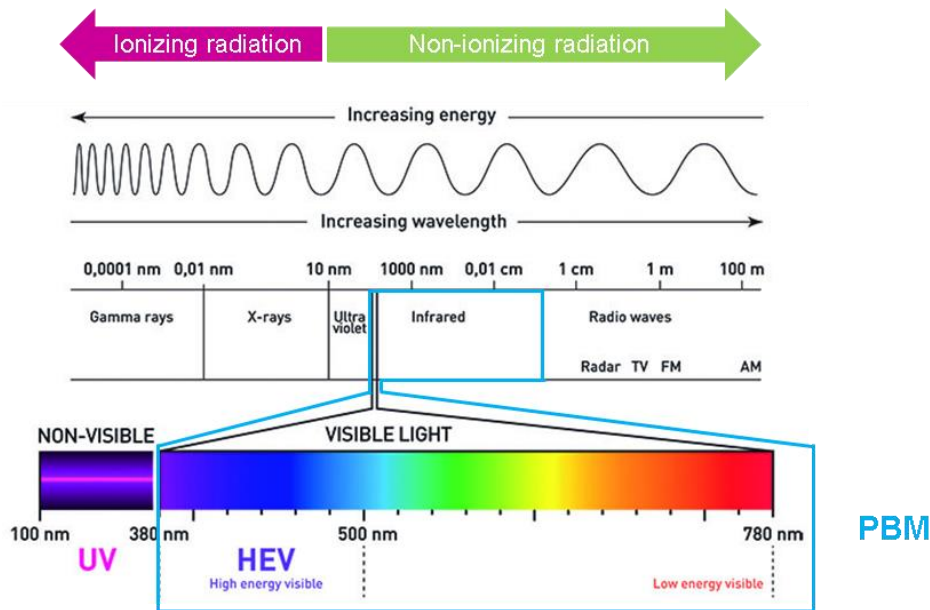


Figure 1: Electromagnetic spectrum differentiating ionizing and non-ionizing radiation with the blue box indicating the typical wavelength range used for photobiomodulation [Modified from⁹].

1.1.1 Irradiation parameters

Besides its inconsistent terminology, significant differences in published study designs, applied irradiation parameters and experimental outcomes depreciate light therapy to an alternative or complementary treatment modality. The most important irradiation parameters represent the wavelength λ [nm], the power [W], the power density or irradiance [W/cm^2], the energy [J] and the energy density or fluence [J/cm^2]. The latter is defined as follows: Irradiance [W/cm^2] x irradiation time [s], and commonly referred to as 'irradiation dose'¹⁰. However, several studies report a non-linear relationship between those two parameters contradicting the Bunsen-Roscoe law of reciprocity, the third law of photobiology¹¹. Therefore, despite of maintaining a constant energy input, mutual changes of both parameters often led to different biological responses^{12, 13}. Other parameters, which have to be considered, are the application mode irradiating either continuously or in pulses/cycles, the number of treatments and the treatment interval. In addition, the coherence and polarization of light might play a pivotal role for the magnitude of biomodulation¹⁰. In total, a vast number of irradiation parameters has to be chosen for each treatment, grading the use of PBM as largely empirical. Moreover, Jenkins et al.¹⁴ underline that irradiation parameters are often reported inaccurately or even incompletely impeding the reproducibility of published results.

1.1.2 Mechanisms of action

Another issue impairing the confidence in light therapy is the ongoing debate about molecular mechanisms underlying photobiomodulatory processes. According to the first law of photobiology, light effects are based on photon absorption by endogenous chromophores, so-called photoacceptors, occurring either in conjugated π -electron systems or metal complexes^{10, 15}. Hence, the biological photoresponse depends on the wavelength, wave number, frequency, photon energy and action spectrum of the respective photoacceptor¹⁶. Different chromophores absorbing light throughout the ultraviolet (UV), VIS and IR wavebands are for instance chlorophyll, rhodopsin, nucleic acids, aromatic amino acids, NADH and NADPH, riboflavin, melanin and melanin precursors, bilirubin, hemoglobin, β -carotene, proteins, lipids and water¹⁷⁻²⁰. Karu et al.¹⁷ postulated four primary mechanisms of photoexcitation resulting in an enhanced biochemical activity: (1) Photoexcitation changes the redox properties of carriers in the respiratory chain accelerating electron transfer²¹, (2) excitation energy gets partly converted to heat causing a local transient heating of the chromophore²², which induces conformational changes triggering biochemical activity, (3) metabolites of oxygen like H_2O_2 , OH^\bullet and O_2^\bullet get reabsorbed by mitochondria leading to an increased redox activity and therefore to an accelerated respiratory chain²³ and (4) photoabsorbing chromophores can be converted to photosensitizers²⁴ transferring energy to adjacent molecules. Such photosensitizers might be components of the respiratory chain like porphyrins, flavins, flavoproteins including cryptochromes, and cytochromes²⁵⁻²⁷. Cytochrome c oxidase, unit 4 of the mitochondrial respiratory chain, represents the best characterized chromophore exhibiting absorption bands in the red to (N)IR range¹⁷, which partly explains the preferred use of red and (N)IR light. Secondary responses after light absorption involve the activation of transcription factors and signaling pathways regulating various cellular processes.

1.1.3 Medical applications

Although PBM is still not considered as a mainstream therapy, it has emerged as a new treatment modality constantly gaining importance for the treatment of various injuries and diseases, in acute and chronic conditions⁸. A literature review showed a variety of ailments in different medical fields to benefit from phototherapy (Figure 2).

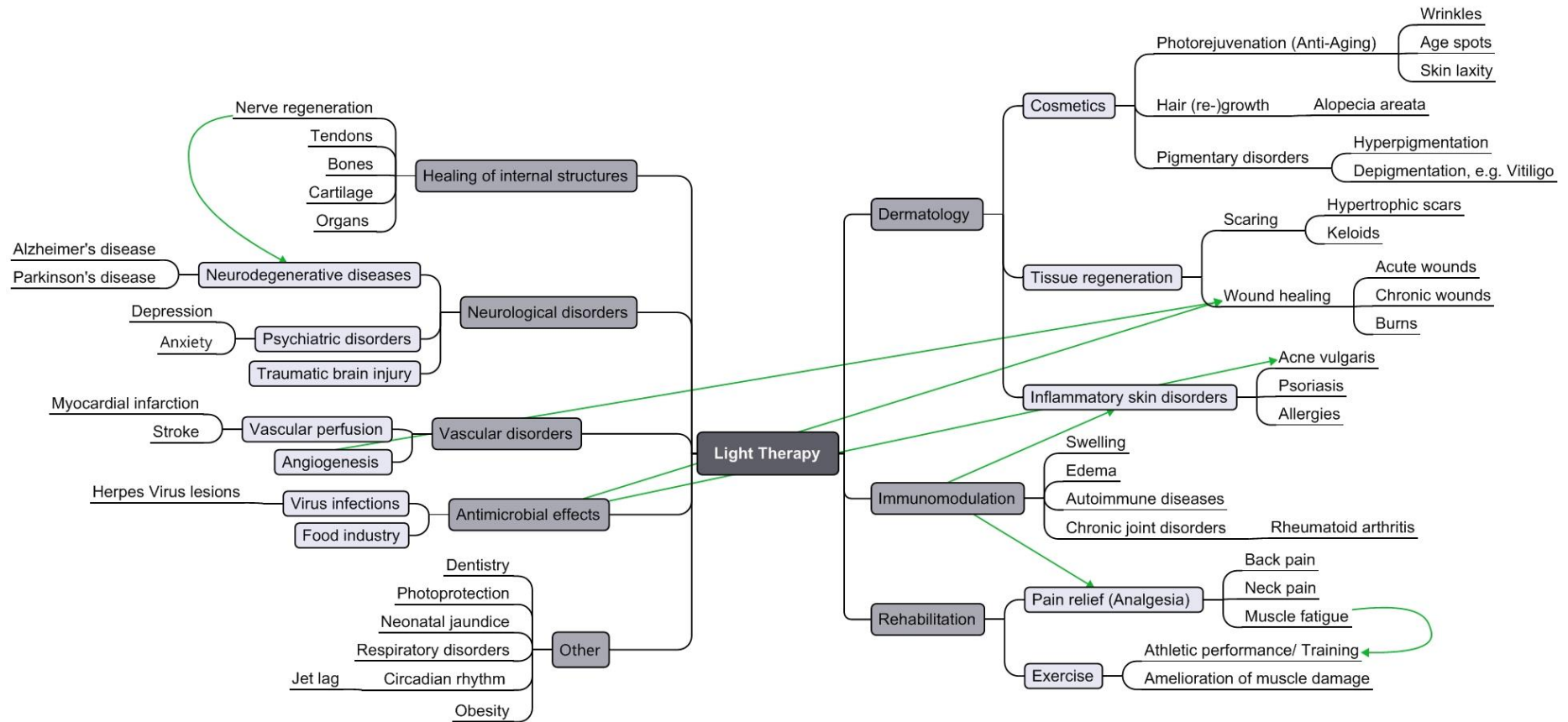


Figure 2: Summary of published LLLT/PBM applications^{28, 29}.

1.2 Human skin

1.2.1 Physiology of human skin

The skin represents the largest organ of the human body, accounting for an area of $1.6 - 2 \text{ m}^2$ and 15% of the total adult body weight with approximately $5 - 10 \text{ kg}$ ^{30, 31}. Besides its main function of forming a protection barrier against environmental insults of mechanical, chemical and biological nature, the skin plays an important role in thermoregulation, in the prevention of excessive transdermal fluid and electrolyte loss as well as in the response to external stimuli including receptors for touch, pain and temperature³¹⁻³⁵. Basically, the skin can be classified into three distinct layers: the epidermis, the dermis and the sub-cutis or hypodermis (Figure 3), which provides an essential energy storage to the human body³¹. Depending on the anatomical location, the composition and thickness of the skin varies. In general, the epidermis is quite thin with an average depth of $0.04 - 1.6 \text{ mm}$, while the dermis is thicker ranging from 0.3 mm to 3.0 mm ³⁶. Besides of dendritic cells, melanocytes, Langerhans cells and Merkel cells, the epidermis consists up to 90 – 95% of keratinocytes, which migrate from the stratum basale through different layers towards the stratum corneum at the skin surface ending up in flattened, anucleated corneocytes^{31, 35}.

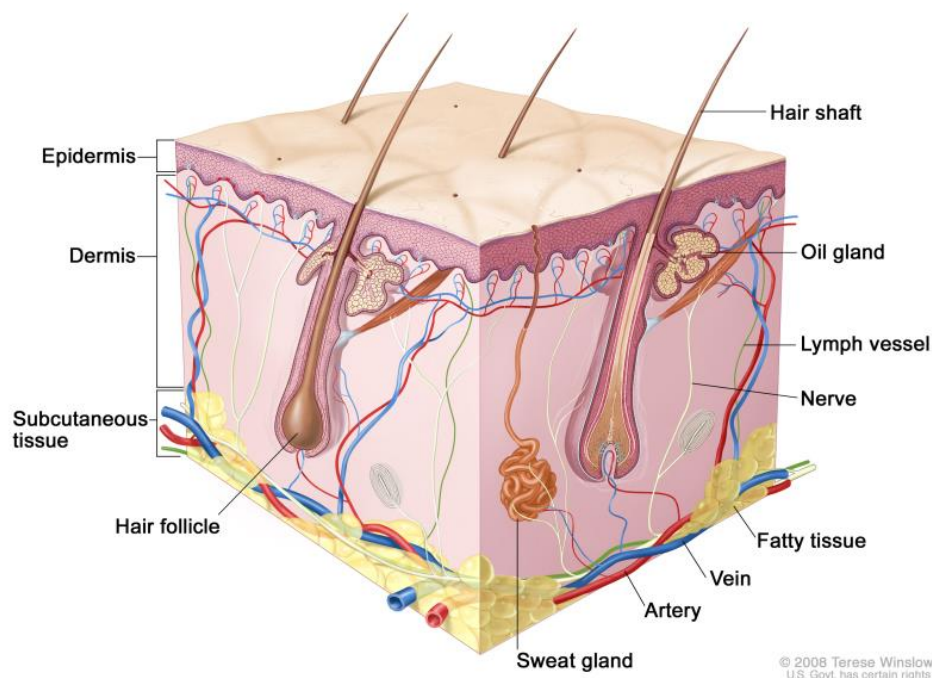


Figure 3: Anatomy of human skin subdivided into epidermis, dermis and subcutaneous tissue (Image reproduced with permission from Reference ³⁷).

As the multi-layered epidermis has no blood vessels, its nutrient supply needed for a continuous renewal is maintained by the underlying dermis comprising numerous blood and lymphatic vessels³⁰. In addition, it includes hair follicles, nerve fibers and secretory glands³⁸. Furthermore, the dermis comprises the connective tissue, which is mainly made up of collagen fibers (> 90%) consisting primarily of interstitial collagen type I and III as well as elastic fibers. Similar to the dynamic epidermis, matrix components of the dermis undergo constant remodeling, not only in pathologic conditions, but also in normal skin³⁸. The connective tissue provides mechanical resistance, tensile strength, elasticity and thus a reversible plasticity to the skin³¹. Due to a varying density and arrangement of collagen fibers, the dermis can be subdivided into two distinct layers, the stratum papillare and the stratum reticulare. Whereas the first is characterized by a relatively thin extracellular matrix (ECM) with loosely arranged collagen fiber bundles and a high cell density, the second shows a very dense network of organized matrix fibers and a low cell density bordering to the fatty tissue of the sub-cutis^{30, 39}. In response to certain stimuli, for instance a skin injury, plasma cells, lymphocytes and other leukocytes are able to enter the dermis.

1.2.2 Fibroblasts in human skin

Fibroblasts are a very dynamic and heterogeneous cell population involved in many physiological processes. There are several distinct fibroblast lineages populating the two-layered dermis: papillary fibroblasts in the superficial layer directly underneath the epidermis, reticular cells located in the deep dermis and another subpopulation associated with hair follicles⁴⁰. Besides different spatial locations and morphological characteristics with papillary fibroblasts showing a lean, spindle-shaped morphology and with reticular ones appearing square and stretched, they exhibit different gene expression patterns and therefore functions⁴¹⁻⁴³. In spite of these differences, their primary function represents ECM deposition, which gets interspersed between skin's appendages, nerves, vessels, receptors and dermal cells forming the connective tissue^{35, 44}. Thus, by providing structural support and maintaining matrix homeostasis, fibroblasts are characterized as the main mediators of scar formation, tissue fibrosis and wound healing⁴⁴⁻⁴⁶. Moreover, especially during cutaneous tissue repair, growth factors, cytokines and chemokines, secreted by fibroblasts, play a crucial role in the regulation of epithelial growth and differentiation, and inflammatory processes^{47, 48}.

1.2.3 Optical properties of human skin

The skin is naturally exposed to light more than any other organ²⁸, whereby the dose of radiation received by the skin is determined by the ozone layer, the position of the sun, the geographical location and altitude as well as cloud covers and ground reflections. Moreover, the photobiological effects evoked do not only depend on the wavelength, frequency and mechanisms of actions induced by UV, VIS or (N)IR radiation, but also on skin characteristics like its structure, thickness, vasculature and pigmentation⁴⁹. The wavelengths used for PBM fall into an ‘optical window’ of the skin reaching from 650 nm to 1200 nm limited by high absorption bands of principal tissue chromophores such as hemoglobin and melanin at < 600 nm and the strong absorption of IR light by water at > 1150 nm (Figure 4, (A))^{10, 16, 49}.

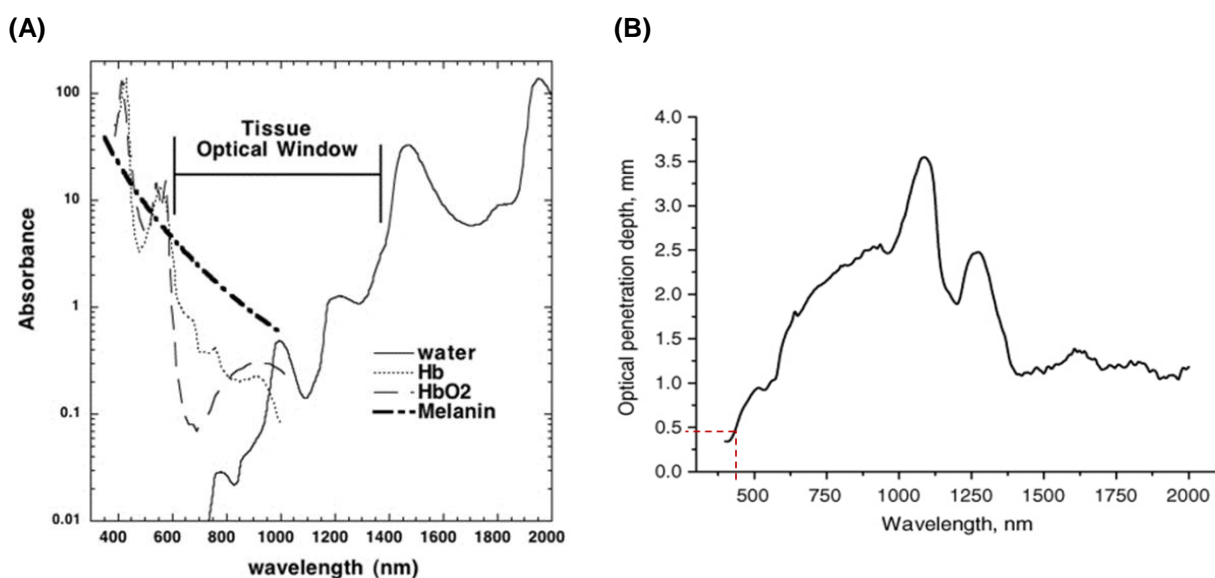


Figure 4: Optical properties of human skin with (A) the ‘optical window’ of tissue¹⁰ showing absorption spectra of different chromophores present in the skin and (B) the optical penetration depth δ of light into human skin for a wavelength range from 400 nm to 2000 nm [Modified from ⁵⁰].

Consequently, the depth of optical penetration δ into human skin highly depends on the wavelength of light. Shorter wavelengths with higher energy, such as UV and parts of VIS light, do not penetrate into the skin as deep as longer wavelengths like IR with less energy even reaching the subcutaneous adipose tissue. Since light absorption and optical tissue scattering are more pronounced in the blue region of the VIS light spectrum, blue light is able to penetrate up to 0.5 mm into human skin (Figure 4, (B))^{50, 51}.

1.3 Blue light

As illustrated in Figure 1, blue light exhibits the highest energy in the VIS part of the electromagnetic spectrum ranging from 380 nm to 500 nm. Due to its proximity to UV, blue light is often connected to damaging and even cytotoxic effects, especially at $\lambda < 450$ nm. For instance, overexposure to high-intensity blue light contributes to oxidative stress in the retina favoring the onset of age-related macular degeneration⁵² or the induction of cataract formation in the eye lens⁵³. Similar to UV light, blue light was shown to be antimicrobial exerting bacteriostatic or even bactericidal effects against numerous gram-positive as well as gram-negative bacterial strains such as *Escherichia coli*, (methicillin-resistant) *Staphylococcus aureus*, *Pseudomonas aeruginosa*, *Klebsiella pneumoniae*, *Propionibacterium acnes*, and many others⁵⁴⁻⁵⁷. Moreover, blue light is well known for its anti-inflammatory properties⁵⁸, explaining its frequent use for inflammatory skin lesions such as psoriasis⁵⁹ and acne⁶⁰. Other common disorders which were shown to benefit from blue light therapy are for instance severe neonatal jaundice⁶¹ as well as back and neck pain.

However, in contrast to red and (N)IR light, blue wavelengths are apparently used for a limited range of applications, especially when reviewing published *in vivo* studies. This discrepancy can be explained by two reasons: (1) the lower penetration depth of blue light (≤ 0.5 mm) restricting its use to rather superficial treatments and (2) less insights into light-triggered signaling cascades. With absorption peaks in the range of VIS blue light, porphyrin ring structures ($\sim 410 - 440$ nm) and flavins (~ 450 nm), which are mainly concentrated in mitochondria, represent the best candidates being activated in response to blue light⁶². Therefore, assessing the effects of blue light on mitochondrial function is a logical consequence. Compared to its rare application for *in vivo* studies, many reports described significant blue light effects on different cell types including inter alia dermal keratinocytes, fibroblasts and melanocytes as well as endothelial cells, stem cells, osteoblasts and several others⁶³⁻⁶⁶. Table 1 summarizes all reports found describing blue light effects on fibroblast cell types with most of them targeting improved wound healing, fibrotic skin diseases or dental treatments. Nearly all of the authors observed a decreased mitochondrial activity, cell proliferation and viability related to an increased production of reactive oxygen species (ROS) probably triggering unbalanced stress responses. In contrast, longer VIS and (N)IR wavelengths frequently exert either neutral or stimulatory effects^{67, 68}.

	Authors	Cell type	Light source	Wavelength [nm]	Irradiance [mW/cm ²]	Time [h:min:s]	Dose [J/cm ²]	#	Effects	Application
1	Akiyama, M. et al. ⁶⁹	Human normal neonatal dermal fibroblasts (NB1RGB)	LED devices	405 471	1.8	03:00:00	16.2	1	– Cell growth Gene expression profiles, qPCR, Immunoblotting: ↑ Mic-1, - Tbp, - β ₂ -Microglobulin	Immune regulation Appetite control
2	Bonatti, S. et al. ⁷⁰	Primary keloid fibroblasts Primary adjacent skin fibroblasts	Quasar Esthetique® (LED device)	470	125	00:01:00 00:02:00 00:03:00	59.9 122.3 183.4	1	Cell counting: – Keloid fibroblasts ↓ Adjacent skin fibroblasts (183.4 J/cm ²)	Keloids
3	Fushimi, T. et al. ⁷¹	Normal human dermal fibroblasts	Mignon Belle LT-1 Crystalline narrow-band LED device	456	0.25	00:20:00	0.3	1	PCR: ↑ HGF, - VEGF-A, ↑ KGF, - IL-8, - Leptin	Wound healing
								3	Growth factor & cytokine levels: ↑ HGF, - VEGF-A, ↑ KGF, - IL-8, - Leptin	
4	Hwang, I. Y. et al. ⁷²	Human gingival fibroblasts (HGF)	Plasma lamp	400 – 500	1900	00:00:01* 00:00:02* 00:00:06* 00:00:13* 00:00:25*	2 4 12 24 48	1	↑ DNA synthesis ↓ Metabolic activity ↑ Cell viability (≥ 24 J/cm ²) ↑ DNA fragmentation ↓ Cell cycle progression ↑ Apoptosis (Sub-G0/G1 phase) ↓ ΔΨm ↑ Poly (ADP ribose) polymerase cleavage	Wound healing (Dentistry)
5	Krassovka, J. et al. ⁷³	Normal palmar fibroblasts Dupuytren's fibroblasts	Narrow-band LED device	453	38	00:02:22* 00:04:23* 00:08:46* 00:17:33* 00:26:19* 00:35:05*	5 10 20 40 60 80	1	↓ Metabolic activity (≥ 60 J/cm ²) – α-SMA expression ↑ ROS – Cell viability	Dupuytren's contracture
6	Kushibiki, T. et al. ⁷⁴	NIH-3T3 fibroblasts	Laser VLM 500®	405	100	00:01:00 00:02:00	6* 12*	1	↑ ROS	N/A
7	Lee, H. S. et al. ⁷⁵	Keloid fibroblasts	Acne photo light (APL®)	410	205	00:00:49	10	2	– Cell proliferation – Cell viability PCR (Collagen biosynthesis): ↓ Collagen I, - TGF-β1, - Smad3, - Smad4 Western Blot (Collagen biosynthesis): ↓ Collagen I, - TGF-β1, - Smad3, -Smad4	Keloids
8	Malcic, A. I. et al. ⁷⁶	Lung fibroblasts of the Chinese hamster (V79 fibroblasts)	Bluephase C8® Light Unit (High-performance LED polymerization light) Irradiation modes: High power (H), low power (LP), soft start (S)	430 – 490	753.9 (H) 751.6 (H) 740.2 (H) 421.5 (L) 421.7 (L) 418.9 (L) 742.2 (S) 719.5 (S) 735.9 (S)	00:00:20 00:00:40 00:00:80 00:00:20 00:00:40 00:00:80 00:00:20 00:00:40 00:00:80	15.1* 30.1* 59.2* 8.4* 16.9* 33.5* 14.8* 28.8* 58.9*	1	– Cell viability – Colony-forming ability ↓ Cell proliferation (S, H mode)	Dentistry

	Authors	Cell type	Light source	Wavelength [nm]	Irradiance [mW/cm ²]	Time [h:min:s]	Dose [J/cm ²]	#	Effects	Application
9	Mamalis, A. et al. ⁷⁷	Primary human skin fibroblasts (adult)	Omnilux Clear-U, (LED array)	415	35	00:01:55 00:03:50 00:05:45 00:11:30 00:17:15 00:30:34	5 10 15 30 45 80	1	- Cell viability ↓ Cell proliferation ↓ Cell migration ↑ ROS	Keloids Other fibrotic skin diseases
10	Masson-Meyers, D. S. et al. ⁷⁸	Primary human dermal fibroblasts (adult)	Dynatron Solaris 708 (LED device)	470	30	00:01:40* 00:30:33* 01:01:07* 02:02:13*	3 55 110 220	1	↓ Metabolic activity (≥ 55 J/cm ²) ↓ Cell viability (≥ 110 J/cm ²)	Safety of light therapy
11	Masson-Meyers, D. S. et al. ⁷⁹	Primary human dermal fibroblasts (adult)	Dynatron Solaris 708 (LED device)	470	30	00:01:40* 00:02:47* 00:05:33* 00:30:33*	3 5 10 55	1	Cell migration: ↑ 5 J/cm ² , ↓ 55 J/cm ² - Cell viability ↑ Protein synthesis Growth factors: - bFGF, - IL-10, ↓ IL-6 - Collagen biosynthesis	Wound healing
12	Mignon, C. et al. ⁸⁰	Primary human reticular dermal fibroblasts Primary human papillary dermal fibroblasts	Proprietary LED-based device prototype	450	30	00:01:07* 00:02:47* 00:04:10* 00:08:20* 00:11:07* 00:16:40* 00:25:00* 00:33:20*	2 5 7.5 15 20 30 45 60	3	↓ Metabolic activity ↓ Cell viability (> 30 J/cm ²) ↑ ROS ↑ Collagen biosynthesis Gene expression profiles, RT-qPCR: ↓ Proliferation, ↓ Metabolism, ↓ Protein synthesis, ↓ Repair (Reticular cells)	Aging skin Non-healing chronic wounds
13	Oplander, C. et al. ⁸¹	Primary human dermal fibroblasts (adult)	Prototypes of narrow-band LED devices	410 420 453 480	50	00:01:40* 00:03:20* 00:05:00* 00:06:40* 00:10:00* 00:16:40* 00:20:00* 00:26:40* 00:30:00*	5 10 15 20 30 50 60 80 90	1	Cell viability: ↓ 410 & 420 nm: ≥ 60 J/cm ² , - 453 nm, ↑ 480 nm: ≥ 30 J/cm ² ROS: ↑ 410 & 420 nm: 10 J/cm ² , - 453 nm, - 480 nm Antioxidative capacity: ↓ 410 & 420 nm: 10 J/cm ² , ↓ 453 nm (30 J/cm ²), - 480 nm	Keloids Hypertrophic scars Fibrotic skin diseases
						00:01:40* 00:05:00* 00:10:00*	5 15 30	4	Cell proliferation: ↓ 410, 420 & 453 nm, - 480 nm	
14	Rotenberg, S. et al. ⁸²	Mouse lung fibroblasts (Balb/c)	Quartz-tungsten halogen (QTH) source	380 – 500	550	00:00:10 00:01:00* 00:02:00 00:04:00*	5 30 60 120	1	↓ Metabolic activity	Dentistry
15	Seo, Y. et al. ⁸³	Rabbit anterior cruciate ligament fibroblasts (ACL)	Low-intensity LED irradiation device	460	45	00:10:00	27	3	- Cell proliferation, - Cell migration PCR: - EGF, ↑ TGF-β1, ↑ IGF, ↓ Collagen I Immunohistochemistry: - Collagen I, - TGF-β1, - Actin, - αVβ3 Integrin	N/A

	Authors	Cell type	Light source	Wavelength [nm]	Irradiance [mW/cm ²]	Time [h:min:s]	Dose [J/cm ²]	#	Effects	Application
16	Tafliński, L. et al. ⁸⁴	Primary human dermal fibroblasts (adult)	Prototype of a narrow-band LED device	420	50	00:05:00* 00:10:00* 00:20:00* 00:30:00*	15 30 60 90	1	↓ Cell viability (≥ 60 J/cm ²) ↑ ROS (15 & 30 J/cm ²) ↓ Antioxidative capacity (15 & 30 J/cm ²) ↓ Contraction of collagen gels	Fibrotic skin diseases
						00:05:00* 00:10:00*	15 30	4	↓ Cell proliferation (15 & 30 J/cm ² with significant results at 2 days of irradiation) ↓ Cell counting ↓ Number of α -SMA positive cells (15 & 30 J/cm ²) ↓ α -SMA expression (15 & 30 J/cm ²)	
17	Taoufik, L. et al. ⁸⁵	Primary human gingival fibroblasts (HGF)	3M/Trilite, Espe (Halogen lamp) The cure, Spring Health Products (LED device) 3M Ortholite (Plasma arc lamp)	/ 420 – 600 450 – 500	750 900 2000	00:04:00 00:03:00 00:02:00	186 162 240	1	– DNA synthesis – Cell proliferation – Immunofluorescent staining for DNA damage (Double-strand breaks)	Dentistry
18	Teuschl, A. et al. ⁸⁶	NIH/3T3 fibroblasts	LEDline2	470	50	00:10:00	30	5	– Metabolic activity ↓ Cell migration ↓ Cell viability	Wound healing
19	Wataha, J. C. et al. ⁸⁷	Balb/c 3T3 mouse fibroblasts	Optilux (QTH) PowerPac (Plasma arc source) Accucure (Argon laser light source)	400 – 500	556 1690 202	00:00:02 00:00:06 00:00:12 00:00:0.5 00:00:1.5 00:00:03 00:00:04 00:00:12 00:00:24	1 3 6 1 3 6 1 3 6	1	Metabolic activity: ↓ QTH, Laser (≥ 3 J/cm ²) ↓ PAC (≥ 1 J/cm ²)	Dentistry
20	Wataha, J. C. et al. ⁸⁸	Diploid human lung fibroblasts (WI-38) Aneuploid mouse lung fibroblasts (Balb/c) Human gingival fibroblasts (HGF)	Optilux (QTH) PowerPac (Plasma arc source) Accucure (Argon laser light source)	400 – 500	556 1690 202	00:02:00 00:00:30 00:00:10	60 5	1	Metabolic activity: ↓ Balb/c (PAC > QTH), ↓ HGF (PAC), ↑ WI-38 (PAC) TEM micrographs: Structural changes in mitochondria for Balb/c fibroblasts Metabolic activity: ↓ Balb/c, ↑ WI-38, ↑ HGF TEM micrographs: see QTH/PAC	Modulating cell growth and survival
21	Yoshida, A. et al. ⁸⁹	Human gingival fibroblasts (HGF)	Techno Light KTL-100 (LED device) Techno Light KTS-150 (QTH)	460	250	00:01:00 00:03:00 00:05:00	15 45 75	1	↓ Metabolic activity (LED > QTH) ↑ ROS (LED > QTH) Electron microscopic analysis: Structural changes in mitochondria	Dentistry

Table 1: Summary of LLLT/PBM publications reporting blue light effects on different types of fibroblasts. * Non-reported parameters (Calculated)

1.4 MEDILIGHT – Light treatment of chronic wounds

Although fundamental PBM mechanisms are not yet fully understood, numerous LED devices were launched to the market with most of them being commercialized for the treatment of cutaneous disorders, such as impaired wound healing. Chronic wounds appear due to a disruption of the classical healing process resulting in a delayed tissue repair beyond the anticipated time, which can take up to several years^{47, 90}. Affecting 3 – 6 million patients only in the US with annual costs of approximately \$10 – 25 billion^{91, 92}, non-healing wounds represent a substantial economic burden to public healthcare systems worldwide. With growing prevalence of vascular disorders and life-style diseases like obesity and diabetes as well as an increasing aging of the population, chronic wounds become a tremendous clinical challenge. According to the Wound Healing Society, chronic wounds can be classified into four categories: (1) pressure ulcers, (2) diabetic ulcers, (3) venous ulcers and (4) arterial ulcers⁹³. Despite their increasing prevalence⁹⁴, many patients still experience insufficient wound care suffering from severe pain and a significantly reduced quality of life often ending in amputation of lower extremities and premature death⁹⁰.

As a new innovation in wound research, the European project MEDILIGHT aimed to develop a medical device which uses proven therapeutic effects of VIS light to improve the self-healing process of wounds and monitor their status during therapy (co-funded by the European Union's Horizon 2020 research and innovation program under Grant Agreement No. 644267). Driven by URGO RID (France), six other partners with different competencies were involved in the consortium: TUB Berlin, University of Heidelberg, CSEM, SignalGeneriX Ltd., Microsemi Semiconductor Ltd. and AMIRES. The whole consortium strived to translate current light technologies, which still mainly rely on bulky and stationary devices in hospitals, into a wearable, light-weight, low cost, and flexible



Figure 5: First prototype of the MEDILIGHT device fixed to a special shoe for diabetic foot ulcer (DFU) patients enabling an easy as well as a comfortable treatment at home.

solution for personalized treatment at home (Figure 5). Besides target applications including DFU and venous leg ulcers (VLU), the device could represent a valuable tool for the therapy of fibrotic skin diseases or even PDT of skin cancer.

1.5 Aim of the study

Nowadays, more and more publications arise in PBM research proposing that light therapy demonstrates a powerful treatment approach for a wide variety of medical conditions. Most *in vivo* studies testing the efficacy of phototherapy, either in animal models or clinical trials, almost exclusively involve red and (N)IR light showing two persuasive advantages. On the one hand, longer wavelengths exhibit a deeper tissue penetration, while, on the other hand, the underlying mechanism of action is more or less elucidated. Consequently, the application of other wavelengths becomes easily underappreciated, even though beneficial effects were already proven for numerous medical disorders. Especially for blue light, many encouraging results were reported; however, its use remains rather controversial, since its higher energy level is often linked to suppression of cellular activity and consequently inhibition of proliferation. Moreover, primary and secondary mechanisms contributing to local and systemic effects remain poorly understood.

Consequently, the main aim of this study was to assess the therapeutic potential of different irradiation doses of VIS blue light in an *in vitro* model of primary normal human dermal fibroblasts (NHDF cells). Driven by the European project MEDILIGHT, studies were mainly focused on testing the modulatory effect of blue light on cell metabolism, proliferation and gene expression profiles. Accordingly, the following issues were addressed in this project:

- Do temperature increases, induced by blue light, contribute to an altered cellular activity and proliferation of NHDF cells?
- Which doses of blue light lead to significant changes in the metabolic activity of NHDF cells and will be chosen for subsequent studies?
- Are light-induced metabolic changes also reflected in altered proliferation rates?
- Does blue light irradiation differentially impact mitochondrial function?
- Are light treatments, especially with higher irradiation doses, safe with respect to cell viability or lead to cytotoxic effects on NHDF cells?
- Which genes and signaling pathways are commonly or differentially expressed at low and/or high dose levels of blue light?
- Does blue light irradiation using the MEDILIGHT prototype show similar effects on the metabolic activity of NHDF cells compared to the BioLight LED Lamp?

2 MATERIAL AND METHODS

2.1 Material

2.1.1 Cell line

The primary cell line 'Normal Human Dermal Fibroblasts' (NHDF), cryopreserved at passage 2 (P2), was obtained from PromoCell GmbH (Heidelberg, Germany). The company had isolated the cells from the dermis of adult human skin, in detail from the temple of a 52-year-old Caucasian female donor. Subsequent quality controls verified typical cell morphology as well as common adherence and viability rates. Phenotypic characterization was performed by immunohistochemical staining of the fibroblast-specific surface antigen CD90, which was identified by flow cytometry analysis. With a population doubling time of 43.4 hours in the log phase, growth performance was tested and guaranteed through multiple passages up to 15 population doublings. The morphology of NHDF cells in passage 6 appeared to be elongated with a branched cytoplasm surrounding oval nuclei (Figure 6).

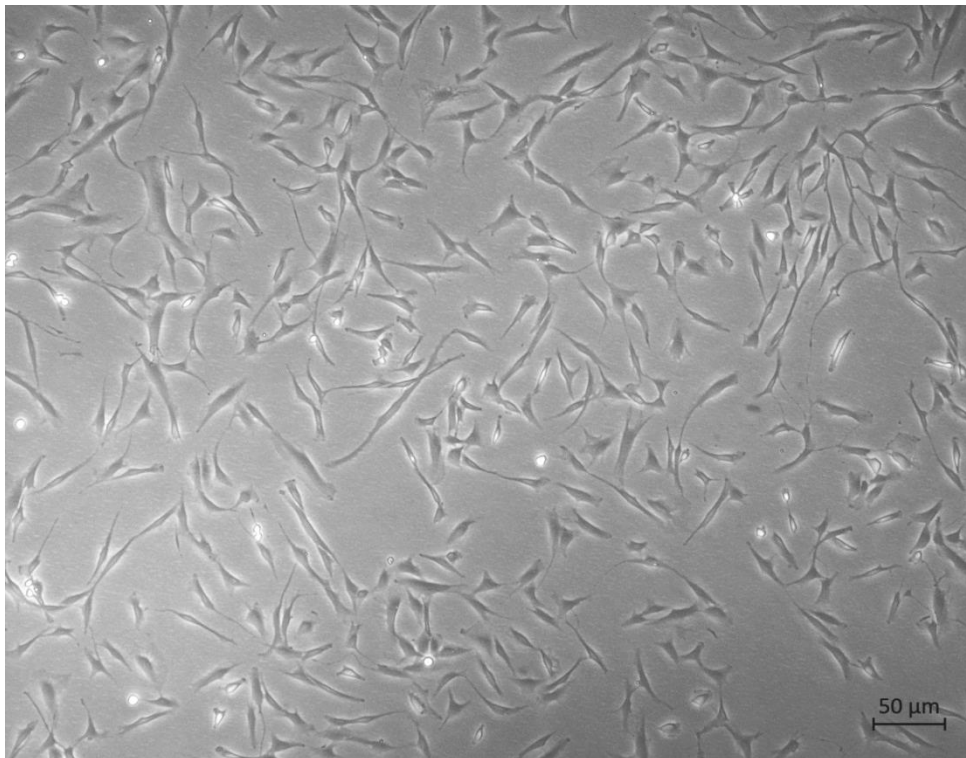


Figure 6: Morphology of normal human dermal fibroblasts (NHDF cells) in passage 6 with mitotic cells. Using an inverted Leica DM IRBE microscope (Leica Mikroskopie & Systeme GmbH, Wetzlar, Germany), the image was acquired in phase contrast with 5x magnification.

2.1.2 Laboratory equipment

The laboratory equipment is outlined in different subgroups. With the corresponding manufacturer specified, the used equipment is listed in subsequent tables as follows: consumables in Table 2, substances in Table 3, kits in Table 4, devices in Table 5 as well as the software used for data evaluation, which is summarized in Table 6.

2.1.2.1 Consumables, substances and kits

Table 2: Overview of consumables with specification of manufacturer

Description	Manufacturer
Cell culture flasks, CELLSTAR® 75 cm ² , 175 cm ²	Greiner Bio-One GmbH, Frickenhausen, Germany
Cell culture plates, 96-well, transparent, flat bottom, with low evaporation lid	Costar® by Corning Incorporated, Kennebunk, ME, USA
Cell culture plates, 96-well, black, clear flat bottom, with low evaporation lid	Costar® by Corning Incorporated, Kennebunk, ME, USA
Cell culture plates, 96-well, white, flat bottom, with low evaporation lid	BRAND GmbH + Co. KG, Wertheim, Germany
Conical tubes (15 mL, 50 mL)	Falcon® by Corning Science México S.A. de C.V., Taumalipas, México
CryoTube™ Vials	Nunc™ by Thermo Fisher Scientific, Roskilde, Denmark
HuGene-2_0st microarrays (Human)	Thermo Fisher Scientific, Waltham, MA, USA
Luna™ Cell counting slides	Logos Biosystems, Anyang-si, Gyeonggi-do, Korea
Pipette tips, graduated, with filter	STARLAB International GmbH, Hamburg, Germany
Round-bottom tubes with cell-strainer cap (5 mL)	Falcon® by Corning Science México S.A. de C.V., Taumalipas, México
Safe-lock tubes (1.5 mL, 2.0 mL)	Eppendorf AG, Hamburg, Germany
Serological pipettes (5 mL, 10 mL, 25 mL)	SARSTEDT AG & Co., Nümbrecht, Germany
URGOSTART, Wound dressing E2723	URGO RID, Chenôve, France

Table 3: Overview of substances with specification of manufacturer

Description	Manufacturer
Allophycocyanin Annexin V	BioLegend, Koblenz, Germany
Amplex® UltraRed Reagent	Molecular Probes™ by Thermo Fisher Scientific, Life Technologies Corporation, Eugene, OR, USA
Annexin V Binding Buffer	BioLegend, Koblenz, Germany
Chloroform	Merck, Darmstadt, Germany
Dimethyl sulfoxide, sterile-filtered	Hybri-Max™ by Sigma-Aldrich Co. LLC, St. Louis, MO, USA
Dulbecco's Modified Eagle Medium (1x) + GlutaMAX™ -I, 500 mL [+] 4.5 g/L Glucose, [-] Pyruvate	Gibco™ by Thermo Fisher Scientific, Waltham, MA, USA
Ethanol, ROTIPURAN®, > 99.8%, p.a.	Carl Roth GmbH & Co. KG, Karlsruhe, Germany
Horseradish peroxidase	Pierce™ by Thermo Fisher Scientific, Rockford, IL, USA

Hydrogen peroxide solution, 30% (w/w) in H ₂ O, with stabilizer	Sigma-Aldrich Chemie, GmbH, Steinheim, Germany
Nuclease-free water	Omega Bio-tek Inc., Norcross, GA, USA
Penicillin/ Streptomycin [+] 10,000 Units/mL Penicillin [+] 10,000 µg/mL Streptomycin	Gibco™ by Thermo Fisher Scientific, Waltham, MA, USA
Phosphate buffered saline (without Mg ²⁺ /Ca ²⁺)	Gibco™ by Thermo Fisher Scientific, Waltham, MA, USA
2-Propanol, ROTIPURAN®, > 99.8%, p.a.	Carl Roth GmbH & Co. KG, Karlsruhe, Germany
Propidium Iodide, 1.0 mg/mL	Invitrogen™ by Thermo Fisher Scientific, Life Technologies Corporation, Eugene, OR, USA
Sodium pyruvate (100 mM)	Gibco™ by Thermo Fisher Scientific, Waltham, MA, USA
Staurosporine (<i>Streptomyces staurosporeus</i>)	Sigma Aldrich, St. Louis, MO, USA
SupplementMix, Fibroblast Growth Medium 3	PromoCell GmbH, Heidelberg, Germany
TRIzol®	Ambion® by Thermo Fisher Scientific, Life Technologies Corporation, Darmstadt, Germany
Trypan Blue stain (0.4%)	Gibco™ by Thermo Fisher Scientific, Waltham, MA, USA
0.25% Trypsin-EDTA (1x)	Gibco™ by Thermo Fisher Scientific, Waltham, MA, USA

Table 4: Overview of kits with specification of manufacturer

Description	Manufacturer
Cell Proliferation ELISA, BrdU (Colorimetric)	Roche Diagnostics GmbH, Roche Applied Science, Mannheim, Germany
CellTiter-Glo® Luminescent Cell Viability Assay	Promega Corporation, Madison, WI, USA
Colorimetric Cell Viability Kit III (XTT)	PromoKine™ by PromoCell GmbH, Heidelberg, Germany
CyQUANT® Direct Cell Proliferation Assay Kit	Invitrogen™ by Thermo Fisher Scientific, Eugene, OR, USA
FITC BrdU Flow Kit	BD Pharmingen™ by BD GmbH, Heidelberg, Germany
GeneChip® Hybridization, Wash and Stain Kit	Thermo Fisher Scientific, Waltham, MA, USA
GeneChip® WT Plus Reagent Kit	Thermo Fisher Scientific, Waltham, MA, USA
Mitochondrial Membrane Potential Assay Kit (II)	Cell Signaling Technology®, Danvers, MA, USA

2.1.2.2 Devices and software

Table 5: Overview of devices with specification of manufacturer

Description	Manufacturer
Agilent 2100 Bioanalyzer	Agilent Technologies, Santa Clara, CA, USA
Axio Observer.Z1 with Lamp Module	Carl Zeiss Microscopy GmbH, Göttingen, Germany
Flow cytometer, BD FACSCanto™ II	BD Biosciences, Heidelberg, Germany
Biofuge primo R, Heraeus®	Kendro Laboratory Products GmbH, Osterode, Germany
BioLight LED Lamp with Lumileds LUXEON Rebel LXML-PR01-0275	Philips Electronics Nederland B.V. Philips Research, Eindhoven, Netherlands Koninklijke Philips N.V., Eindhoven, Netherlands

Centrifuge Rotanta 96 RC	Hettich GmbH & Co. KG, Tuttlingen, Germany
CO ₂ Incubators HERAcell™ 240i, HERAcell™ VIOS 160i	Thermo Electron LED GmbH, Thermo Scientific, Langenselbold, Germany
Diffusor	CSEM, Basel, Switzerland
Laser Power Meter, 843-R	Newport Corporation, Irvine, CA, USA
GeneChip® Fluidics Station 450	Affymetrix UK Ltd., High Wycombe, UK
GeneChip® Hybridization Oven 640	Affymetrix UK Ltd., High Wycombe, UK
GeneChip® Scanner 3000	Affymetrix UK Ltd., High Wycombe, UK
Laminar flow, Heraeus®, HERAsafe	Kendro Laboratory Products GmbH, Hanau, Germany
Leica DM IRB, IRBE	Leica Mikroskopie & Systeme GmbH, Wetzlar, Germany
Luna™ Automated cell counter	Logos Biosystems, Anyang-si, Gyeonggi-do, Korea
MEDILIGHT prototypes, 1 st generation	MEDILIGHT consortium (EU Horizon H2020, # 644267)
Microplate reader, Spark® 10M	Tecan Austria GmbH, Grödig, Austria
myFuge™ Mini centrifuge C1008	Benchmark Scientific, Edison, NJ, USA
Mr. Frosty™ Cryo 1°C Freezing container	Nalgene® by Thermo Fisher Scientific, Waltham, MA, USA
NanoQuant plate™	Tecan Austria GmbH, Grödig, Austria
Neutral density filter, D1.0, NG4	Advanced Optics Schott AG, Mainz, Germany
pH Meter, pH 540 GLP, MultiCal®	WTW, Weilheim, Germany
Thermocouple Data Logger, USB TC-08	Pico Technology, St. Neots, Cambridgeshire, UK
Thermocouple, Type K, RS PRO	RS Components Ltd., Corby, Northamptonshire, UK
918 UV-SI Wand detector, 200 – 1100 nm, OD3 Attenuator, DB15	Newport Corporation, Irvine, CA, USA

Table 6: Overview of software with specification of manufacturer

Description	Manufacturer
BD FACSDiva, version V6.X	BD Biosciences, Heidelberg, Germany
FlowJo™ 10, version 2.5.1	FlowJo LLC, Ashland, OR, USA
Fiji, Image processing package of ImageJ	Free software for image analysis
JMP® Genomics, version 7.1	SAS Institute Inc., Cary, NC, USA
SparkControl, version 1.2	Tecan Austria GmbH, Grödig, Austria
ZEN 2 pro	Carl Zeiss AG, Oberkochen, Germany

2.1.3 Light sources

Two LED systems were used for the blue light treatment of human dermal fibroblasts. For most of the studies, cells were irradiated with the BioLight LED Lamp provided by Philips Research (Eindhoven, Netherlands) serving as a benchmark, since the device developed by MEDILIGHT was designed and manufactured during the project period. In April 2018, the 1st generation of prototypes was provided for *in vitro* testing.

2.1.3.1 BioLight LED Lamp

The BioLight LED Lamp, accompanied by a current modulator, which enabled pulsed driving, was set up and calibrated by Philips Electronics Nederland B.V., Philips Research (Eindhoven, Netherlands). It was equipped with two power supplies with one delivering 1 A at 300 V (direct current) to drive the LEDs via defined presets. The second one powered the fan with a fixed voltage of 24 V (direct current) and 0.1 A protecting the lamp against overheating, especially when using higher irradiances or longer irradiation times (Figure 7, (A)). The illumination field was composed of LEDs (Philips Lumileds LUXEON Rebel LXML-PR01-0275 from Koninklijke Philips N.V. (Eindhoven, Netherlands)). The latter, showing a royal blue color (Figure 7, (A)) and a beam divergence of $\pm 15^\circ$, were covered by a set of lenses (Figure 7, (B)).



Figure 7: (A) Experimental set-up of the BioLight LED Lamp with a current modulator and two power supplies provided by Philips Electronics Nederland B.V., Philips Research (Eindhoven, Netherlands). (B) Lens-covered illumination field (LED aperture).

This set-up provided a homogenous light distribution, which was determined by Philips Research using an average central irradiance of 10 mW/cm^2 at a distance of 50 mm from the lamp casing (Figure 8, (A)). The maximum time-averaged emittance was given at 100 mW/cm^2 , corresponding to 15 W for the 10 cm x 15 cm emission aperture. Moreover, the maximum peak emittance equaled 350 mW/cm^2 . According to the company's specification, the LED device was distance and power adjusted to deliver a fixed irradiance of 23 mW/cm^2 at the surface of irradiated cell culture plates.

The peak wavelength, which was measured at a central irradiance of 12 mW/cm² and a distance of 50 mm, was given at $\lambda = 453$ nm (Figure 8, (B)). For all experiments the irradiation was performed continuously with a duty cycle of 100%. Prior to each light treatment, the LEDs were pre-run for a few seconds in order to stabilize their output.

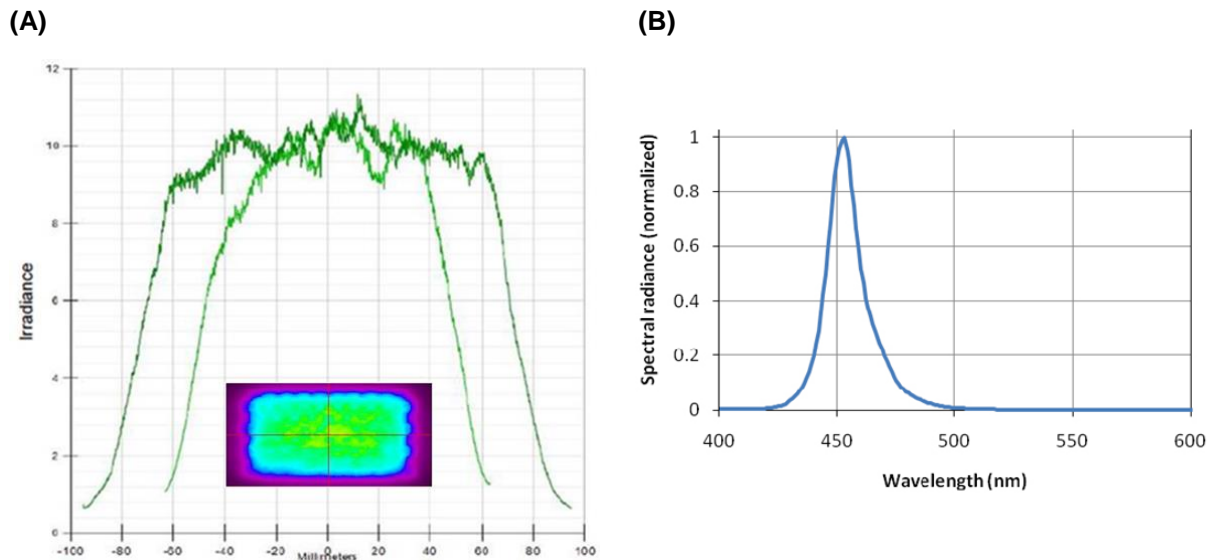


Figure 8: Lamp specifications of the BioLight LED lamp with (A) the spatial distribution of irradiance at a distance of 50 mm from the lamp casing and (B) the emission spectrum with a peak wavelength at 453 nm, which was measured at a central irradiance of 12 mW/cm² and a distance of 50 mm.

2.1.3.2 MEDILIGHT system

Seven consortium partners of the European project MEDILIGHT had developed a wearable and highly integrated medical device, which was intended to improve the impaired healing process of chronic wounds. In respect of hygienic requirements for medical devices, the prototype was divided into two parts. The first part consisted of a re-usable LED-based illumination and sensing system, which was placed on top of a disposable wound dressing and fixed by a customized pocket. Although it sealed the wound hermetically, the adhesive and absorbent dressing (E2723), developed by URGO RID (Chenôve, France), was still breathable. Besides providing homogenous illumination through the dressing, the flat and flexible LED foil was equipped with an integrated smart sensing system. This enabled continuous monitoring of temperature changes and simultaneous mapping of blood oxygenation levels. The second, also re-usable part represented an encasement, which enclosed an electronic module and a rechargeable battery with its status indicated by one of the light displays on top of the encasement (Figure 9).

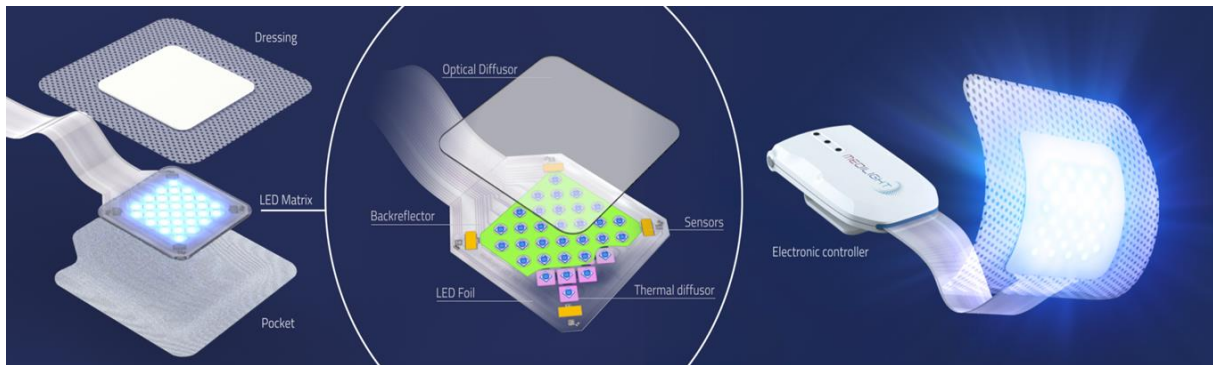


Figure 9: MEDILIGHT system including a thin and flexible LED foil with integrated temperature and pulse oximetry sensors illuminating the wound area through the disposable absorbent wound dressing E2723. The rechargeable system was controlled by an electronic module via wireless communication.

Moreover, an application software was developed in order to drive the LED array and its integrated sensors as well as to analyze acquired data transmitted via Bluetooth. In order to be compliant with hygienic conditions, URGO RID encapsulated the LED foil together with a thin-film back-reflector from CSEM (Basel, Switzerland) in silicone. The addition of the latter was intended to yield a higher light efficiency (Figure 10).

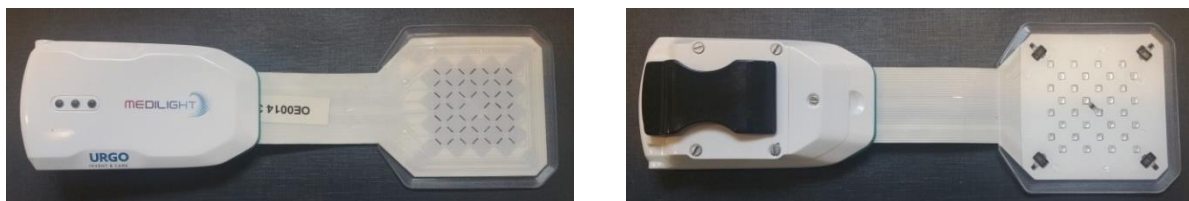


Figure 10: Holistical MEDILIGHT prototype from (A) top side and (B) bottom side showing the thin-film back-reflector attached to the flexible LED foil, increasing light efficiency within the surrounding silicone encapsulation.

Since the prototype missed any optical lenses diffusing the light (Figure 11, (A), (B)), the light emission of single LED spots was homogenized by adding another layer, an opaque diffuser, which was also provided by CSEM (Figure 11, (C)).

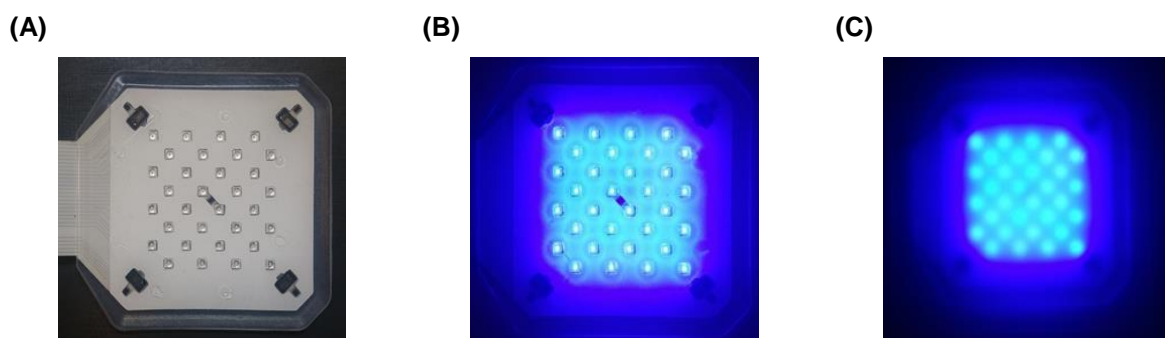


Figure 11: (A) Illumination field of the MEDILIGHT prototype either (B) without diffuser or (C) with diffuser.

2.2 Methods

2.2.1 Cell culture

NHDF cells were cultured in Dulbecco's Modified Eagle Medium (DMEM, high glucose, GlutaMAX™ Supplement), which was complemented with 100 units/mL penicillin/streptomycin as well as 1 mM sodium pyruvate (Gibco™ by Thermo Fisher Scientific, Waltham, MA, USA). Moreover, a SupplementMix from PromoCell GmbH (Heidelberg, Germany) was added, completing the medium with 0.1 mL/mL fetal calf serum (FCS) (10%) (v/v), 1 ng/mL basic fibroblast growth factor and 5 µg/mL insulin. Standard culture conditions were maintained in a humidified atmosphere at 37°C and 5% CO₂. In order to ensure logarithmic growth and prevent senescence, the cells were only used up to 15 population doublings, which corresponded to about 6 – 8 passages. At subconfluence (70 – 80%), NHDF cells were re-seeded according to the instructions of PromoCell keeping a plating density of 3.500 – 7.000 cells/cm². For cell detachment, 0.25% Trypsin/EDTA (1x) was diluted to 0.04% using phosphate buffered saline (PBS) without Mg²⁺ and Ca²⁺ (Gibco™ by Thermo Fisher Scientific, Waltham, MA, USA) and added for an incubation time of 3 minutes at 37°C and 5% CO₂. Then, viable cells, determined by Trypan Blue exclusion, were quantified with a Luna™ automated cell counter and seeded in new flasks or multiwell plates at the suggested plating density. For culture flasks, split ratios of 1:6 – 1:10 were obtained with medium renewal twice a week, whereas for 96-well plates the plating density was adjusted according to the experiment duration: 5,000 cells/well for 3 culture days; 2,500 cells/well for 4 culture days and 1,250 cells/well for 5 days of culturing. Unless otherwise specified, NHDF cells were seeded into black 96-well plates, which prevented light crosstalk between single wells, and incubated for 24 hours at 37°C and 5% CO₂ before exposing them to the light treatment.

2.2.2 Light treatment

At 24 hours after seeding, the medium was renewed at 30 minutes prior to irradiation in order to provide an appropriate amount of nutrients to the cells. Then, following another incubation for 30 minutes at 37°C and 5% CO₂, NHDF cells were treated with different blue light doses. All light treatments were performed outside the incubator.

2.2.2.1 BioLight LED Lamp

As already described in 2.1.3.1, the BioLight LED Lamp provided by Philips Research (Eindhoven, Netherlands) operated at a steady irradiance level, yielding 23 mW/cm² at the surface of irradiated cell culture plates (50 mm distance from the lamp casing). However, since the black plate, the lid and the medium led to a power loss of about 50% due to light absorption, the irradiance was attenuated to about 12 mW/cm²⁹⁵. In consequence, the dose resulting from different irradiation times also changed. Blue light doses, which were tested in this study, are listed in Table 7.

Table 7: Different irradiation times [min] with corresponding doses [J/cm²] at an irradiance level of about 12 mW/cm². The left column lists irradiation times assigned to low – mid blue light doses, while the right column summarizes irradiation times corresponding to mid – high blue light doses.

Low – Mid Dose		Mid – High Dose	
Irradiation time [min]	Dose [J/cm ²]	Irradiation time [min]	Dose [J/cm ²]
2.5	1.8	22.5	16.2
5.0	3.6	25.0	18.0
7.5	5.4	30.0	21.6
10.0	7.2	45.0	32.4
12.5	9.0	60.0	43.2
15.0	10.8	90.0	64.8
17.5	12.6	120.0	86.4
20.0	14.4	240.0	172.8

Concerning the experimental set-up, the left part of the plate (Col. #1-6) was treated with blue light, while the right side (Col. #7-12) was dark taped representing the untreated control (Figure 12). Hence, apart from blue light irradiation, untreated control cells were always kept under the same environmental conditions, which excluded a plate effect between light-treated and untreated groups.

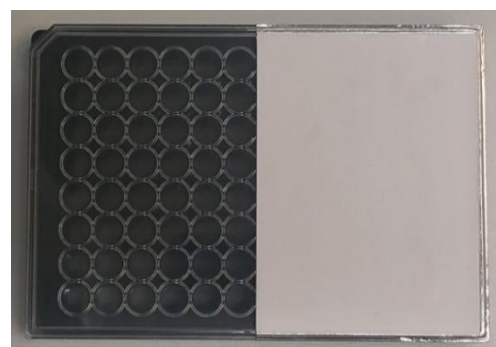


Figure 12: Lid of a black 96-well plate with the right side (Col. #7-12) dark taped setting up the non-irradiated control.

Throughout this study, two experimental light schedules were followed involving either single treatments with a defined irradiation dose or multiple treatments, with the same dose each, summing up in an equivalent irradiation dosage (Figure 13).

Using the latter, cells were treated once a day over two or three consecutive days with the medium being renewed before each treatment. Following multiple treatments long-term effects, for example changes in cell activity and proliferation, were always studied at 24 hours after the last irradiation (Figure 13, (B)). In contrast, different time points were tested after single blue light exposures to assess fast responses like changes in ROS or ATP levels (Figure 13, (A)). To perform direct comparisons, two independent methods were often combined on the same test plate, such as the XTT assay and time-matched RNA isolation with subsequent gene expression profiles.

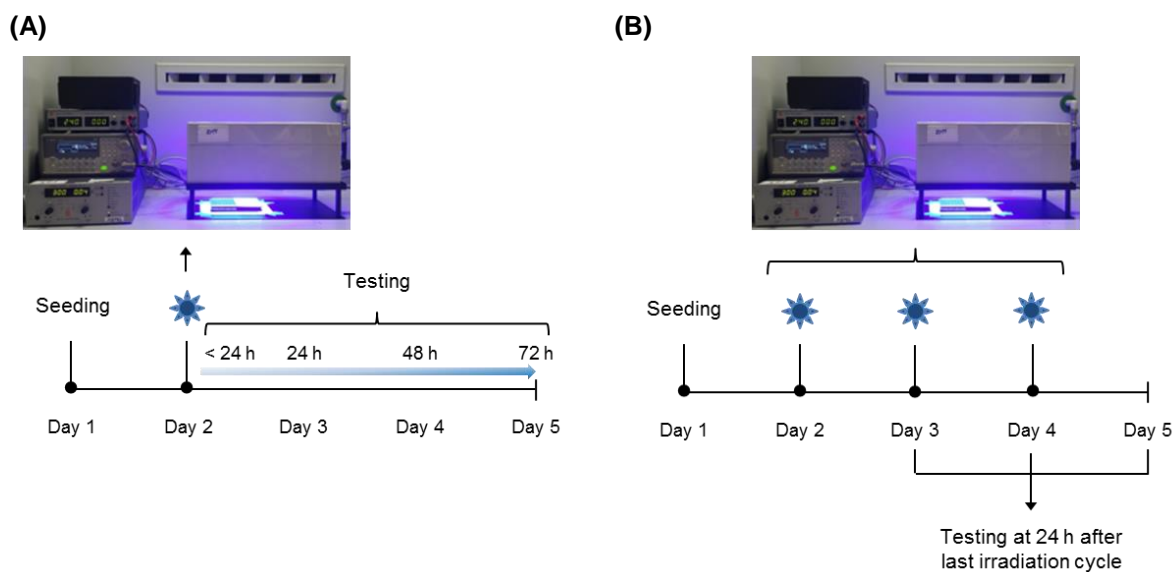


Figure 13: Experimental light schedules for (A) single and (B) multiple treatments. (A) At 24 hours after seeding into black 96-well plates, NHDF cells were irradiated on the second day with assays being performed within the next 72 hours after irradiation. (B) Starting at 24 hours after seeding, NHDF cells were treated once a day on consecutive days, while the assays were performed at 24 hours after the first, second or third irradiation.

2.2.2.2 MEDILIGHT system

As a prerequisite for subsequent *in vivo* studies, the efficacy of different MEDILIGHT prototypes had to be assessed *in vitro*. Since its illumination field housing 450 nm LEDs was too small to treat half of the multiwell plate, lids with a defined irradiation area were prepared (Col. #2-5, Row #C-F). Moreover, irradiation was performed in direct contact to the plate. Using an 843-R laser power meter (Newport Corporation, Irvine, CA, USA), the irradiance resulting underneath the entire component stack was adjusted to 23 mW/cm^2 , which coincided with the setting of the BioLight LED Lamp. Involving the diffusor (CSEM, Basel, Switzerland) or E2723 (URGO RID, Chenôve, France), duty cycles (DCs) of respectively 38% and 68% were obtained (Figure 14).

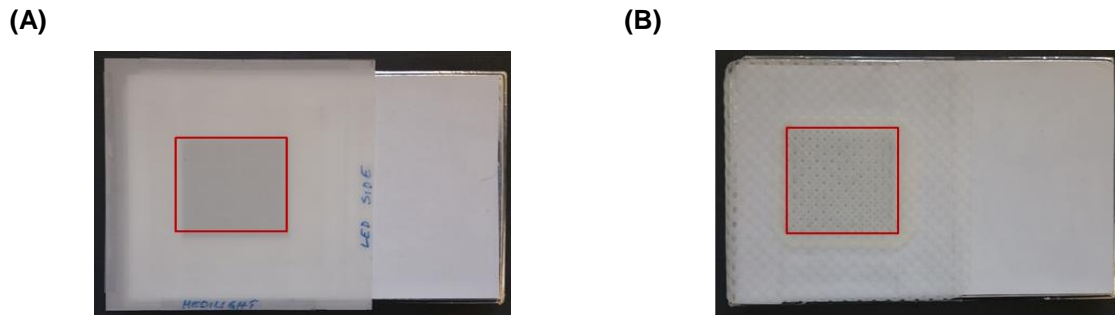


Figure 14: Experimental design for *in vitro* validation of the MEDILIGHT prototype – Plate set-up with (A) diffuser (CSEM, Basel, Switzerland) and (B) wound dressing E2723 (URGO RID, Chenôve, France). The red rectangle indicates the irradiated area.

To determine whether the illumination field provided a homogenous light distribution, NHDF cells were seeded into transparent 96-well plates, which allowed light crosstalk between single wells. For these light experiments, the center of the lid (Col. #5-8, Row #C-F), adapted to the size of the illumination field, was left untaped, while the surrounding was dark taped excluding any light penetration (Figure 15, (A)). Light distribution was varied by adding the diffuser or E2723 (Figure 15, (B) & (C)).

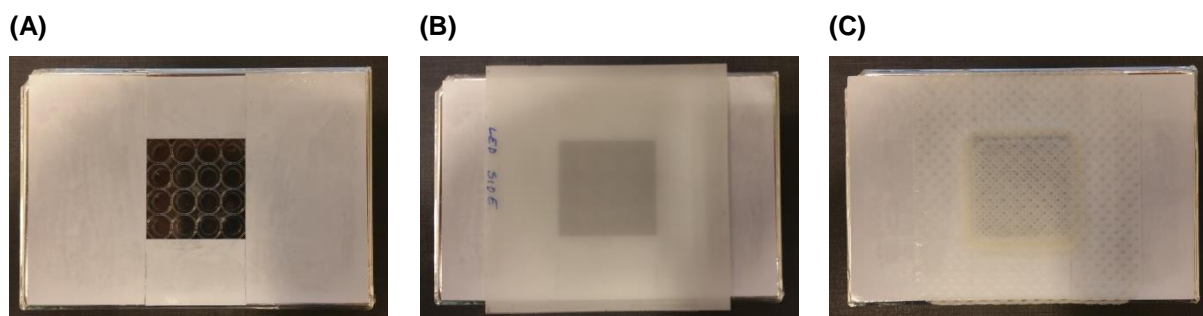


Figure 15: Experimental design for light distribution studies with the MEDILIGHT prototype – Plate set-up for (A) center irradiation covered with (B) the diffuser or (C) the wound dressing E2723.

2.2.3 Temperature measurements

2.2.3.1 BioLight LED Lamp

In order to exclude thermal effects influencing cellular processes apart from blue light treatment, the temperature of cell culture medium was recorded during continuous irradiations of 120 minutes. First, the wells of a black 96-well plate were filled with 100 μ L of medium followed by an incubation at 37°C and 5% CO₂ for 30 minutes before irradiation, imitating experimental conditions.

Meanwhile, a pre-run of 15 minutes without light irradiation was performed at room temperature (RT) in order to stabilize the measuring system. Afterwards, through openings constructed at the side of the cell culture plate, a thermocouple (type K) was placed into one of the inner wells and the irradiation was started (Figure 16). Connected to a Pico Technology USB TC-08 data logger (RS Components Ltd., Corby, Northamptonshire, UK), data were visualized and immediately analyzed.

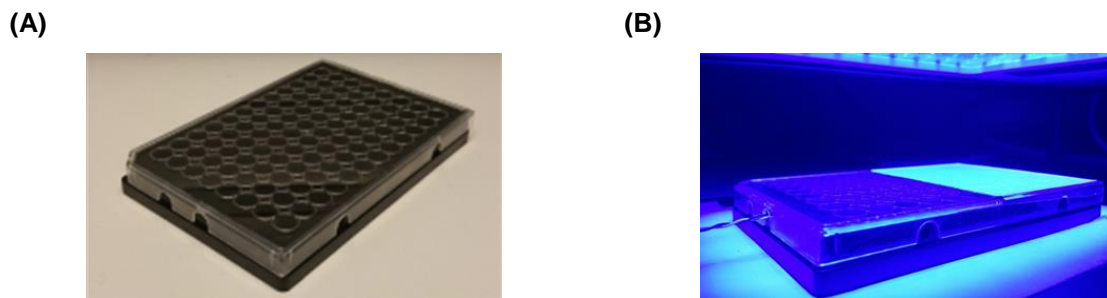


Figure 16: Experimental design for temperature measurements performed *in vitro* using the BioLight LED Lamp. (A) Black 96-well plate with openings at the side allowing the placement of thermocouples inside the plate for *in vitro* temperature measurements, (B) performed during blue light irradiation.

2.2.3.2 MEDILIGHT system

Owing to the risk of inducing cutaneous hyperalgesia due to significant temperature increases ($> 40^{\circ}\text{C}$), *in vitro* and *in vivo* temperature measurements were performed to guarantee patient safety. Besides recordings in cell culture plates as described in 2.2.3.1, temperature changes were followed on a skin-like polymer from URGO RID (Chenôve, France) as well as on porcine and human skin. In addition to integrated sensors monitoring the temperature on the LED array, external sensors were placed at different positions underneath the dressing E2723 to record direct changes on the polymer or skin. Due to different wound healing stages requiring either stimulated cell responses with $10 \text{ mW}/\text{cm}^2$ ⁹⁵ or antibacterial effects at $23 \text{ mW}/\text{cm}^2$ ⁹⁶, the irradiance was adjusted accordingly underneath the respective component stacks.

2.2.4 Cell metabolism and proliferation assays

With respect to the interests of MEDILIGHT, blue light effects on cell metabolism and proliferation were studied using various methods. Besides metabolic activity assays, changes in cell cycle distributions, DNA synthesis rates and cell counts were tested.

2.2.4.1 Metabolic activity – XTT reduction

Metabolic activity was assessed using the colorimetric Cell Viability Kit III (XTT) from PromoKine (PromoCell GmbH, Heidelberg, Germany). In presence of the activation reagent, N-methyl dibenzopyrazine methyl sulfate (PMS), mitochondrial enzymes of metabolic active and viable cells reduce the yellow tetrazolium salt XTT to a water-soluble, orange-colored formazan dye. Therefore, resulting absorbance intensities directly correlate with the activity of mitochondrial enzymes of viable and active cells metabolizing XTT. Following irradiation, a reaction mixture of XTT and PMS (1:200) was added to the medium (50% by volume) and incubated for 1 hour at 37°C and 5% CO₂. With a Spark® 10M microplate reader (Tecan Austria GmbH, Grödig, Austria) absorbance signals were quantified at 450 nm with a reference reading at 690 nm. Non-specific signals were identified by adding XTT/PMS only to cell culture medium.

2.2.4.2 Metabolic activity – ATP concentration

The CellTiter-Glo® Luminescent Cell Viability Kit (Promega Corporation, Madison, WI, USA) indicates metabolic active cells by ATP quantification. Light and oxyluciferin are formed upon the mono-oxygenation of luciferin, which is catalyzed by Ultra-Glo™ Recombinant Luciferase in the presence of Mg²⁺, ATP and molecular oxygen. As stated in the enclosed protocol, kit reagents were mixed and added to the cells after irradiation (100% by volume). Following cell lysis, induced by shaking for 2 minutes, the luminescent signal was allowed to stabilize for 10 minutes at RT. Then, the contents of each well were transferred to a white, opaque-walled 96-well plate. With an integration time of 500 ms, luminescence was recorded using the Spark® 10M microplate reader. Read-outs were supposed to be directly proportional to the ATP amount present in culture, representing the count of viable and thus metabolic active cells. Background signals were identified by including wells containing only medium.

2.2.4.3 Cell proliferation – Determination of cell cycle distribution

Since the previously described methods depend on metabolic changes and thus only represent an indirect measure of proliferation, cell cycle distributions were analyzed using the FITC BrdU Flow Kit provided by BD Pharmingen™ (Heidelberg, Germany).

5-Bromo-2'-deoxyuridine (BrdU) represents a synthetic thymidine analogue, which is incorporated into newly synthesized DNA of cells entering and progressing through the S phase of the cell cycle. Therefore, combining immunofluorescent staining of BrdU with a total DNA stain allowed the enumeration and characterization of cells with respect to their cell cycle position. Following seeding and a 24-hour incubation, cells were synchronized by serum starvation (0% FCS) for another day. Afterwards, cells were resupplied with full culture medium, treated with blue light and labeled with 1 mM BrdU for 24 hours at 37°C and 5% CO₂, which was repeated for consecutive irradiations. At 24 hours after the last treatment, cells were harvested and stained according to the manufacturer's protocol. First, with intermediate washing, NHDF cells were fixed and permeabilized in several steps performed on ice. Then, the cells were incubated with 300 µg/mL of DNase for 1 hour at 37°C exposing incorporated BrdU. With further washing steps in between, BrdU was stained with fluorescein isothiocyanate (FITC)-conjugated antibodies for 20 minutes at RT. Finally, the cells were labeled with the total DNA stain 7-Aminoactinomycin D (7-AAD) enabling two-color flow cytometry analyses using a BD FACSCanto™ II from BD Biosciences (Heidelberg, Germany). In total, 10,000 events were recorded for each sample and analyzed with the FlowJo software, version 2.5.1 (FlowJo LLC, Ashland, USA).

2.2.4.4 Cell proliferation – DNA synthesis

Similar to the FITC BrdU Flow Kit, the colorimetric Cell Proliferation ELISA from Roche Diagnostics (Mannheim, Germany) quantifies cell proliferation based on BrdU incorporation. At first, NHDF cells were synchronized by serum depletion (0% FCS) for 24 hours. Afterwards, cells were resupplied with full cell culture medium, treated with blue light and incubated with 10 µM BrdU for 24 hours at 37°C and 5% CO₂, which was repeated for consecutive irradiations. At 24 hours after the last blue light treatment, the labeling medium was aspirated and cells were fixed for 30 minutes, while the DNA was denatured. This enabled an increased accessibility for the anti-BrdU antibody, which was incubated for 90 minutes, while free, unbound antibodies were removed by three subsequent washing steps with 1x PBS. As the antibody was conjugated to peroxidase, tetramethyl-benzidine was added for 3 minutes. Then, the reaction was stopped with 1 M H₂SO₄. The Spark® 10M microplate reader was used to quantify immune complexes at 450 nm with a reference reading at 690 nm.

Thus, measured absorbance values correlated with the extent of BrdU incorporation into newly synthesized DNA, indicating changes in the number of actively replicating cells. For each test, two controls were included: (1) A blank without cells identifying unspecific binding of BrdU and the antibody to the plate and (2) a background control assessing unspecific binding of the antibody to cells in the absence of BrdU.

2.2.4.5 Cell proliferation – Nuclei/Cell counting

Besides experiments involving BrdU incorporation, cell counting was used to assess light-induced changes in cell proliferation. Instead of using the Luna™ automated cell counter yielding highly variable results, NHDF cells were labeled with a nucleic acid stain followed by immediate image acquisition of entire wells (Figure 17).

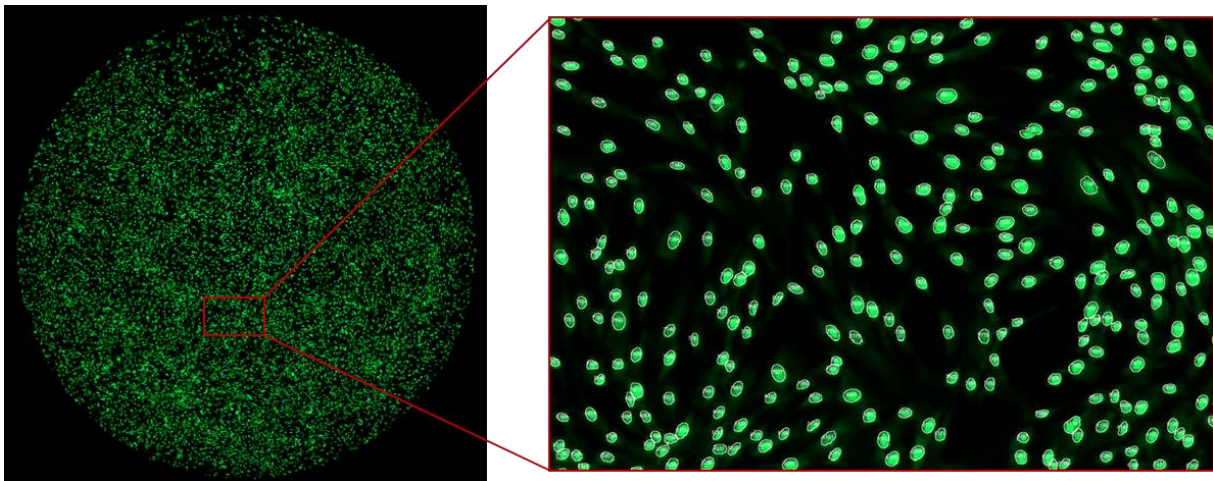


Figure 17: Stitched fluorescent image acquired and processed using the inverted microscope Axio Observer.Z1 (Carl Zeiss Microscopy GmbH, Göttingen, Germany) showing stained nuclei of NHDF cells, which were segmented and counted using Fiji, an image processing package of ImageJ.

Therefore, the green fluorescent, live cell-permeable CyQuant® Direct nucleic acid stain (Thermo Fisher Scientific, Eugene, OR, USA) was selected, which evaluates changes in cell proliferation and viability based on DNA content and membrane integrity. At 24 hours after blue light treatment, the nucleic acid stain was mixed with a background suppression dye (1:5) using full cell culture medium, added to the cells (100% by volume) and incubated for 60 minutes at 37°C and 5% CO₂. Using the inverted fluorescence microscope Axio Observer.Z1 (Carl Zeiss Microscopy GmbH, Göttingen, Germany), 6 wells per condition, treated and untreated, were imaged with the GFP filter set ($\lambda_{Ex} = 489 \text{ nm}$ / $\lambda_{Em} = 519 \text{ nm}$), accounting for 1,900 tiles per plate.

After stitching individual tiles with the ZEN 2 pro software, single-color fluorescence images were evaluated with a macro written in Fiji analyzing several parameters of single particles, respectively cell nuclei. Subsequent to contrast enhancement and background subtraction, images were converted into binary masks and holes were filled. Using a watershed algorithm, individual cell nuclei were segmented based on minimum and maximum threshold values (Figure 17). Besides total cell nuclei counts, the area (in pixels) and shape of single particles were analyzed. Finally, processed images and corresponding results were saved automatically (.jpeg and .txt format).

2.2.5 Functional assays

Since photosensitization processes activated by blue light are said to occur mainly in mitochondria, cell metabolism tests were substantiated with assays further studying mitochondrial function. Furthermore, cell viability was determined following different doses of blue light irradiation.

2.2.5.1 Mitochondrial function – Generation of hydrogen peroxide (H₂O₂)

The generation of H₂O₂ induced by blue light irradiation was assessed using the Amplex® UltraRed Reagent (AUR) from Molecular Probes™ (Life Technologies™ by Thermo Fisher Scientific, Carlsbad, CA, USA). It represents a fluorogenic substrate for horseradish peroxidase (HRP) reacting with H₂O₂ in a stoichiometric ratio of 1:1, which forms brightly fluorescent Amplex® UltroXRed. After light treatment, a solution of 100 µM AUR and 0.2 U/mL HRP was prepared with a 0.1 M potassium phosphate buffer (pH 6.0) and added to the cells (100% by volume) for 20 minutes in the dark at RT. Several controls were included identifying unspecific signals (Table 8).

Table 8: Amplex® UltraRed assay – Selected controls identifying non-specific fluorescence signals.

	Medium	Cells	Irradiation	AUR
Control 1	✓	X	X	X
Control 2	✓	X	✓	X
Control 3	✓	X	X	✓
Control 4	✓	X	✓	✓
Control 5	✓	✓	X	X
Control 6	✓	✓	✓	X

The Spark® 10M microplate reader was used to read-out fluorescence signals from the bottom at $\lambda_{Ex} = 490 \text{ nm}$ / $\lambda_{Em} = 581 \text{ nm}$.

2.2.5.2 Mitochondrial function – Mitochondrial membrane potential $\Delta\Psi_m$

Changes in the mitochondrial membrane potential ($\Delta\Psi_m$) were quantified using the cell membrane-permeable cationic dye tetramethylrhodamine ethyl ester perchlorate (TMRE). Upon its addition, TMRE accumulates in active mitochondria of living cells and indicates them by an orange fluorescent signal at $\lambda_{Ex} = 550 \text{ nm}$ / $\lambda_{Em} = 575 \text{ nm}$. Consequently, cells showing a decrease of $\Delta\Psi_m$ due to mitochondrial depolarization or inactivation are characterized by less TMRE accumulation. After light treatment, NHDF cells were incubated with a 200 nM TMRE labeling solution for 20 minutes at 37°C and 5% CO₂. Following three washing steps, cells were kept in 1x PBS for later analyses using the Spark® 10M microplate reader and the fluorescence microscope Axio Observer.Z1. Prior to TMRE labeling of cells, controls were treated with 50 μM of carbonyl cyanide 3-chlorophenylhydrazone (CCCP) for 15 minutes at 37°C and 5% CO₂. The ionophore blocks the formation of an electrochemical proton gradient and thus uncouples oxidative phosphorylation, which finally leads to $\Delta\Psi_m$ disruption.

2.2.5.3 Cell viability – Flow cytometry analysis

To assess whether blue light treatment induces cell death, the supernatant of treated and untreated cells was collected at 24 hours after irradiation. Remaining adherent cells were harvested by trypsinization and combined with the respective supernatants collected before. Viable (negative) and dead (positive) control samples were obtained according to the same procedure. Cytotoxicity was induced with 1 μM staurosporine (*Streptomyces staurosporeus* by Sigma Aldrich, St. Louis, MO, USA), which was incubated for 24 hours at 37°C and 5% CO₂ prior to cell harvesting. The samples were centrifuged (2,000 \times g, 3 minutes, RT) and supernatants were discarded. First, the negative control was washed with a Hank's Balanced Salt Solution including 2% FCS, 2 mM EDTA as well as 10 mM HEPES (Staining buffer (SB)). After a second centrifugation (2,000 \times g, 3 minutes, RT), NHDF cells were dissolved in 500 μL of SB in order to pre-adjust the flow cytometer BD FACSCanto™ II (Heidelberg, Germany) by defining appropriate voltage settings for the required fluorescence channels.

Table 9 shows that light-treated, untreated and dead cell populations were, according to the number of tests, dissolved using different SB volumes. Then, 200 μ L of each sample was added to one well of a 96-well plate with U-bottom, which was thereafter centrifuged (2,000 \times g, 3 minutes, RT). The supernatant was discarded, while the samples were washed with 200 μ L SB each and centrifuged again. Adding 100 μ L of Annexin Binding Buffer (ABB), samples were either single stained, double stained or left unstained in order to identify autofluorescence (Table 9). Annexin V (BioLegend, San Diego, CA, USA), which was conjugated to the fluorophore allophycocyanin (AV-APC), and Propidium Iodide (PI) (Invitrogen™, Life Technologies™ by Thermo Fisher Scientific, Carlsbad, CA, USA) were used to mark apoptotic and necrotic cells. With 3 μ L and 2 μ L respectively, both stains were added and incubated simultaneously for 15 minutes in the dark at RT. Finally, 100 μ L of ABB was added and cell viability was examined using the pre-adjusted BD FACSCanto™ II. In total, 20,000 events were recorded per sample and analyzed with the FlowJo software, version 2.5.1.

Table 9: Cell viability testing using flow cytometry – Summary of test conditions including the negative control, the positive control as well as untreated and light-treated samples. Besides the staining buffer volume, in which the cells were dissolved, the resulting sample number and type of stainings are indicated.

	Test condition	Buffer volume [μ L]	Sample	Staining
1	Negative control	500	1	Unstained
2	Positive control (Staurosporine-treated)	800	1	Unstained
			2	Single stained: AV-APC+
			3	Single stained: PI+
			4	Double stained: AV-APC+/PI+
3	Test samples (Blue Light)	400	1	Unstained
			2	Double stained: AV-APC+/PI+
4	Test samples (No Light)	400	1	Unstained
			2	Double stained: AV-APC+/PI+

2.2.6 Gene expression analysis

2.2.6.1 RNA isolation

At different time points after irradiation, NHDF cells were harvested and lysed with TRIzol (Ambion®, Life Technologies™ by Thermo Fisher Scientific, Carlsbad, CA, USA). Lysates of untreated and blue light-treated cells were pooled from 15 wells of a 96-well plate (Figure 12), with three replicates each, and shortly after stored at -80°C.

To isolate the RNA, 200 μ L of chloroform was added for 1 mL TRIzol and incubated for 3 minutes at RT. Then, the samples were vortexed and centrifuged (12,000 \times g, 15 minutes, 4°C) yielding three different phases: a lower organic phase with proteins and lipids, an interphase with DNA and an upper aqueous phase containing the desired RNA. The upper phase was transferred to a new tube and precipitated by the addition of 500 μ L isopropanol for 1 mL TRIzol. Afterwards, the tubes were inverted, incubated for 10 minutes at RT and centrifuged (12,000 \times g, 10 minutes, 4°C). The supernatant was discarded and two washing steps followed adding 1 mL of 80% ethanol each. After centrifugation (12,000 \times g, 5 minutes, 4°C), the RNA pellet was air-dried and dissolved in 20 μ L of RNase-free water.

2.2.6.2 RNA quantification and quality control

Extracted RNA was quantified by spectrophotometric analysis using the Spark® 10M microplate reader. In addition to the concentration, RNA purity was determined by measuring the absorbance ratio at A260/280 with acceptable values of 1.7 – 2.1. Moreover, the RNA integrity was assessed by capillary electrophoresis on an Agilent 2100 Bioanalyzer (Agilent Technologies, Santa Clara, CA, USA) revealing the RNA Integrity Number (RIN), with RIN > 7 indicating sufficient RNA quality. Following the standard labeling protocol from Affymetrix, a total amount of 100 ng RNA was used to prepare biotinylated antisense cDNA using the GeneChip® WT Plus Reagent Kit and the GeneChip® Hybridization, Wash and Stain Kit (both kits from Thermo Fisher Scientific, Waltham, MA, USA). Then, using a GeneChip Hybridization Oven 640, fragmented and labeled cDNA was hybridized into Affymetrix HuGene-2_0-st microarrays for 16 hours at 45°C. Finally, the arrays were dyed and washed on a GeneChip Fluidics Station 450 and scanned with a GeneChip Scanner 3000. All equipment was provided by Affymetrix UK Ltd. (High Wycombe, UK).

For bioinformatic evaluation of microarray data, a Custom CDF, version 21, including ENTREZ based gene definitions was used for annotation⁹⁷. Fluorescence intensity values were processed by quantile normalization and Robust Multi-Array Average (RMA) background correction. Using the commercial software package JMP10® Genomics, version 7.1 (SAS, SAS Institute Inc., Cary, NC, USA), one-way analysis of variance (ANOVA) was performed to identify differentially expressed genes.

Corresponding plots like 3D scatter plots, correlation heat maps and Venn diagrams were prepared with JMP10® Genomics, version 7.1. Gene Set Enrichment Analysis (GSEA) was performed to determine whether defined lists or sets of genes exhibited a statistically significant bias in their distribution within a ranked gene list using the software GSEA (see <http://www.broadinstitute.org/gsea/>)⁹⁸. With the public external database Kyoto Encyclopedia of Genes and Genomes (KEGG), which combines expression patterns of selected genes, differentially regulated pathways for various cell functions were obtained. The latter are grouped in seven main categories, which are further classified into subcategories (<https://www.genome.jp/kegg/pathway.html>). Whereas pathway analysis was considered significant at a nominal p-value of < 0.05, statistical significance for differentially expressed genes was specified at a false discovery rate (FDR) of < 0.05 corresponding to the adjusted p-value (q-value).

2.2.7 Statistical analysis

Depending on the type and size of data sets, numerical data were either represented as points showing means \pm standard deviation (SD) or box-and-whisker plots. For the latter, the lower quartile (1st quartile) and upper quartile (3rd quartile) were depicted with their difference specified as the interquartile range (IQR). The whiskers were set at the 3rd quartile +1.5 (IQR) for the maximum and at the 1st quartile -1.5 (IQR) for the minimum. In addition, the median was represented as a white band in the middle of the boxes. Fold changes were obtained by normalizing the data to time-matched, non-irradiated controls. Statistical analyses were performed using JMP® Genomics, version 7.1. After confirming a normal data distribution (Shapiro-Wilk normality test), one-way ANOVA and a Student's t-test for pairwise comparisons were applied. If the null hypothesis H_0 assuming a normal data distribution was rejected, nonparametric statistics were employed using the Wilcoxon test for pairwise comparisons. For all statistical tests, differences were considered statistically significant at a false positive rate of $\alpha = 0.05$. Unless otherwise specified, the number of repetitions and replicates performed for each test method is indicated as follows: N (# repetitions, # replicates).

3 RESULTS

3.1 BioLight LED Lamp

3.1.1 Temperature measurements

In order to exclude biological effects induced by high temperatures during irradiation, thermal changes of the cell culture medium were monitored during continuous blue light treatment. After stabilizing the measuring system with a pre-run of 15 minutes at RT, a thermocouple (type K) was placed into one of the inner wells of a pre-warmed black 96-well plate, which was filled with 100 μ L of medium. At the same time, blue light irradiation was started for 120 minutes. Initially, a fast temperature rise was observed since the 96-well plate was directly taken from the incubator. However, in the following time course, the temperature remained constant in a range between 32°C to 35°C (Figure 18). As NHDF cells were cultivated in a humidified atmosphere at 37°C, light-generated heat stress could be excluded. Therefore, biological effects shown below were caused by blue light treatment instead of thermal (de-)activation.

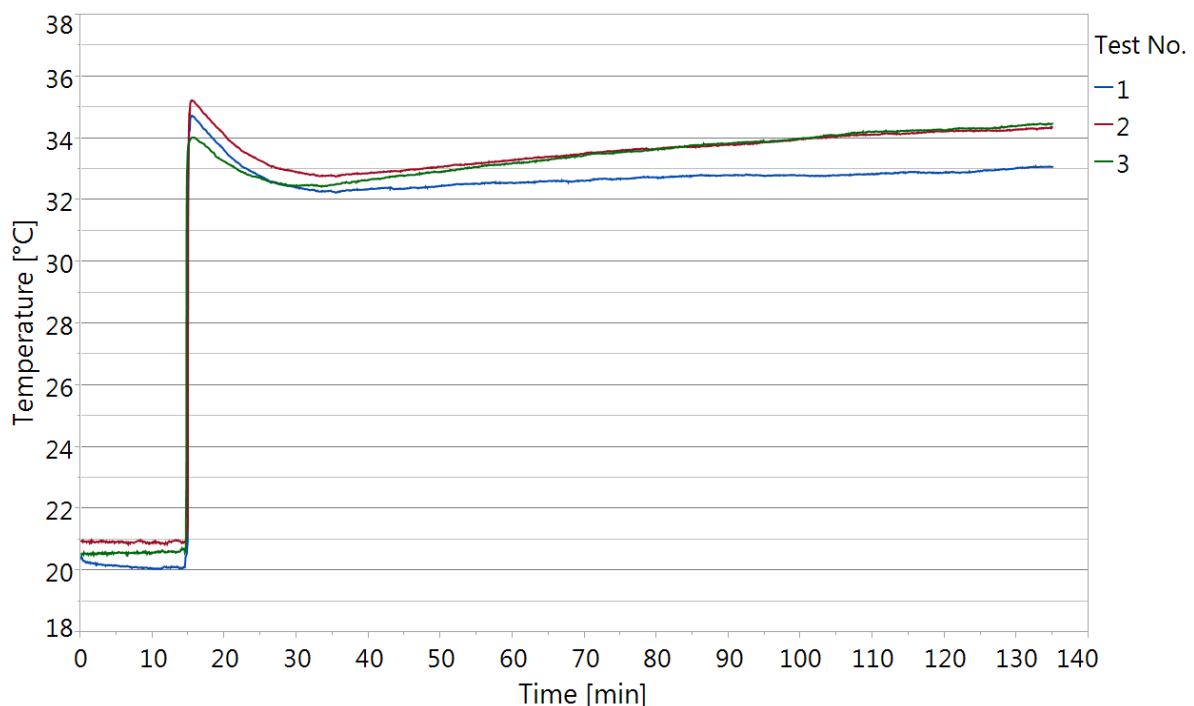


Figure 18: Temperature measurements performed during 120 minutes of continuous blue light irradiation using the BioLight LED Lamp from Philips Research (Eindhoven, Netherlands). First, the measurement was started with a pre-run of 15 minutes without irradiation at RT in order to stabilize the system. Afterwards, a thermocouple (type K) was placed into one of the inner wells of a pre-warmed black 96-well plate, which was filled with 100 μ L of cell culture medium, and the irradiation was started for 120 minutes. Experiments were performed in three independent test runs (N = 3 repetitions).

3.1.2 Cell metabolism assays

At first, changes in the metabolism of NHDF cells following blue light irradiation were determined based on the activity of mitochondrial enzymes and the quantification of ATP present in cell culture.

3.1.2.1 Assessment of XTT linearity revealed an optimal incubation time of 1 hour

Since the color change, XTT undergoes upon reduction by viable cells, and thus the resulting absorbance read-out increases over time, the optimal incubation time had to be determined in order to verify signal linearity. For this purpose, a range of different NHDF cell numbers including 1,500; 1,750; 2,000; 2,500; 4,000; 5,000; 6,000; 7,500; 7,750 and 8,000 cells/well was seeded into black 96-well plates. At 48 hours after seeding, imitating an experiment duration of three days, activated XTT was added and incubated for 30 minutes up to 2.5 hours (Figure 19).

Figure 19 shows a linear increase in absorbance values, which directly correlate to an increasing number of viable and metabolic active cells as well as to a longer incubation time of activated XTT. With $R^2 = 0.98$, which indicates the goodness-of-fit of linear regression, excellent linearity was obtained for incubation times ranging from 1 hour to 2 hours. In contrast, a shorter (30 minutes) or longer (2.5 hours) incubation period showed lower R^2 values. Especially for an incubation time of 2.5 hours, absorbance values for higher plated cell numbers, particularly from 4,000 cells/well on, reached a plateau, recommending a shorter incubation time of XTT (Figure 19). Nevertheless, the signal seemed to be proportional over a wide range of different cell numbers and incubation times, demonstrating that the XTT assay provided a reliable quantification of viable and metabolic active cells in unknown samples.

Although the Spark® 10M microplate reader from Tecan Austria GmbH (Grödig, Austria) is said to provide signal linearity for optical densities from 0 – 3 OD, an incubation time of activated XTT for 1 hour was chosen, showing about 0.7 – 0.8 AU for a seeded cell number of 5,000 cells/well (Figure 19). While meeting the Lambert-Beer law, this cell number yielded about 80% confluence on the third culture day in 96-well plates, excluding any impact of contact inhibition on cellular activity.

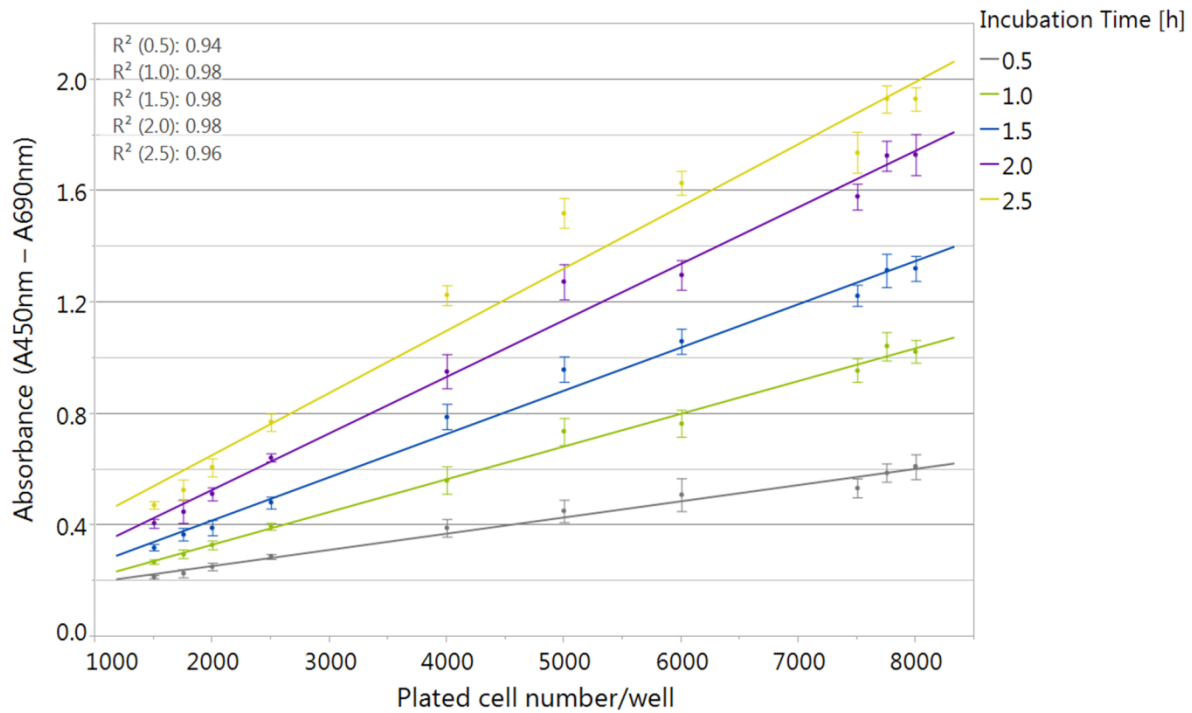


Figure 19: XTT results for varying NHDF cell concentrations seeded into black 96-well plates (1,500; 1,750; 2,000; 2,500; 4,000; 5,000; 6,000; 7,500; 7,750 and 8,000 cells/well) and different XTT incubation times of 30 minutes, 1 hour, 1.5 hour, 2 hours and 2.5 hours (N = 1 repetition, 3 replicates). Linear relationships between increasing absorbance values, cell numbers and XTT incubation times were verified by R^2 .

3.1.2.2 Different blue light irradiation times showed a biphasic dose-response curve of cellular metabolism

First, NHDF cells were exposed to different irradiation times or respectively doses of blue light (Table 7), while the XTT assay was constantly performed at 24 hours after continuous irradiation. For lower light doses ($< 9.0 \text{ J/cm}^2$), the mitochondrial activity was slightly increased with a maximum effect of 7.10% ($p < 0.0001$) after blue light treatment with 5.4 J/cm^2 . However, exposing the cells to higher blue light doses and respectively longer irradiation times, an inflection point to inhibitory effects was found after 10.8 J/cm^2 of blue light, corresponding to 15 minutes of irradiation. With an attenuation by 25.09% ($p < 0.0001$) in comparison to the non-irradiated control, the metabolic activity of NHDF cells was constantly decreasing up to a mid irradiation dose of 21.6 J/cm^2 . For subsequent, even higher, doses ($> 21.6 \text{ J/cm}^2$), the inhibition of cellular activity was further enhanced by 6.04% ($p < 0.0001$) following blue light irradiation using 86.4 J/cm^2 (Figure 20). Therefore, blue light-triggered changes in cell metabolism were characterized by a biphasic dose-response curve showing an accelerated metabolic activity after lower blue light doses ($< 10.8 \text{ J/cm}^2$), whereas cell activity was slowed down using higher irradiation doses ($> 10.8 \text{ J/cm}^2$).

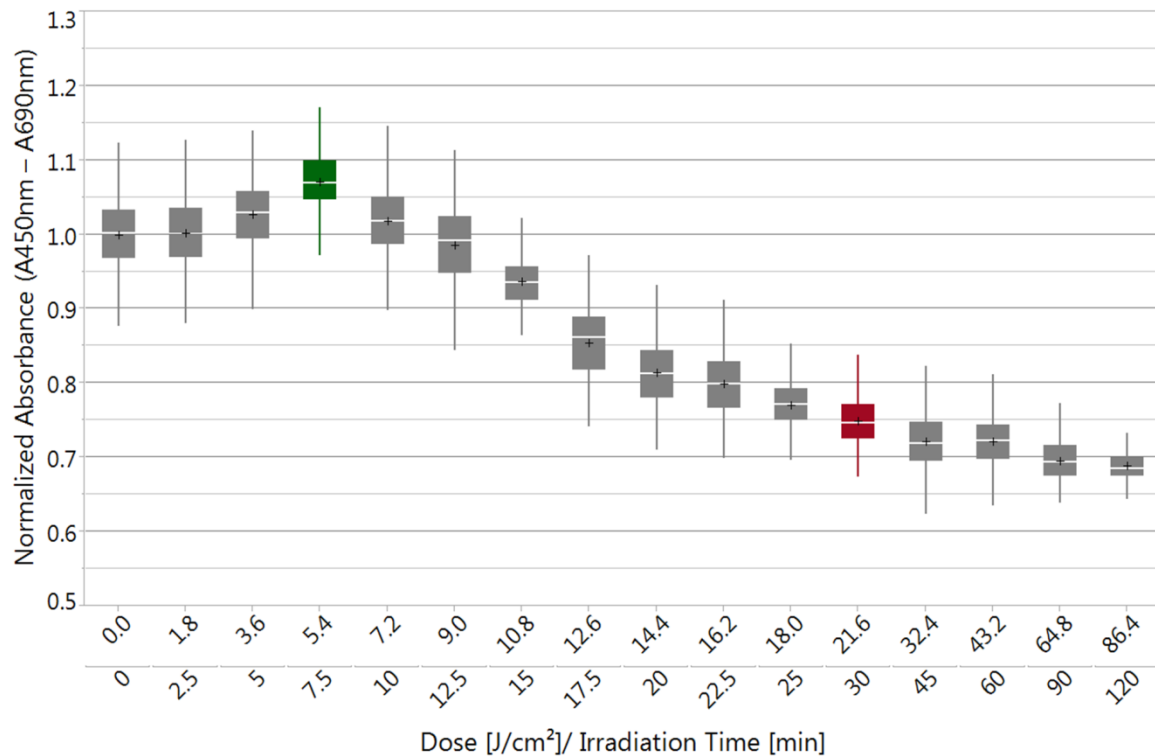


Figure 20: Changes in the metabolic activity of NHDF cells following different blue light doses with a constant time point of XTT testing at 24 hours after irradiation. Single blue light treatments were performed in continuous mode. Fold changes were evaluated versus time-matched, non-irradiated controls. Data are presented as box plots with means displayed as + (N = 3 repetitions, 3 replicates). Corresponding statistics are summarized in Table 17 (Appendix).

To study both, stimulatory and inhibitory light effects, blue light doses of 5.4 J/cm² and 21.6 J/cm² were chosen for subsequent analyses investigating cellular processes following either single or multiple light treatments.

3.1.2.3 Changes in metabolic activity after single blue light treatments with 5.4 J/cm² and 21.6 J/cm² were time-dependent

Furthermore, changes in the mitochondrial activity of NHDF cells were assessed at different time points after continuous exposure to either 5.4 J/cm² or 21.6 J/cm² of blue light (Figure 21). In direct comparison to the non-irradiated control, light-treated cells showed an increased metabolic activity by 6.09% ($p < 0.0001$) at 1 hour following 5.4 J/cm² of blue light, which slowly attenuated within the next 11 hours. During this time period, a significant difference of 2.39% ($p < 0.0001$) was observed at 3 hours after irradiation, while no significant effects were found after 6 hours with 0.24% ($p = 0.5560$) and after 12 hours with 0.17% ($p = 0.2366$).

Nonetheless, a second increase in cellular metabolism of NHDF cells was present at 24 hours (6.86%, $p < 0.0001$), which corresponds to the time-matched result depicted in Figure 20. In the further time course, mitochondrial activity decreased down to 2.42% ($p < 0.0001$) at 48 hours after irradiation reaching a non-significant difference of 0.26% ($p = 0.4001$) after 72 hours (Figure 21).

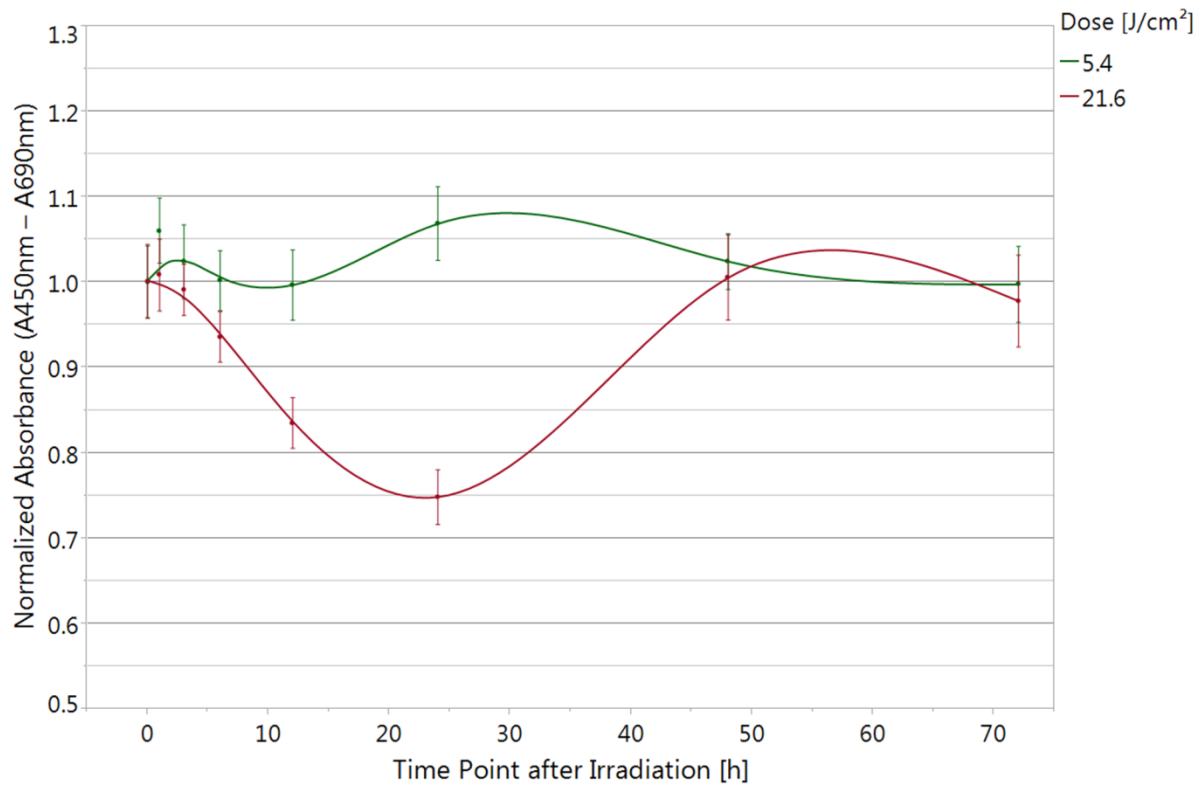


Figure 21: Changes in the metabolic activity of NHDF cells at different time points following a single blue light exposure to either 5.4 J/cm² or 21.6 J/cm². Blue light treatments were performed in continuous mode. Fold changes were evaluated versus time-matched, non-irradiated controls. Data are presented as mean \pm SD (N = 3 repetitions, 3 replicates). Corresponding statistics are summarized in Table 18 (Appendix).

When using a higher irradiation dose of 21.6 J/cm², changes in cellular metabolism showed a delayed onset, which started to be significantly different after 6 hours with a decrease by 6.53% ($p < 0.0001$). Subsequently, a continuous decline in cell activity was noted with 16.62% ($p < 0.0001$) less active cells after 12 hours. With a reduction by 25.31% ($p < 0.0001$), the inhibition of metabolic activity was even more enhanced after 24 hours. This finding was in line with the outcome obtained for the first set of experiments (25.09% ($p < 0.0001$)), in which cell metabolism was tested at 24 hours following different doses of continuous blue light treatment (Figure 20). Nevertheless, in the course of progressing metabolic inhibition, NHDF cells were able to recover already at 48 hours after light exposure, which was similar to the trend seen for the lower blue light dose of 5.4 J/cm² (Figure 21).

3.1.2.4 Consecutive single irradiations of 21.6 J/cm² enhanced metabolic inhibition, while multiple treatments with 5.4 J/cm² did not increase cell stimulation

Subsequent to studies testing blue light effects on cell metabolism at various time points after single irradiations with different doses, NHDF cells were treated multiple times. To test whether the differential effects of 5.4 J/cm² and 21.6 J/cm² could be maintained or even enhanced, consecutive blue light irradiations were performed every 24 hours, applying both blue light doses in separate experiments. The XTT test was performed at 24 hours after the last blue light treatment. For this purpose, the seeded cell number was adjusted preventing the occurrence of cell confluency and therefore contact inhibition since metabolic activity greatly varies with cell density. At the same time, the increasing cell density limited the experimental duration to five days allowing three days of blue light irradiation with 24-hour time intervals.

Treating NHDF cells twice using a single irradiation dose of 5.4 J/cm² each (2x (24), 10.8 J/cm²) could not enhance the stimulatory effect on cellular metabolism found at 24 hours after a single light treatment (0.30%, $p=0.5359$). However, the acceleration of mitochondrial activity following a single irradiation was reproducible in comparison to the outcomes depicted in Figure 20 and Figure 21. Compared to one irradiation (1x (24)), three consecutive light treatments (3x (24), 16.2 J/cm²) slightly decreased the metabolic activity of NHDF cells by 1.89% ($p<0.0001$) (Figure 22).

In contrast, a second irradiation with the higher blue light dose of 21.6 J/cm² (2x (24), 43.2 J/cm²) revealed an even stronger decrease in mitochondrial activity (Figure 22). Numerically speaking, the difference between a two-fold irradiation returning a decrease by 35.69% compared to a reduction of metabolically active cells by 25.54% after one treatment resembled to approximately 10% ($p<0.0001$). Again, the latter outcome confirmed the effects previously found (Figure 20, Figure 21). Moreover, it was possible to maintain the inhibitory effect, which was lost at 48 hours following a single blue light treatment (Figure 21). However, the difference between two (2x (24), 43.2 J/cm²) and three consecutive blue light treatments (3x (24), 64.8 J/cm²) was not significant ($p=0.9727$) (Figure 22).

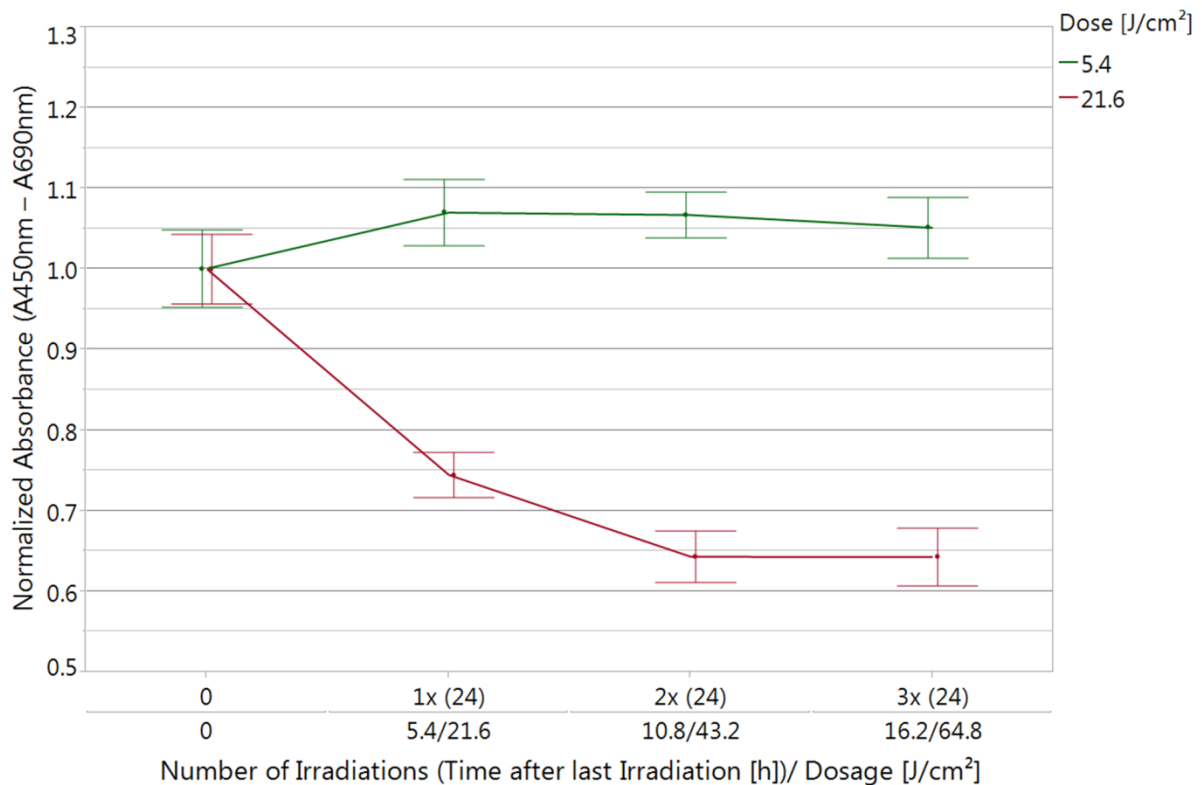


Figure 22: Changes in the metabolic activity of NHDF cells following single (1x (24)) and consecutive (2x (24), 3x (24)) treatments with either 5.4 J/cm² or 21.6 J/cm² of blue light. Consecutive irradiations were performed every 24 hours in continuous mode. XTT tests were carried out at 24 hours after the last light treatment. Fold changes were evaluated versus time-matched, non-irradiated controls. Data are presented as mean \pm SD (N = 3 repetitions, 3 replicates). Corresponding statistics are summarized in Table 19 (Appendix).

3.1.2.5 Multiple daily treatments with 5.4 J/cm² of blue light enhanced the stimulatory effect on cell metabolism

Since the metabolic stimulation of NHDF cells could not be enhanced with single irradiations of 5.4 J/cm² over consecutive days, two and three daily exposures were performed with 3-hour time intervals. The XTT test was carried out at 24 hours after the last irradiation. Compared to a single irradiation per day (1x), two irradiations (2x) revealed a continuous increase in cell metabolism. While the respective differences on the first (3.76%, $p < 0.0001$) and second day of irradiation (2.13%, $p < 0.0001$) were hardly distinct, a significant difference of 9.71% ($p < 0.0001$) was reached after the third treatment day (differences between single groups were evaluated with the non-parametric Wilcoxon method). Thus, compared to the control, two irradiations per day showed the highest effect of 14.88% ($p < 0.0001$) following three consecutive days of blue light treatment. In contrast, three irradiations per day (3x) reduced the metabolic activity by 17.10% ($p < 0.0001$) already after the first treatment day.

However, mitochondrial activity seemed to recover slowly decreasing the difference to the first day of irradiation by 6.16% ($p < 0.0001$) on day 2 and by additional 2.86% ($p < 0.0001$) on day 3 (Figure 23).

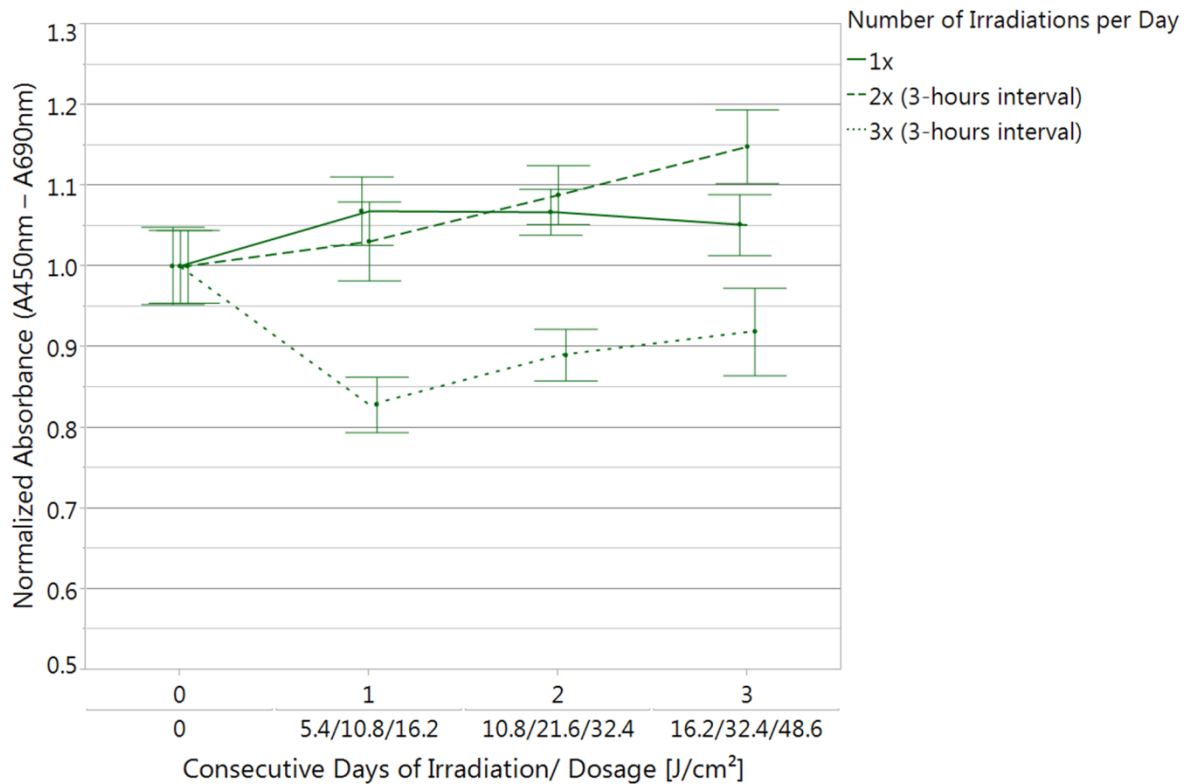


Figure 23: Changes in the metabolic activity of NHDF cells following single (1x) and multiple blue light treatments (2x, 3x) of 5.4 J/cm² per day with a time interval of 3 hours in between. Irradiations were performed in continuous mode. XTT tests were carried out at 24 hours after the last light treatment. Fold changes were evaluated versus time-matched, non-irradiated controls. Data are presented as mean \pm SD (N = 3 repetitions, 3 replicates). Corresponding statistics are summarized in Table 20 (Appendix).

3.1.2.6 Energy metabolism increased using an irradiation dose of 5.4 J/cm², while 21.6 J/cm² of blue light decreased the ATP concentration

The amount of viable and metabolic active cells was further determined based on cellular ATP quantification. As changes in ATP levels represent a fast response, the assay was performed at different time points following single irradiations with either 5.4 J/cm² or 21.6 J/cm² of blue light. As shown in Figure 24, at 30 minutes after irradiation, the energy metabolism of NHDF cells slightly decreased with significant differences of 1.58% ($p = 0.0169$) for 5.4 J/cm² and 3.29% ($p < 0.0001$) for 21.6 J/cm² of blue light. However, in comparison to the untreated controls, the ATP levels found at 1 hour following light exposure were contrasting for both irradiation doses.

While it increased to 3.20% ($p < 0.0001$) after 5.4 J/cm^2 of blue light, the higher dose led to a reduction by additional 1.19% ($p = 0.0055$) (Figure 24). Then, both curves converged each other reaching a difference of 2.88% ($p < 0.0001$) at 6 hours after irradiation. Subsequently, the effect for 21.6 J/cm^2 of blue light remained constant within the next 18 hours (0.25%, $p = 0.6599$), while another peak of 4.69% ($p < 0.0001$) was present at 24 hours following irradiation with 5.4 J/cm^2 , which indicated a higher ATP concentration compared to the control (Figure 24).

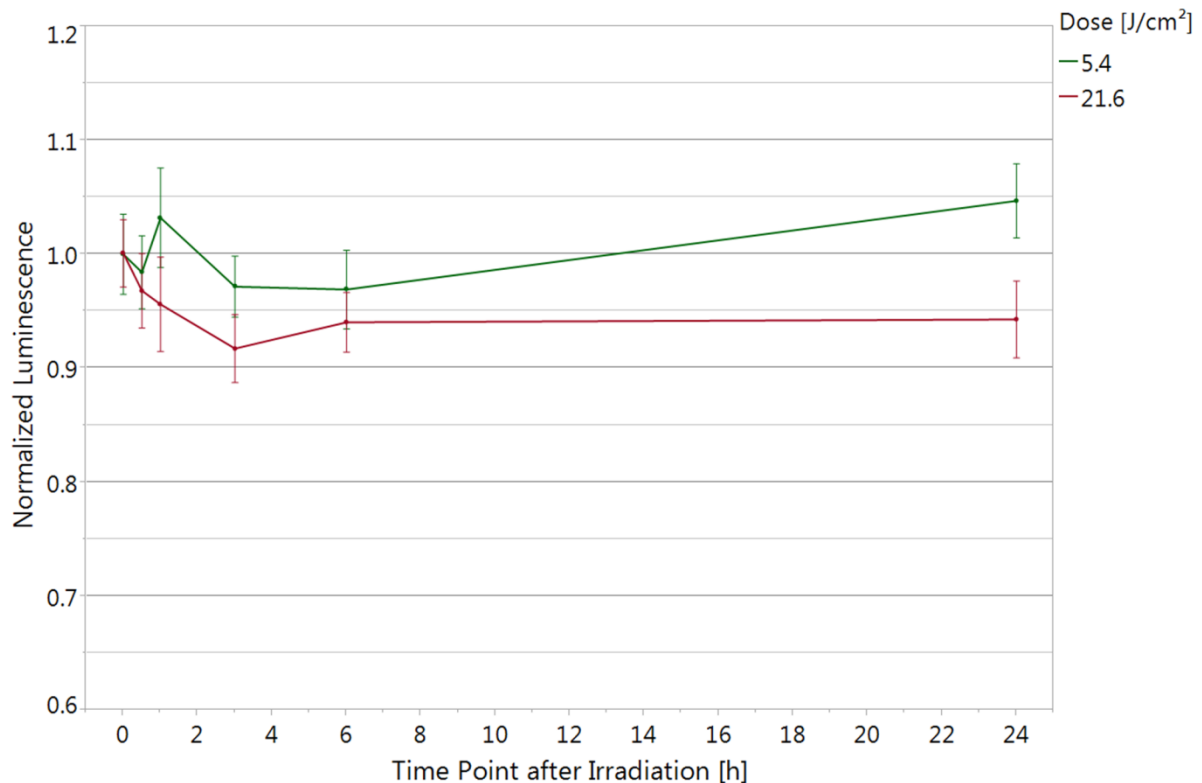


Figure 24: Changes in the ATP concentration of NHDF cells present at different time points following a single blue light exposure to either 5.4 J/cm^2 or 21.6 J/cm^2 . Blue light treatments were performed in continuous mode. Fold changes were evaluated versus time-matched, non-irradiated controls. Data are presented as mean \pm SD (N = 3 repetitions, 3 replicates). Corresponding statistics are summarized in Table 21 (Appendix).

3.1.3 Cell proliferation assays

Since the colorimetric XTT Cell Viability Kit and the luminescent ATP Cell Viability Assay evaluate changes in cell metabolism, they only represent an indirect measure of cell proliferation. Consequently, proliferation rates may not be reflected accurately. Therefore, various strategies were used to quantify proliferative activity of NHDF cells following blue light irradiation with different doses, involving analyses of cell cycle distribution, DNA synthesis and cell count.

3.1.3.1 Consecutive irradiations using a blue light dose of 5.4 J/cm^2 each led to an accumulation of S-phase cells, while multiple treatments with 21.6 J/cm^2 of blue light increased the amount of G0/G1-phase and G2/M-phase cells

The first experimental approach chosen was based on the determination of cell cycle distribution following single and consecutive irradiations with flow cytometry analysis. The proportion of NHDF cells in each cell cycle phase was quantified by staining their total DNA content with 7-AAD and combining it with an immunofluorescent staining of BrdU, detecting active DNA synthesis. Thus, cell populations staying in different cell cycle phases could be clearly differentiated depending on their staining intensities. Figure 25 shows representative density plots with the populations of interest being marked in terms of their cell cycle position – Region 1: Sub-G0/G1 phase, Region 2: G0/G1 phase, Region 3: early and late S phase as well as Region 4: G2/M phase.

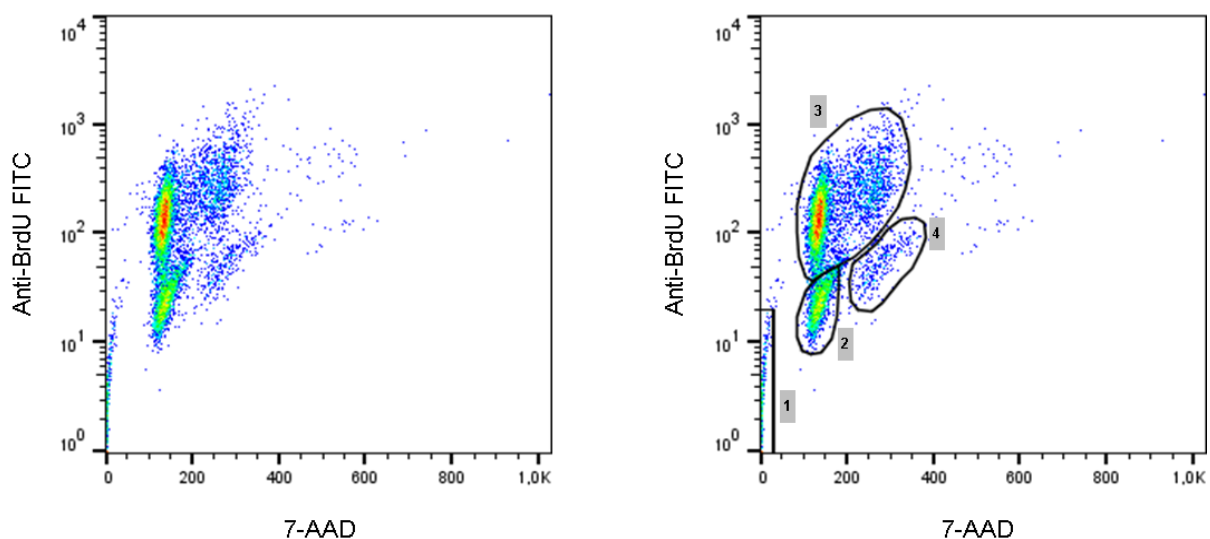


Figure 25: Representative pseudocolor density plots of NHDF cells stained by the total DNA dye 7-AAD and an anti-BrdU antibody, conjugated to FITC. In each plot 8,000 events are depicted.

Cell populations showing 7-AAD fluorescence intensities in the range of $\sim 100 - 150$ exhibited low DNA contents, with R2 representing cells in the G0/G1 phase, while cells in R3 could be assigned to the early S phase, since they were positive for BrdU. Equally, cells with higher DNA contents either stayed in the late S phase (R3, BrdU+) or the G2/M phase (R4, BrdU-). R1, specified at 7-AAD fluorescence intensities < 50 , identified apoptotic, fragmented cells characterized by degraded DNA (Figure 25). After synchronization, cells were resupplied with full medium and treated with single or consecutive irradiations of 5.4 J/cm^2 and 21.6 J/cm^2 , followed by BrdU addition.

The staining protocol was started at 24 hours after the last light treatment. For both doses, time-matched controls showed a similar cell cycle distribution with ~ 4.67% in Sub-G0/G1, ~ 25.90% in G0/G1, ~ 66.55% in S and ~ 2.52% in G2/M (Figure 26).

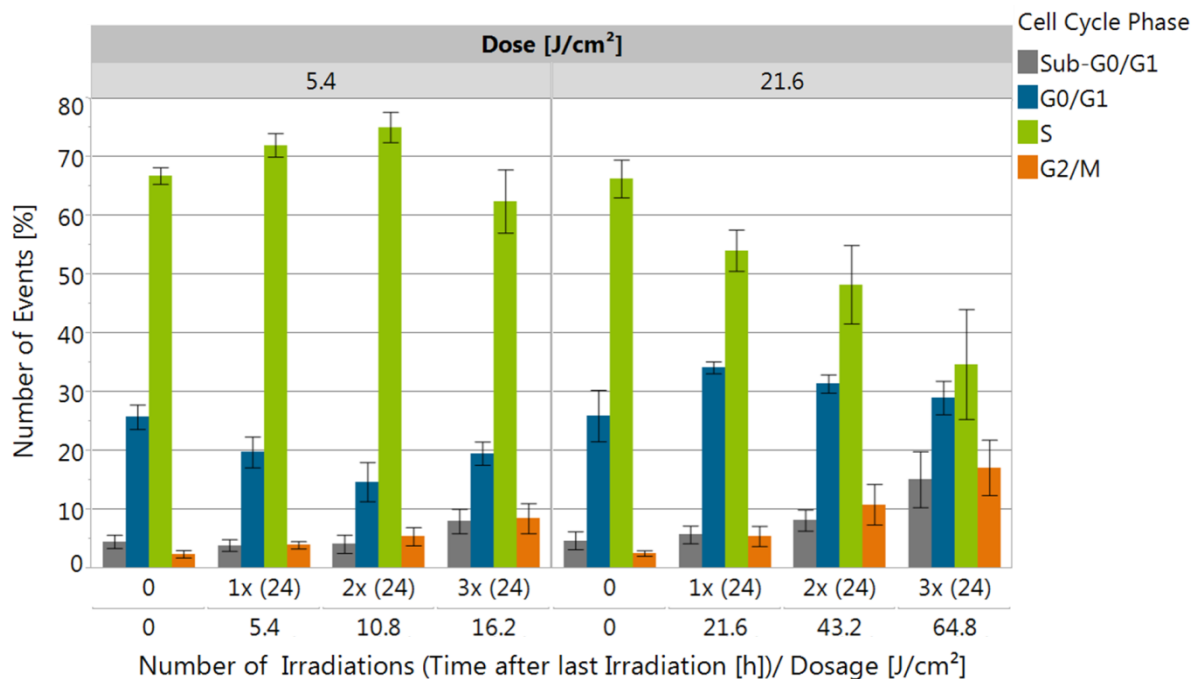


Figure 26: Changes in the cell cycle distribution of NHDF cells following single (1x (24)) and consecutive (2x (24), 3x (24)) treatments with either 5.4 J/cm² or 21.6 J/cm² of blue light. Consecutive irradiations were performed every 24 hours in continuous mode. Flow cytometry analyses were carried out at 24 hours after the last light treatment and subsequent addition of BrdU. Bars display mean values \pm SD (N = 3 repetitions, 3 replicates). Corresponding statistics for each cell cycle phase are summarized in Table 22 (Appendix).

A single treatment with 5.4 J/cm² of blue light elevated the number of S-phase cells by 5.20% ($p=0.0017$) accompanied by a decrease of G0/G1-phase cells by 6.00% ($p<0.0001$). This effect was slightly enhanced with a second irradiation on the next day, with 75.10% of the entire cell population showing an active DNA replication, while 14.70% of NHDF cells stayed in G0/G1. However, three exposures reset the cell cycle distribution close to control values along with an increase of the Sub-G0/G1 phase to 8.02% and the G2/M proportion to 8.51%. In contrast, consecutive blue light irradiations with 21.6 J/cm² each led to a continuous decrease of NHDF cells present in the S phase from 66.30% after a single light exposure down to 34.70% ($p<0.0001$) following three irradiations. The reduction in S-phase cells after one irradiation was accompanied by an increase of the G0/G1 phase by 8.20% ($p<0.0001$), which was not enhanced with additional light treatments. In contrast, two (2x (24), 43.2 J/cm²) and three (3x (24), 64.8 J/cm²) irradiations showed a higher frequency of cells staying in Sub-G0/G1 and G2/M (Figure 26).

3.1.3.2 Two consecutive blue light irradiations using 5.4 J/cm² each stimulated DNA replication, whereas proliferation was blocked with 21.6 J/cm² of blue light

Besides flow cytometry analyses, a colorimetric ELISA based on BrdU incorporation was performed in order to confirm changes in the number of actively replicating cells following blue light treatment. After synchronization by serum starvation, NHDF cells were resupplied with full cell culture medium and treated with single or consecutive irradiations of 5.4 J/cm² and 21.6 J/cm², while multiple treatments were performed every 24 hours. The ELISA was carried out at 24 hours after the last irradiation and subsequent addition of BrdU. Compared to the untreated control, DNA synthesis increased by 3.34% ($p=0.0007$) following one irradiation with 5.4 J/cm² of blue light (1x (24)). This effect was enhanced to 5.40% ($p<0.0001$) with two consecutive light treatments accounting for 10.8 J/cm² (2x (24)), whereas a third irradiation, yielding a dosage of 16.2 J/cm² (3x (24)), led to a reduction by 3.36% ($p=0.0073$) (Figure 27).

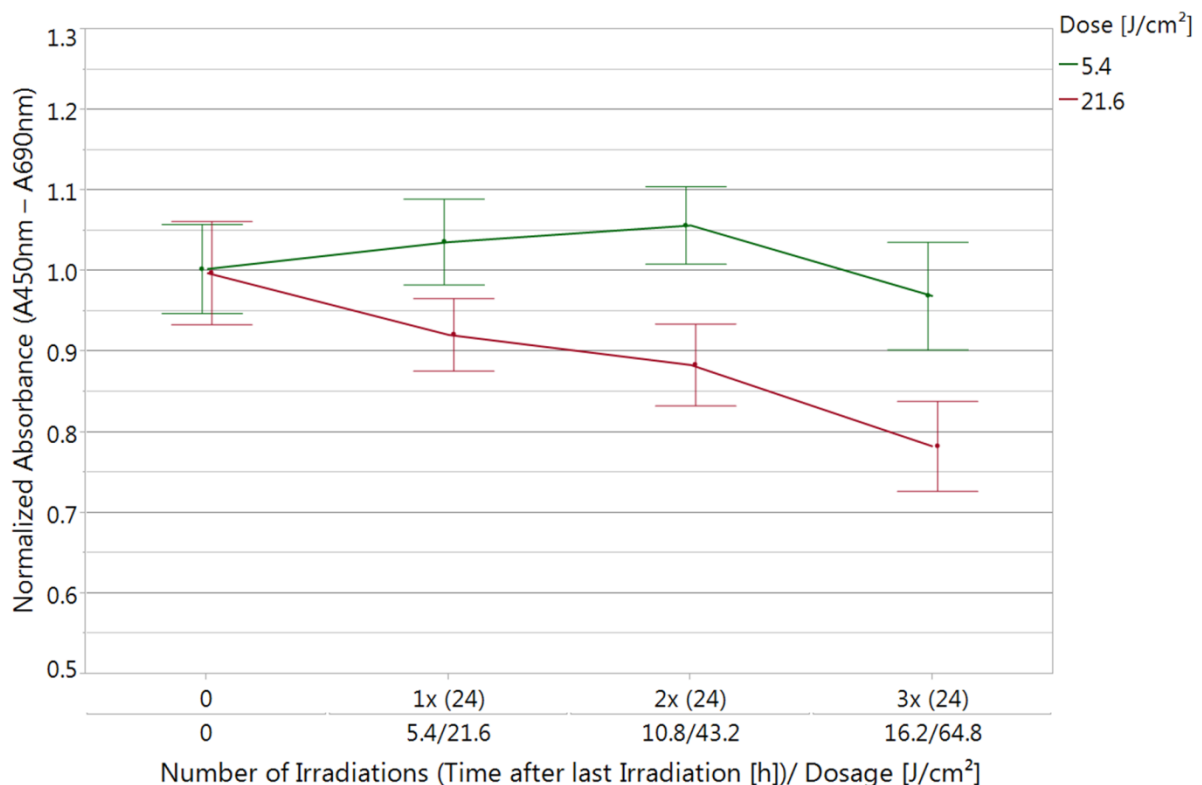


Figure 27: Changes in the DNA synthesis of NHDF cells following single (1x (24)) and consecutive (2x (24), 3x (24)) treatments with either 5.4 J/cm² or 21.6 J/cm² of blue light. Consecutive irradiations were performed every 24 hours in continuous mode. BrdU-ELISAs were carried out at 24 hours after the last light treatment and subsequent addition of BrdU. Fold changes were evaluated versus time-matched, non-irradiated controls. Data are presented as mean \pm SD (N = 3 repetitions, 3 replicates). Corresponding statistics are summarized in Table 23 (Appendix).

When exposing NHDF cells to the higher blue light dose of 21.6 J/cm², active DNA synthesis was reduced down to 92.32% (p<0.0001) following a single light treatment (1x (24)). After two treatments (2x (24)), accounting for a total dosage of 43.2 J/cm², it was further blocked by another 3.73% (p=0.0197). Moreover, three irradiations (3x (24), 64.8 J/cm²) decreased BrdU incorporation by actively replicating cells to 78.49% (p<0.0001) indicating an enhanced inhibition of cell proliferation (Figure 27).

3.1.3.3 Blue light treatment with either 5.4 J/cm² or 21.6 J/cm² differentially modulated nuclei counts, respectively cell counts, and nuclei sizes

In addition to experiments involving BrdU incorporation to evaluate DNA synthesis, stained nuclei of living cells were counted after single and consecutive treatments with either 5.4 J/cm² or 21.6 J/cm² of blue light. At 24 hours after the last irradiation, cell nuclei were stained with the fluorescent dye CyQuant® in order to assess changes in total cell numbers and therefore proliferation. Analyzing the acquired fluorescence images with a macro written in Fiji, nuclei counts were evaluated for entire wells representing a measure for the total cell count. In addition, the area of single nuclei and different shape descriptors were determined.

Treating NHDF cells either once or twice with 5.4 J/cm² of blue light led to increased cell counts compared to the control. Numerically speaking, 1.99% (p<0.0001) more cells were found following a single irradiation (1x (24)), which was enhanced up to 8.39% (p<0.0001) following two treatments performed on consecutive days (2x (24), 10.8 J/cm²). However, three light treatments (3x (24), 16.2 J/cm²) revealed a reduced cell count by 5.94% (p<0.0001) compared to the non-irradiated control (Figure 28). In contrast, with a single blue light irradiation using 21.6 J/cm² (1x (24)), the cell count decreased by 6.59% (p<0.0001) intensifying to 10.89% (p<0.0001) less cells after two light treatments (2x (24), 43.2 J/cm²). A third irradiation (3x (24)), yielding a total dosage of 64.8 J/cm², showed a reduced cell count by 32.51% (p<0.0001) revealing a stronger inhibition of cell proliferation with an increasing number of light treatments using 21.6 J/cm² (Figure 28).

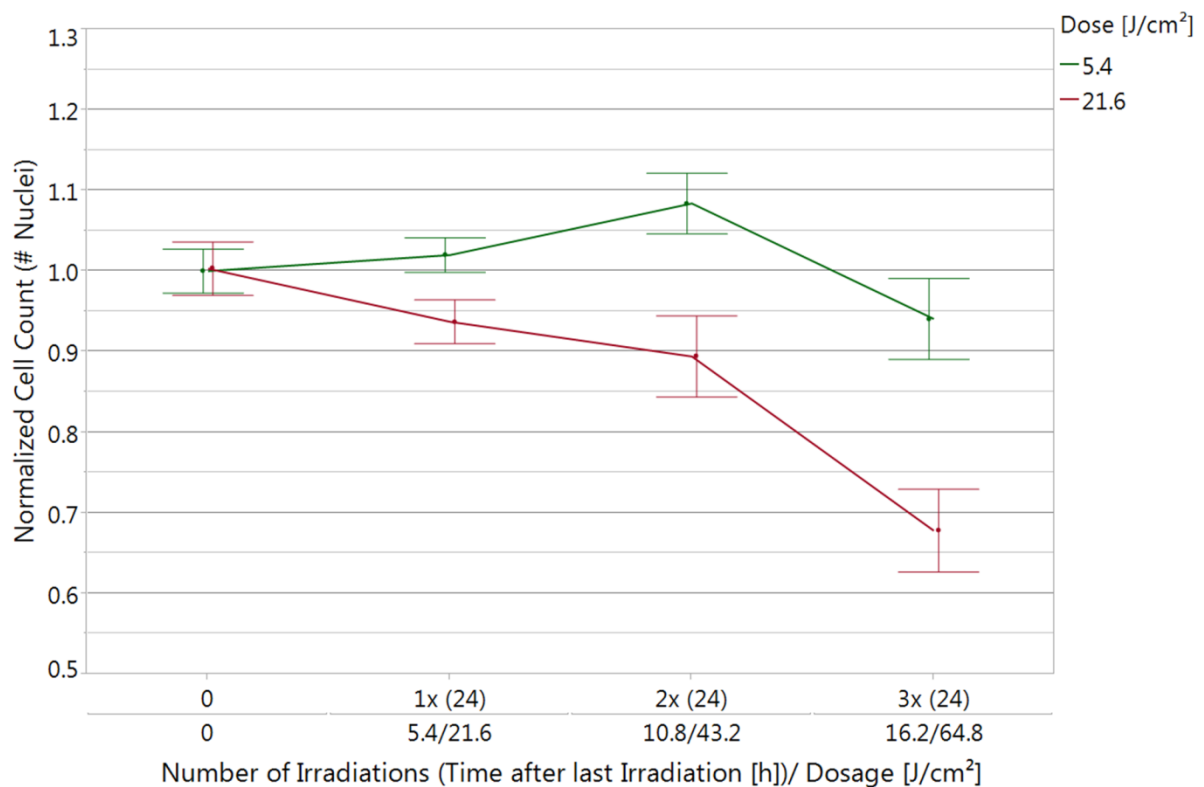


Figure 28: Changes in nuclei or respectively NHDF cell counts following single (1x (24)) and consecutive (2x (24), 3x (24)) treatments with either 5.4 J/cm² or 21.6 J/cm² of blue light. Consecutive irradiations were performed every 24 hours in continuous mode. Staining of cell nuclei was carried out at 24 hours after the last light treatment. Fold changes were evaluated versus time-matched, non-irradiated controls. Data are presented as mean \pm SD (N = 4 repetitions, 3 replicates). Corresponding statistics are summarized in Table 24 (Appendix).

In addition to the count, the area of single nuclei was analyzed. Figure 29 illustrates slight changes found after consecutive irradiations with single doses of 5.4 J/cm² of blue light. With two light treatments (2x (24), 10.8 J/cm²), smaller nuclei sizes were indicated by a decrease of 2.01% ($p=0.0005$), while after three irradiations (3x (24), 16.2 J/cm²) a minor trend to bigger cell nuclei was observed (1.57%, $p=0.0047$). In contrast, consecutive irradiations with 21.6 J/cm² of blue light, which were performed every 24 hours, yielded more pronounced effects showing a continuous rise of nuclei sizes with an increasing dose. Whereas one (1x (24), 21.6 J/cm²) and two (2x (24), 43.2 J/cm²) treatments revealed similar increases by 4.59% and 6.13% ($p<0.0001$), a third one (3x (24)), yielding a dosage of 64.8 J/cm², increased the average size of cell nuclei by additional 5.19% adding up to 11.32% ($p<0.0001$) (Figure 29).

The determination of different shape descriptors, like circularity, roundness as well as aspect ratio did not reveal statistically significant differences.

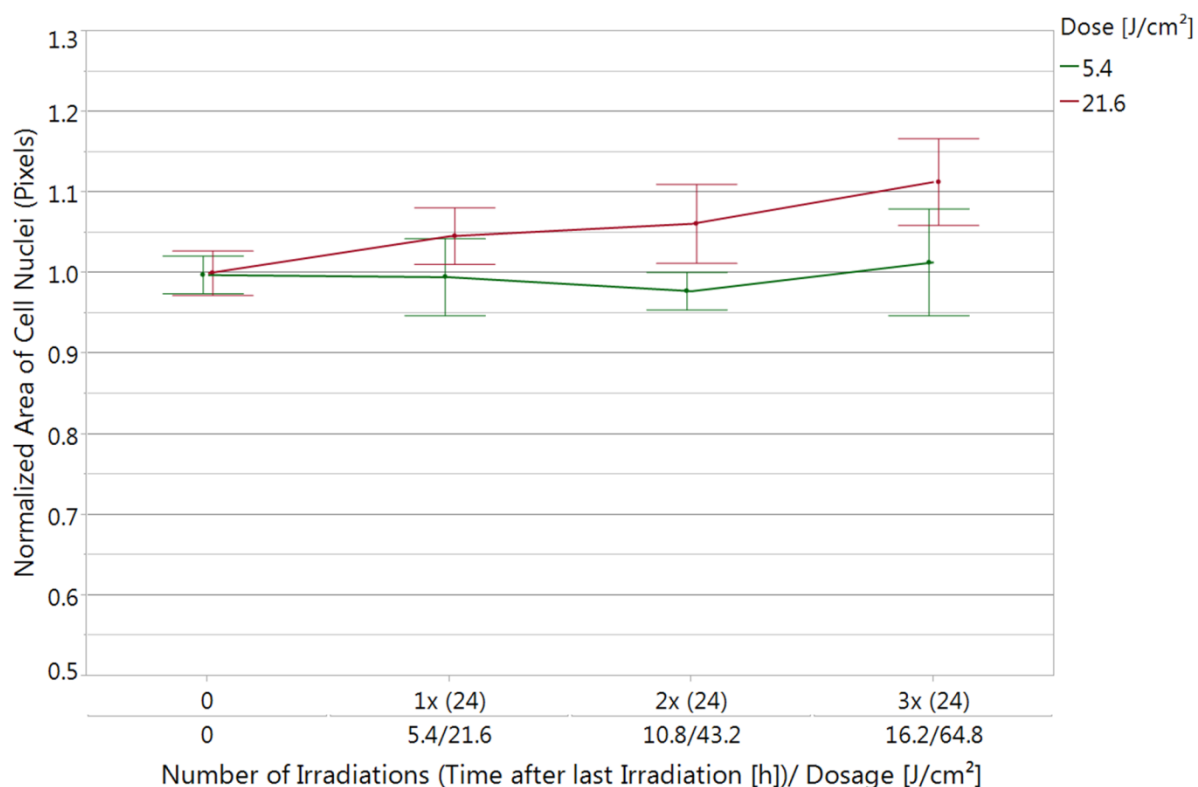


Figure 29: Changes in the average area of NHDF cell nuclei following single (1x (24)) and consecutive (2x (24), 3x (24)) treatments with either 5.4 J/cm² or 21.6 J/cm² of blue light. Consecutive irradiations were performed every 24 hours in continuous mode. Staining of cell nuclei was carried out at 24 hours after the last light treatment. Fold changes were evaluated versus time-matched, non-irradiated controls. Data are presented as mean \pm SD (N = 4 repetitions, 3 replicates). Corresponding statistics are summarized in Table 25 (Appendix).

3.1.4 Functional assays

3.1.4.1 Blue light irradiation triggered immediate generation of H₂O₂

The formation of ROS, which play a crucial role as second messengers in numerous signaling pathways, is known to be modulated by blue light irradiation. Since ROS production represents a fast response, the generation of H₂O₂ was investigated at different time points following single irradiations with 5.4 J/cm² or 21.6 J/cm² of blue light (Figure 30). Directly after irradiation, corresponding to 30 minutes due to the incubation time of Amplex® UltraRed, the fluorescent signal was highly elevated for both irradiation doses. Using 5.4 J/cm², an initial rise in H₂O₂ by 193.26% (p<0.0001) was observed, whereas the level of H₂O₂ following the higher dose of 21.6 J/cm² was increased approximately two-fold by 114.49% (p<0.0001). However, increased H₂O₂ concentrations were normalized to the control level within 1 hour following a single irradiation with 21.6 J/cm² of blue light, while it took about 3 hours for the lower dose.

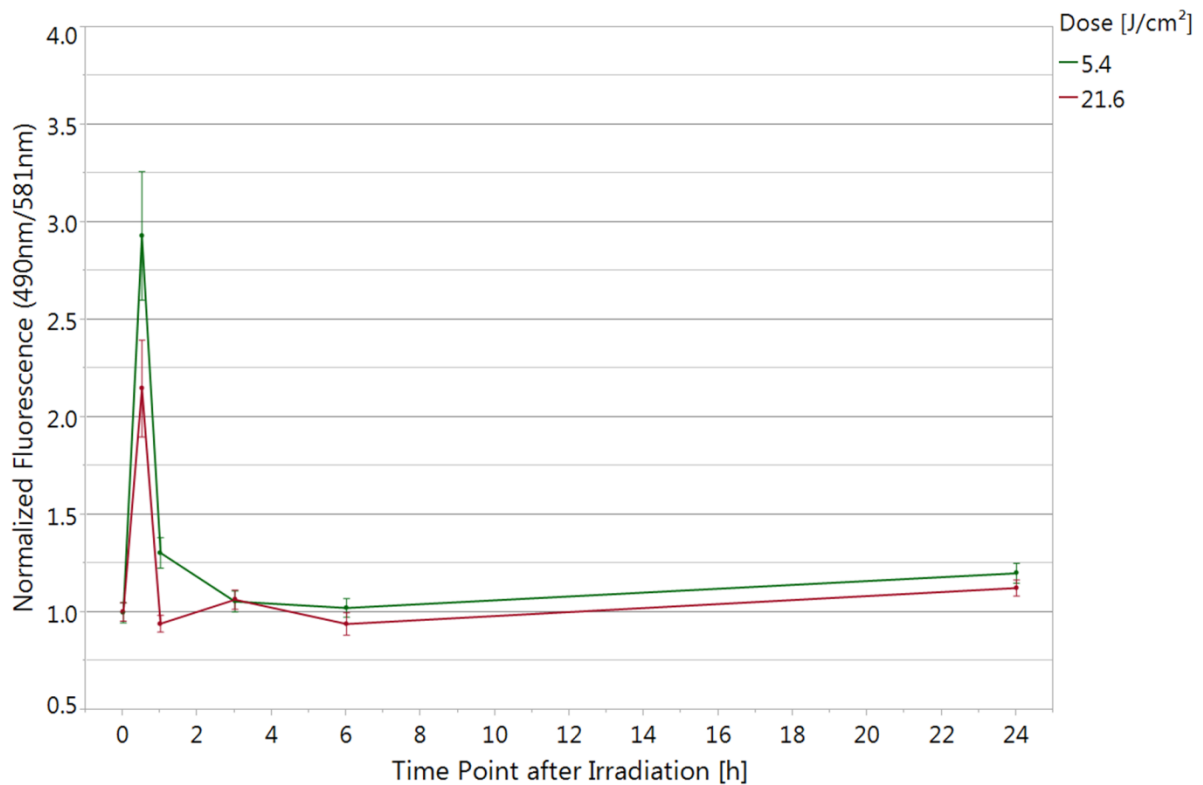


Figure 30: Changes in H₂O₂ levels of NHDF cells measured at different time points following a single blue light exposure to either 5.4 J/cm² or 21.6 J/cm². Blue light treatments were performed in continuous mode. Amplex® UltroXRed was excited at $\lambda_{Ex} = 490$ nm, while its fluorescence emission was measured at $\lambda_{Em} = 581$ nm. Fold changes were evaluated versus time-matched, non-irradiated controls. Data are presented as mean \pm SD (N = 3 repetitions, 3 replicates). Corresponding statistics are summarized in Table 26 (Appendix).

In contrast, the formation of H₂O₂ was again elevated to 6.28% ($p < 0.0001$) at 3 hours following irradiation with 21.6 J/cm² of blue light. At 6 hours and 24 hours afterwards, the amount of H₂O₂ fluctuated in comparison to preceding time points. Numerically speaking, slight reductions in H₂O₂ concentrations by 3.28% ($p = 0.1243$) for 5.4 J/cm² and by 12.46% ($p < 0.0001$) for 21.6 J/cm² at 6 hours were turned back to respective increases by 17.76% ($p < 0.0001$) and 18.45% ($p < 0.0001$) at the last time point. Thus, NHDF cells seemed to balance sudden H₂O₂ bursts within 24 hours (Figure 30).

3.1.4.2 TMRE staining revealed an impairment of mitochondrial function directly after blue light irradiation

Since Figure 30 indicates a sharp rise in H₂O₂ shortly after irradiation of NHDF cells, the question was whether light-triggered ROS generation exceeds physiological levels, which in turn may impair mitochondrial function. Thus, $\Delta\Psi_m$ was measured at different time points following single irradiations with 5.4 J/cm² and 21.6 J/cm² of blue light using the fluorescent probe TMRE, which concentrates in active mitochondria.

At 30 minutes after exposing NHDF cells to 21.6 J/cm^2 of blue light, the fluorescence signal was significantly attenuated by 12.36% ($p < 0.0001$), which demonstrated less accumulation of TMRE and therefore a higher number of depolarized mitochondria. In the further time course, the initial decrease slowly turned back to the control level with significant differences of 6.67% at 1 hour ($p < 0.0001$) and 4.99% ($p < 0.0001$) at 3 hours after blue light treatment. Thereafter, the inhibitory effect on $\Delta\Psi_m$ was balanced with non-significant changes by 1.10% ($p = 0.3604$) at 6 hours and 1.14% ($p = 0.1222$) at 24 hours (Figure 31).

Following a single treatment with 5.4 J/cm^2 of blue light, a similar trend was found at 30 minutes after irradiation, except that the lower decrease in $\Delta\Psi_m$ by 4.31% ($p < 0.0001$) was compensated within 1 hour. At later time points, up to 24 hours, no significant differences were found compared to the untreated control (Figure 31). CCCP, an uncoupler of mitochondrial oxidative phosphorylation, suppressed TMRE staining intensities by 67.5% on average, which revealed not only a successful depolarization control, but also validated the staining characteristics of TMRE.

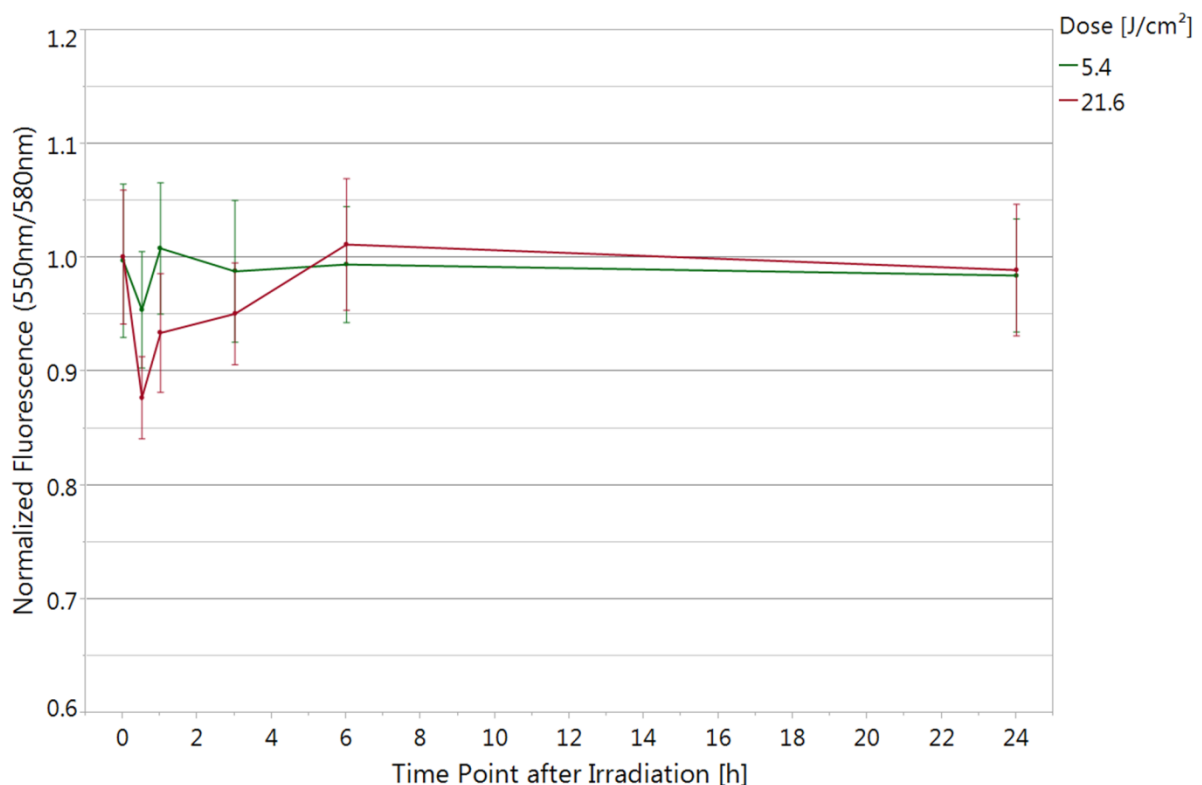


Figure 31: Changes in the mitochondrial membrane potential $\Delta\Psi_m$ of NHDF cells at different time points following a single blue light exposure to either 5.4 J/cm^2 or 21.6 J/cm^2 . Blue light treatments were performed in continuous mode. TMRE was excited at $\lambda_{\text{Ex}} = 550 \text{ nm}$, while its fluorescence emission was measured at $\lambda_{\text{Em}} = 580 \text{ nm}$. Fold changes were evaluated versus time-matched, non-irradiated controls. Data are presented as mean \pm SD (N = 2 repetitions, 3 replicates). Corresponding statistics are summarized in Table 27 (Appendix).

In addition to spectrophotometric measurements, TMRE intensities were verified with fluorescence microscopy. Figure 32 displays exemplary images acquired immediately after microplate readings with (A) showing the positive control with $\Delta\Psi_m$ disruption induced by CCCP as well as (B) the untreated sample and treated samples at (C) 30 minutes and (D) 3 hours following irradiation with a blue light dose of 21.6 J/cm^2 . While the positive control showed low fluorescence intensities as a consequence of mitochondrial depolarization (Figure 32, (A)), the untreated control displayed brightly fluorescent cells with TMRE accumulated in active mitochondria (Figure 32, (B)). In contrast, blue light irradiation led to a reduction of the signal indicating changes of the mitochondrial polarization status. Viewing the corresponding images (Figure 32, (C) & (D)), a slight difference was observed, while the fluorescence intensity of TMRE seemed to be slightly higher at 3 hours following 21.6 J/cm^2 of blue light.

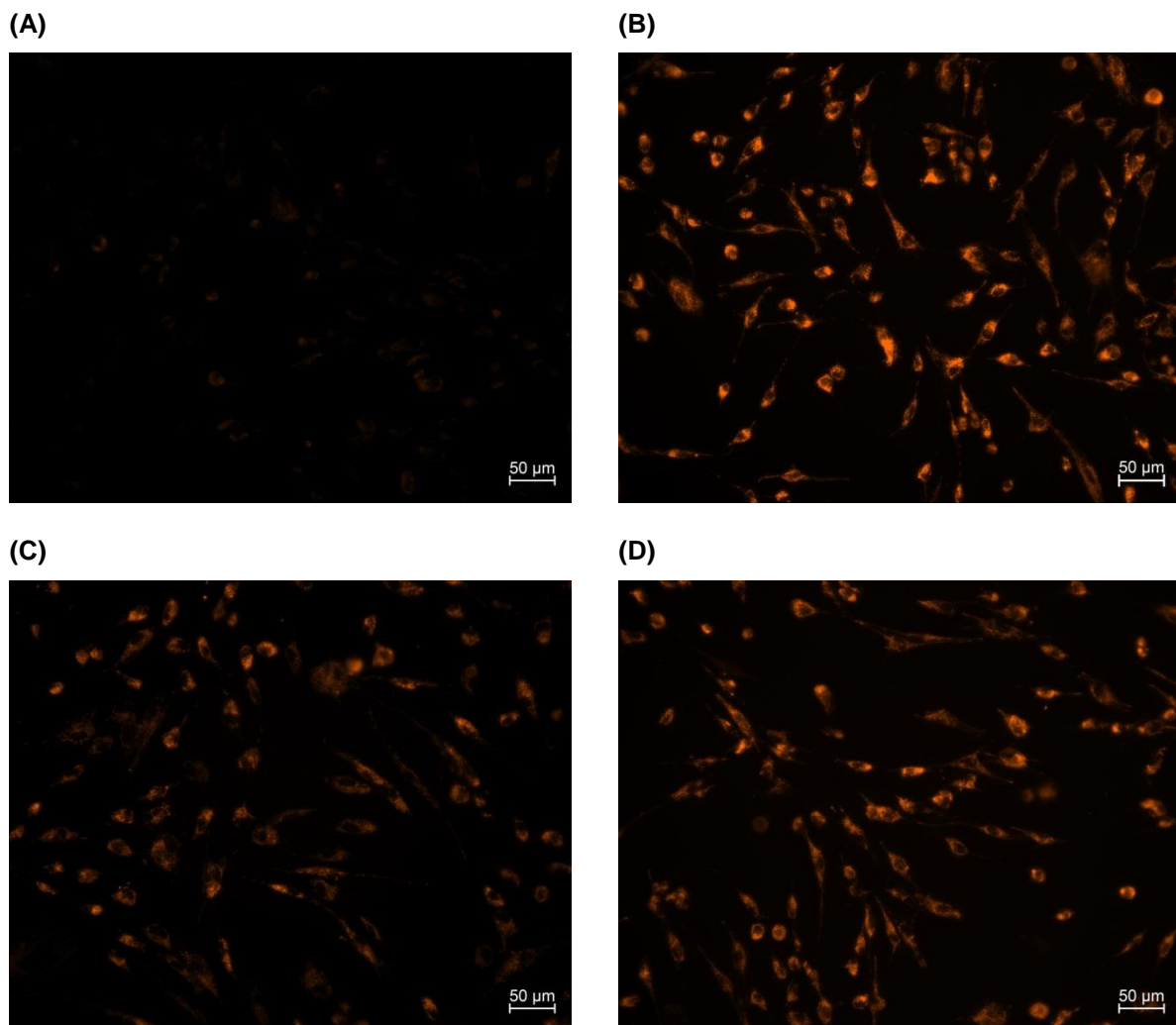
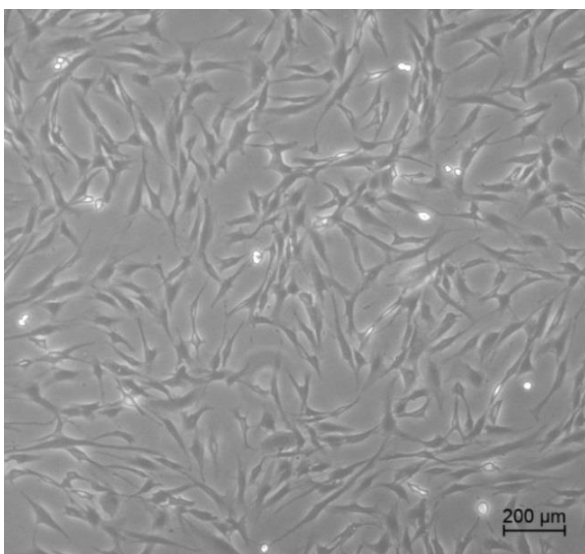


Figure 32: Representative fluorescence images showing the extent of TMRE accumulation in NHDF cells following different treatments. (A) The positive control sample, in which $\Delta\Psi_m$ disruption was induced with $50 \mu\text{M}$ of CCCP, (B) the untreated sample receiving no light and the treated sample at (C) 30 minutes and (D) 3 hours after irradiation with 21.6 J/cm^2 of blue light.

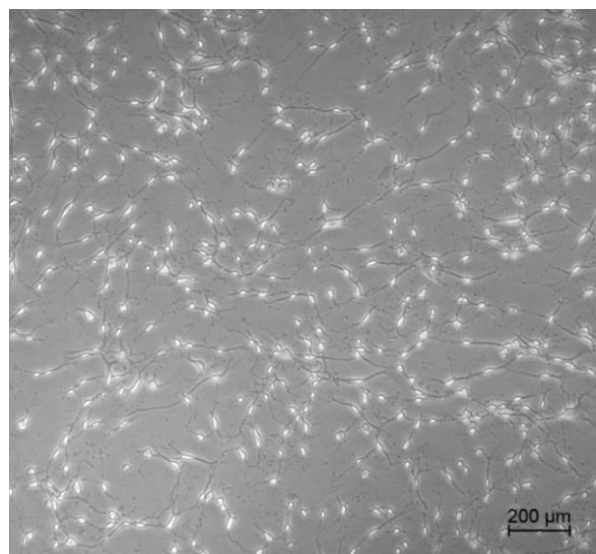
3.1.4.3 Single blue light treatments did not induce cell death up to an irradiation dose of 172.8 J/cm²

To elucidate whether the found reductions in cellular activity and proliferation resulted from growth inhibition instead of cell death, flow cytometry analyses were performed at 24 hours following single blue light treatments. Besides using prechosen blue light doses of 5.4 J/cm² and 21.6 J/cm², NHDF cells were treated with up to 172.8 J/cm² in order to guarantee safety of high-energy light treatments. For the positive control, cytotoxic effects were induced by exposing NHDF cells to 1 μM of staurosporine (*Streptomyces staurospores*), a non-selective protein kinase inhibitor, for 24 hours at 37°C and 5% CO₂. At different time points following staurosporine administration, respectively at 2 hours, 6 hours and 24 hours, cell morphology was documented by acquiring phase contrast images using an inverted Leica DM IRBE microscope (Leica Mikroskopie & Systeme GmbH, Wetzlar, Germany) (Figure 33, (B) – (D)). Already after 2 hours of incubation at 37°C and 5% CO₂ (Figure 33, (B)), the apoptotic stimulus exerted by staurosporine revealed a remarkable induction of cell shrinkage compared to untreated control cells (Figure 33, (A)). In the following time course, cell shrinkage was enhanced (Figure 33, (C)), and finally, at 24 hours of incubation, a lot of NHDF cells were found to be detached from the adherent surface (Figure 33, (D)), showing a time-dependent cytotoxic effect.

(A)



(B)



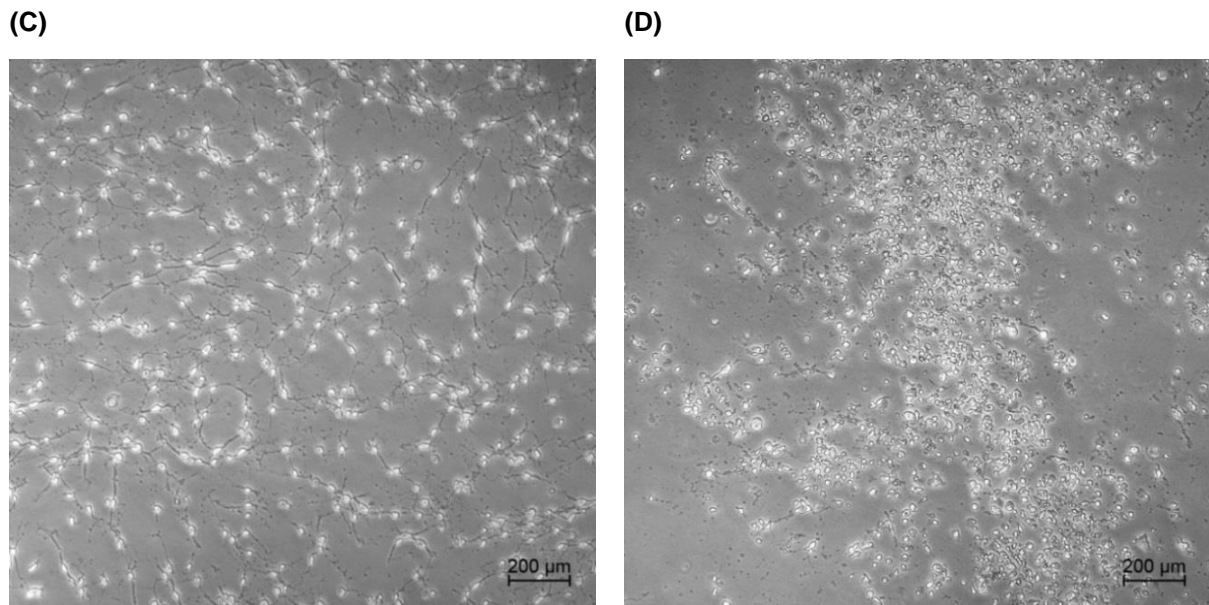


Figure 33: NHDF morphology before treatment with staurosporine (A) and following incubation with 1 μM of staurosporine for (B) 2 hours, (C) 6 hours and (D) 24 hours. Images were acquired using an inverted Leica DM IRBE microscope (Leica Mikroskopie & Systeme GmbH, Wetzlar, Germany) in phase contrast with 5x magnification.

Single cells were analyzed with respect to their scatter parameters and their light emission properties generated by two different fluorescent stains. The measurement of forward scatter (FSC) allowed to discriminate cell populations by size, whereas the intensity of side scatter (SSC) provided information about the granularity and thus internal complexity of cells. In contrast to living cells (Figure 34, (A)), dead cells were characterized by forward and side scatters of low intensities indicating smaller cell sizes and a lower degree of internal complexity or granularity (Figure 34, (B)).

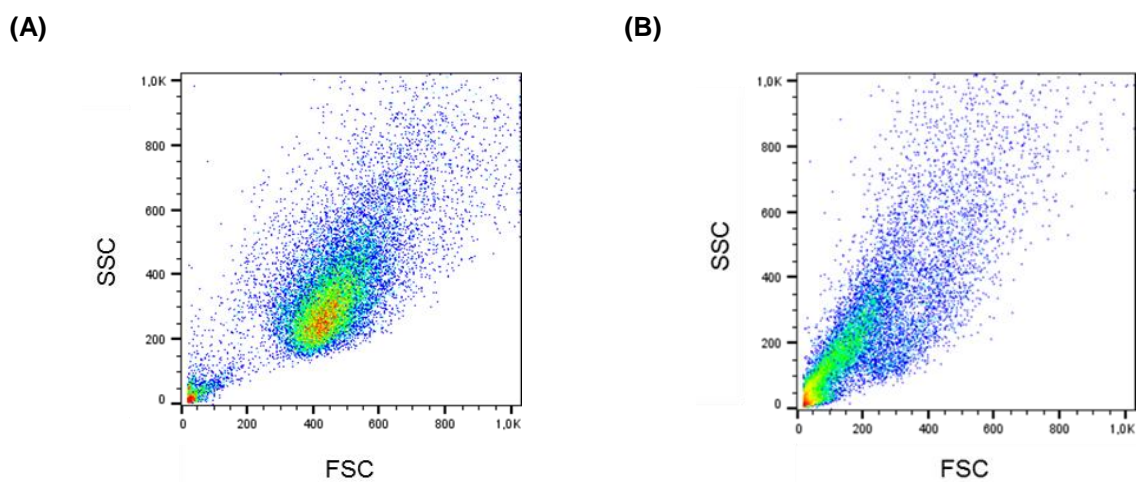


Figure 34: Representative pseudocolor density plots of NHDF cells either (A) untreated or (B) exposed to 1 μM of staurosporine for 24 hours inducing cytotoxicity. In each plot 8,000 events are depicted.

In Figure 35 exemplary forward vs. side scatter plots are represented for untreated and treated fibroblasts, either irradiated with 5.4 J/cm^2 or 21.6 J/cm^2 of blue light, as well as for the respective positive controls. For a better comparison of the individual dot plots, overlays were compiled. Comparing the dot plots of untreated and treated cells with the ones for the positive control, they represented a rather healthy cell population with forward and side scatters of higher intensities. However, the difference between untreated and light-treated samples was negligible, since their measured scatter intensities were similar, which can be easily inferred from the overlays shown in Figure 35. This observation applied for both blue light doses. Therefore, the discrimination of dead and living NHDF cells based on their scatter parameters suggested that samples, treated with 5.4 J/cm^2 and 21.6 J/cm^2 of blue light, exhibited a similar amount of dead cells compared to untreated samples.

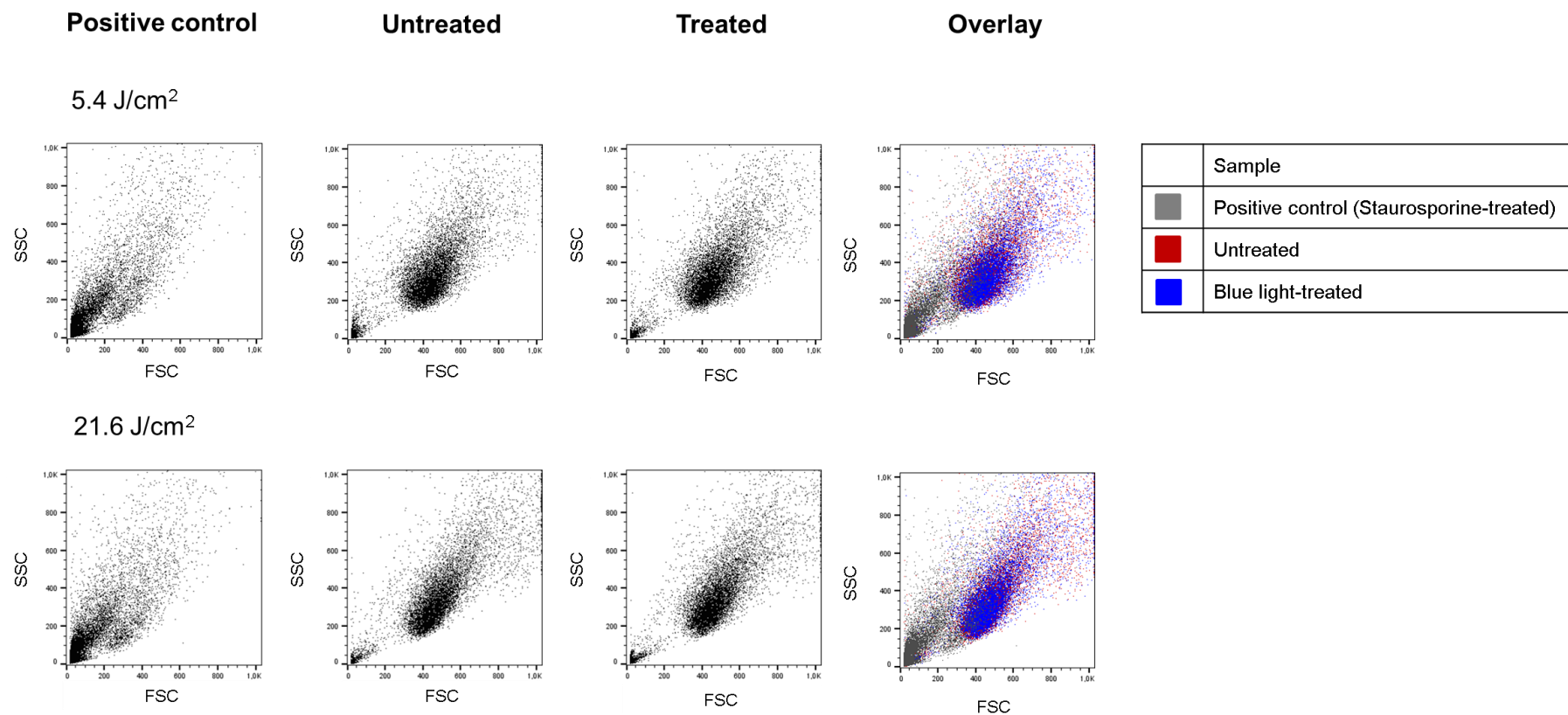


Figure 35: Representative two-parameter dot plots showing scatter parameters (forward scatter (FSC), side scatter (SSC)) of NHDF cells following different treatments. From left to right: The positive control sample, in which cytotoxicity was induced with 1 μM of staurosporine for 24 hours, the untreated sample receiving no light, the blue light-treated sample and finally the overlay of all three conditions. Flow cytometry analysis was performed at 24 hours following staurosporine treatment of the positive control as well as continuous blue light treatment of irradiated samples with either 5.4 J/cm² or 21.6 J/cm². In each plot 8,000 events are depicted.

To mark apoptotic and necrotic cells, Allophycocyanin (APC)-conjugated Annexin V (AV-APC) and Propidium Iodide (PI) were chosen. Unstained samples were prepared to determine background autofluorescence in order to set appropriate PMT voltages and derive proper gating strategies (Figure 36, (A)). AV-APC identifies cells in which phosphatidylserine gets exposed at the outer leaflet of the plasma membrane, which is typical of early apoptotic cells (AV-APC+/PI-) shown in the lower right quadrant Q3 of the dot plot (Figure 36, (B)). In contrast, necrotic cells are characterized by a loss of their membrane integrity resulting in an increased permeability. Therefore, the second stain PI, a fluorescent DNA intercalating dye, detects necrotic cells, which accumulate in the upper left quadrant Q1 of the plot (Figure 36, (C)). However, it has to be noted that AV-APC also binds to internal phosphatidylserine following complete cell rupture indicating late apoptotic/necrotic cells. Consequently, double labeling shows a complete representation of dead cells and allows the distinction of early apoptotic cells (AV-APC+/PI-) from necrotic cells (AV-APC+/PI+) (Figure 36, (D)).

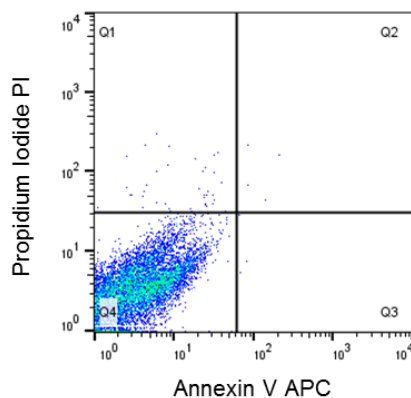
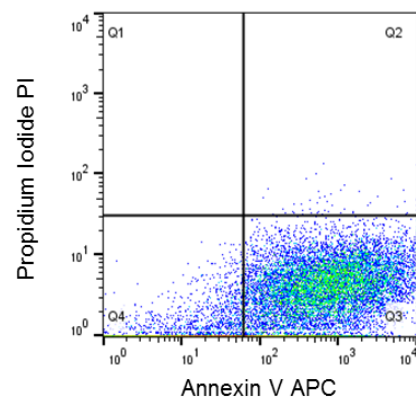
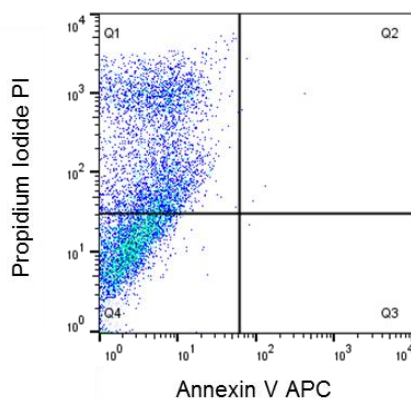
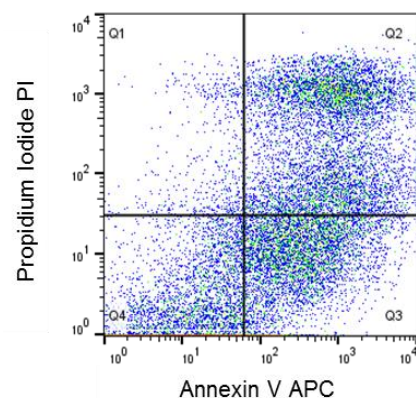
(A) Unstained**(B) Single stained (AV-APC+)****(C) Single stained (PI+)****(D) Double stained (AV-APC+/PI+)**

Figure 36: Representative pseudocolor density plots of NHDF cells exposed to 1 μ M of staurosporine for 24 hours inducing cytotoxicity. (A) Unstained, (B) Single stained with AV-APC, (C) Single stained with PI and (D) Double stained with AV-APC and PI. In each plot 8,000 events are depicted.

In the following figures, representative two-parameter dot plots and single-parameter histograms are shown for double stained samples containing positive control cells as well as untreated and blue light-treated cells. Latter were either treated with a blue light dose of 5.4 J/cm^2 depicted in Figure 37 or 21.6 J/cm^2 displayed in Figure 38. For the positive control, fluorescence intensities of AV-APC and PI were increased, which was visualized by definite shifts in both graphics, the dot plots and the histograms. In contrast, untreated and light-treated samples showed lower fluorescence intensities accounting for higher numbers of living cells in the respective cell populations, which was clearly illustrated by the overlays for AV-APV and PI (Figure 37, Figure 38). Therefore, the exemplary dot plots and histograms shown for both irradiation doses, 5.4 J/cm^2 and 21.6 J/cm^2 , gave a first indication that blue light does not induce cell death up to a mid irradiation dose. In addition, the observation of irradiated NHDF cells during experiments did not reveal rounding or other stress signs after exposure to different blue light doses.

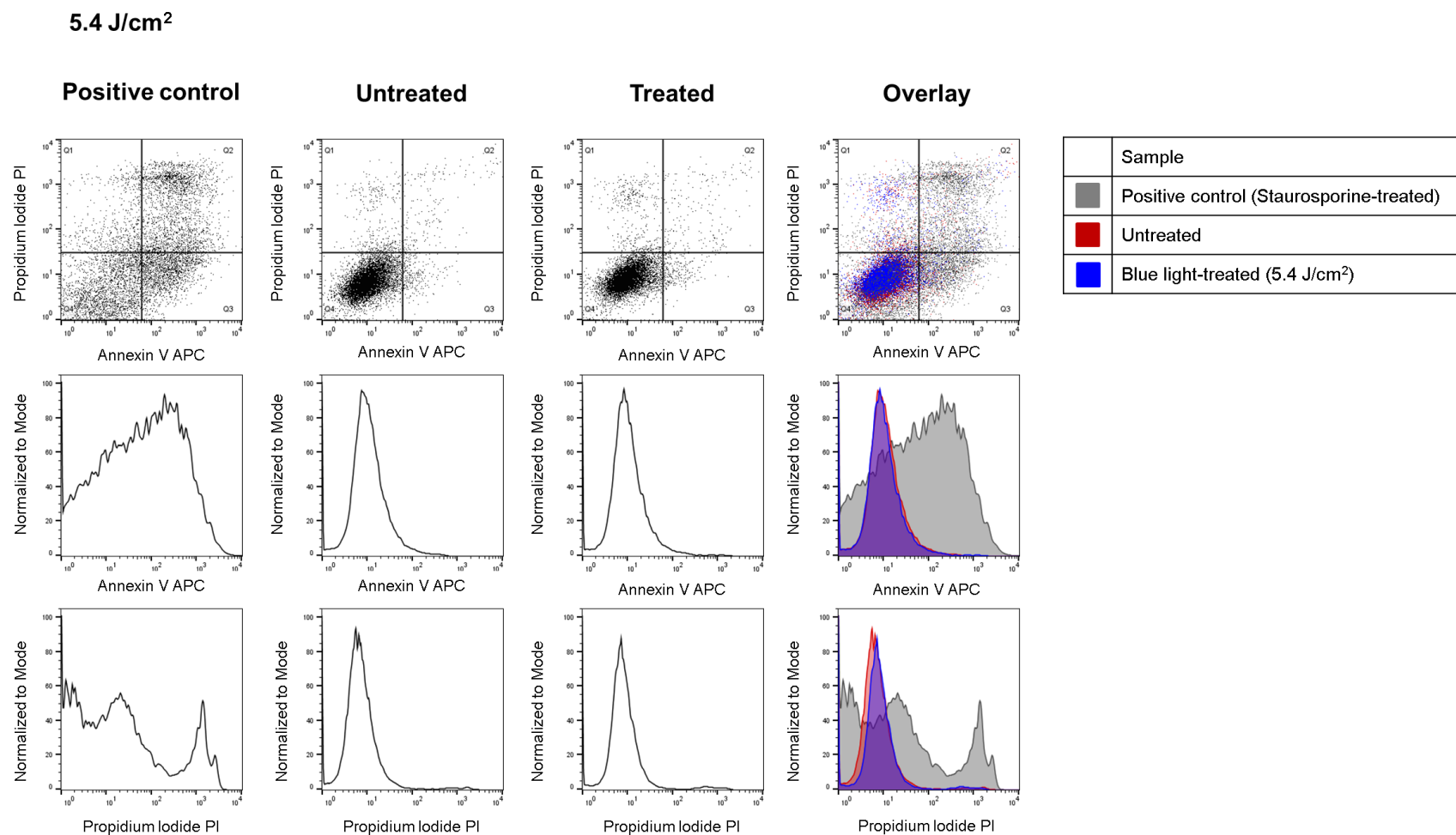


Figure 37: Exemplary two-parameter dot plots and single-parameter histograms showing fluorescence intensities of NHDF cells stained with AV-APC and PI following different treatments. From left to right: The positive control sample, in which cytotoxicity was induced with 1 μM of staurosporine for 24 hours, the untreated sample receiving no light, the treated sample with 5.4 J/cm² of blue light and finally the overlay of all three conditions. Flow cytometry analysis was performed at 24 hours following staurosporine treatment of the positive control as well as continuous blue light treatment of irradiated samples. The dot plots are subdivided by four quadrants with living cells being located in the lower left quadrant (Q4). Cells in early apoptosis, stained by AV-APC, can be assigned to the lower right quadrant (Q3), whereas the upper right quadrant depicts the percentage of cells staying in late apoptosis (Q2). Necrotic cells, stained by PI, can be found in the upper left quadrant (Q1). In each plot 8,000 events are depicted.

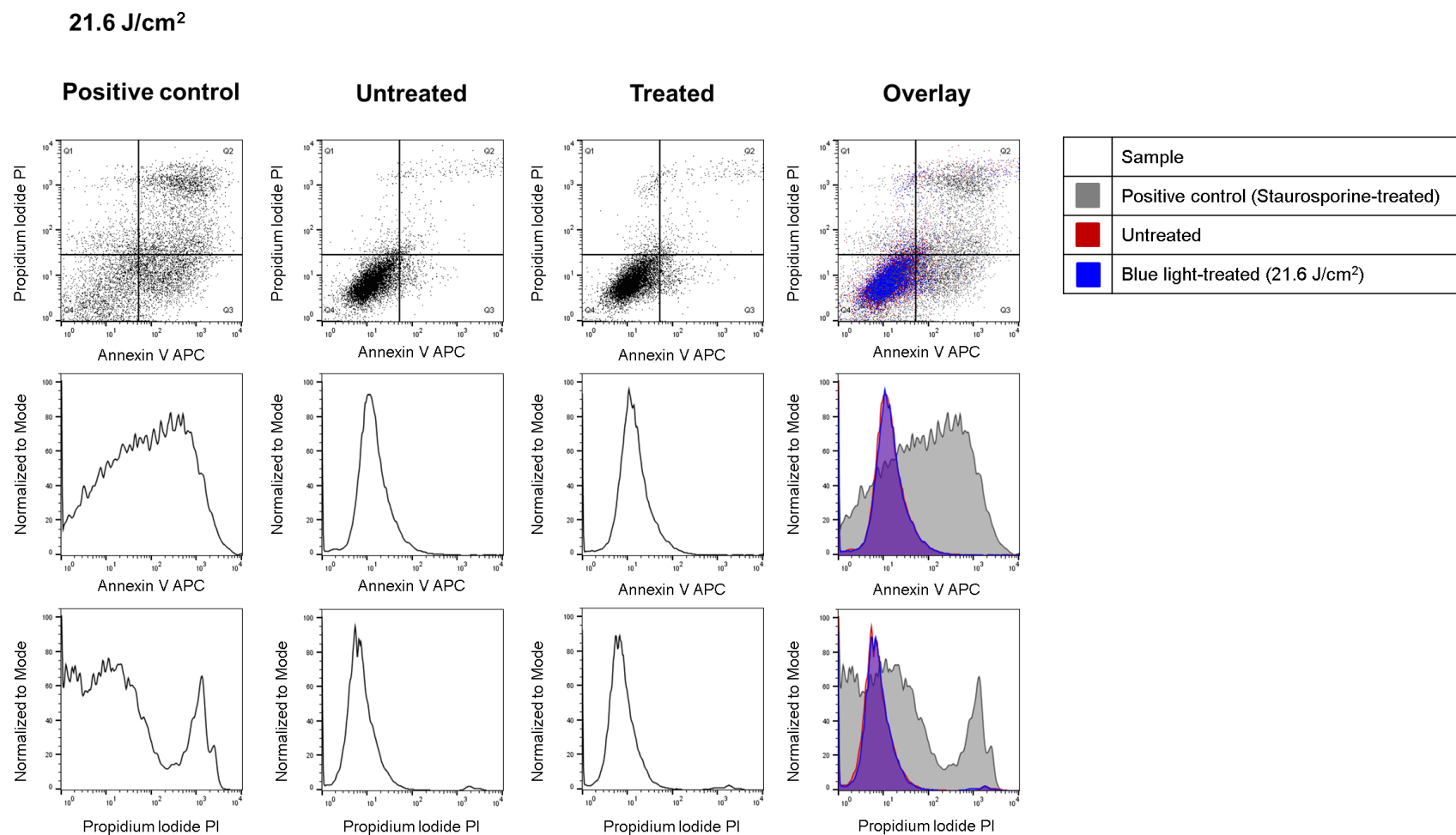


Figure 38: Exemplary two-parameter dot plots and single-parameter histograms showing fluorescence intensities of NHDF cells stained with AV-APC and PI following different treatments. From left to right: The positive control sample, in which cytotoxicity was induced with 1 μM of staurosporine for 24 hours, the untreated sample receiving no light, the treated sample with 21.6 J/cm² of blue light and finally the overlay of all three conditions. Flow cytometry analysis was performed at 24 hours following staurosporine treatment of the positive control as well as continuous blue light treatment of irradiated samples. The dot plots are subdivided by four quadrants with living cells being located in the lower left quadrant (Q4). Cells in early apoptosis, stained by AV-APC, can be assigned to the lower right quadrant (Q3), whereas the upper right quadrant depicts the percentage of cells staying in late apoptosis (Q2). Necrotic cells, stained by PI, can be found in the upper left quadrant (Q1). In each plot 8,000 events are depicted.

However, for quantitative data analysis, counts of living cells were inferred from the lower left quadrant Q4, whereas the overall number of dead cells was added up by summarizing Q1, Q2 and Q3. Whereas the positive control showed an overall rate of cell death by approximately 50% ranging from 42.1% to 53.8% for the individual samples, untreated and blue light-treated samples yielded about 90% living cells and 10% dead cells. Comparing the respective event numbers of living and dead cells for untreated and blue light-treated samples, no significant differences were observed up to a light dose of 86.4 J/cm², corresponding to an irradiation time of 120 minutes. However, a significant change of 3.5% ($p=0.0160$) was noted for the highest dose of 172.8 J/cm² (Figure 39), which was negligible with respect to the questioned safety of high-energy light treatments. Hence, flow cytometry results obtained for increasing doses, did not reveal an energy-density dependent induction of cell death by blue light irradiation.

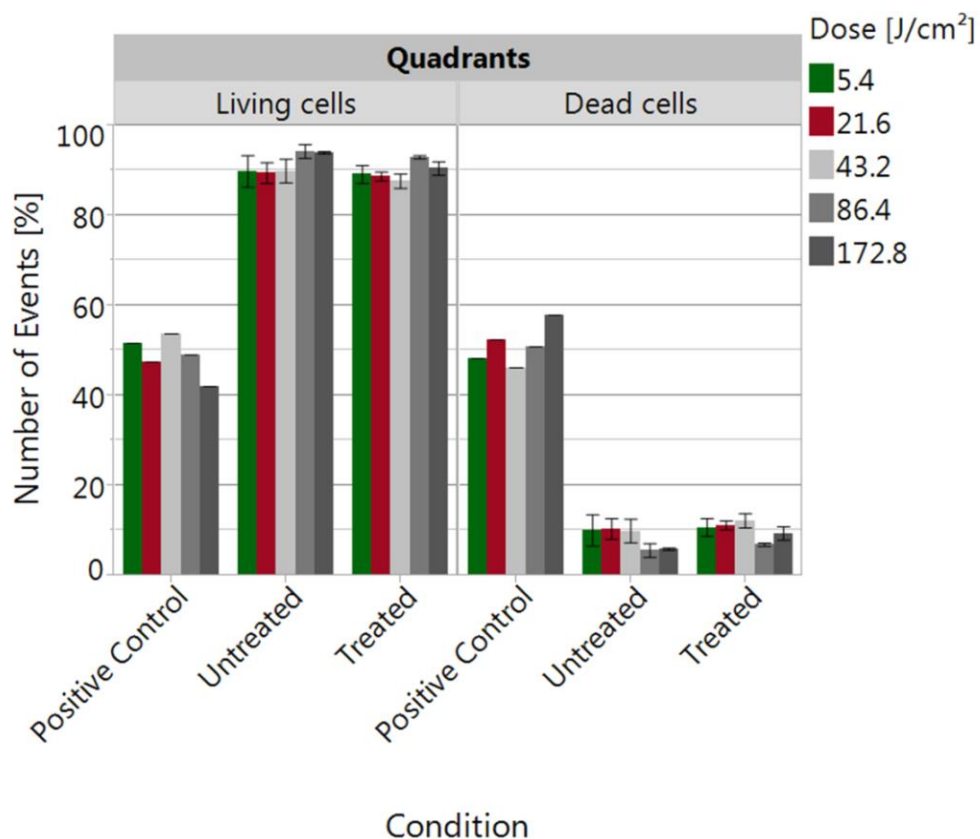


Figure 39: Number of events [%] for living and dead NHDF cells inferred from two-parameter dot plots showing fluorescence intensities of AV-APC and PI following different treatments. From left to right: The positive control samples, in which cytotoxicity was induced with 1 μ M of staurosporine for 24 hours, the untreated samples receiving no light, and the blue light-treated samples, which were irradiated with different blue light doses. Flow cytometry analyses were performed at 24 hours following staurosporine treatment of the positive control as well as continuous blue light treatment of irradiated samples. Living cell counts were inferred from the lower left quadrant (Q4), whereas the total amount of dead cells was added up by summarizing the number of events in Q1, Q2 and Q3. Bars display mean values \pm SD ($N = 1$ repetition, 3 replicates). Corresponding statistics are summarized in Table 28 (Appendix).

3.1.5 Gene expression analysis

Subsequent to cell harvesting at different time points (1 hour, 3 hours and 24 hours) following irradiation, RNA extraction and respective quality controls (RIN = 10 for all samples), time-dependent changes in gene expression of NHDF cells were studied using transcriptome analysis. As single blue light treatments using either 5.4 J/cm² or 21.6 J/cm² revealed contrary effects on metabolism, proliferation and mitochondrial function, it was examined whether both irradiation doses differentially impact gene expression. For the respective time points after single treatments with different blue light doses, gene expression analyses were performed once with three replicates for each condition tested, light-treated and untreated (see 2.2.6.1). Following distribution analysis and batch normalization for separate experiments, correlation heatmaps and principal component analyses showed an unambiguous differentiation of irradiated and non-irradiated samples into distinct clusters. Figure 40 depicts a representative correlation matrix compiled for 24 hours of harvesting after 5.4 J/cm² of blue light with the Pearson's correlation coefficient r indicating negative correlations between blue light and control samples. Moreover, the similarity dendrogram illustrates dissimilar relations between light-treated and untreated data sets (Figure 40).

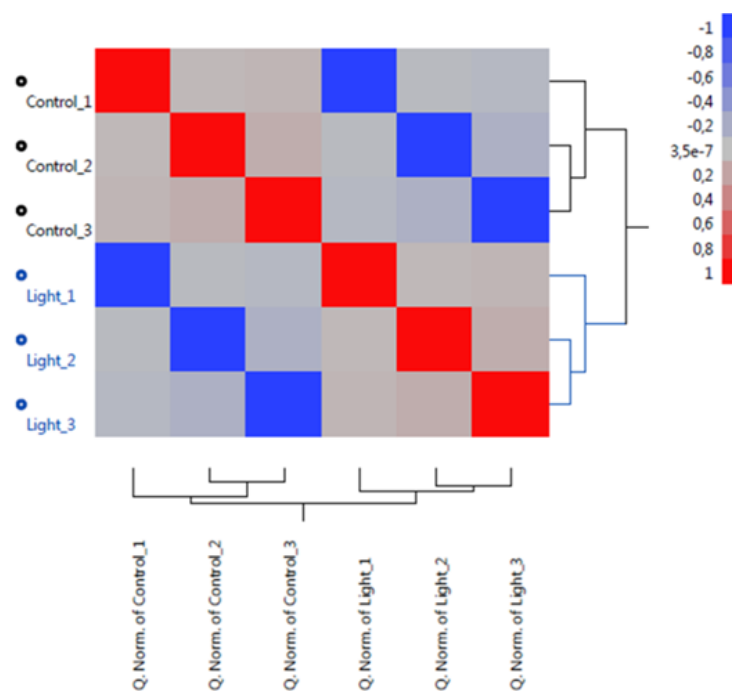


Figure 40: Representative Pearson correlation heatmap showing cluster analysis of untreated (control, N = 1 repetition, 3 replicates) and treated (light, N = 1 repetition, 3 replicates) samples following a single blue light treatment of NHDF cells with 5.4 J/cm² and cell harvesting at 24 hours afterwards. Red indicates positive linear correlations ($r = 1$), while blue shows negative linear correlations ($r = -1$). The matrix reveals strong correlations between light-treated samples, which can be clearly differentiated from untreated samples.

Out of 24,733 genes, screened with the Affymetrix HuGene-2_0-st microarrays, on average 1,300 significant genes (FDR < 0.05) were differentially expressed in each experiment corresponding to approximately 5% of the complete array. Since previous test methods revealed dose-dependent effects of blue light, it was reviewed whether both irradiation doses used, 5.4 J/cm² and 21.6 J/cm², triggered commonly and/or rather differentially expressed genes. Figure 41 illustrates that only a few genes shared in common were affected, while the amount increased for longer time points following irradiation. Whereas at 1 hour after exposure to blue light of either 5.4 J/cm² or 21.6 J/cm², only 47 genes were found in common, the number of shared genes at 24 hours after irradiation accounted for 139 in total. Nevertheless, the proportion of commonly shared genes stayed below 5%, as their increasing number over time was accompanied by a cumulative amount of overall differentially expressed genes. Apparently, most of the genes were differentially affected when comparing both blue light doses, 5.4 J/cm² and 21.6 J/cm² (Figure 41).

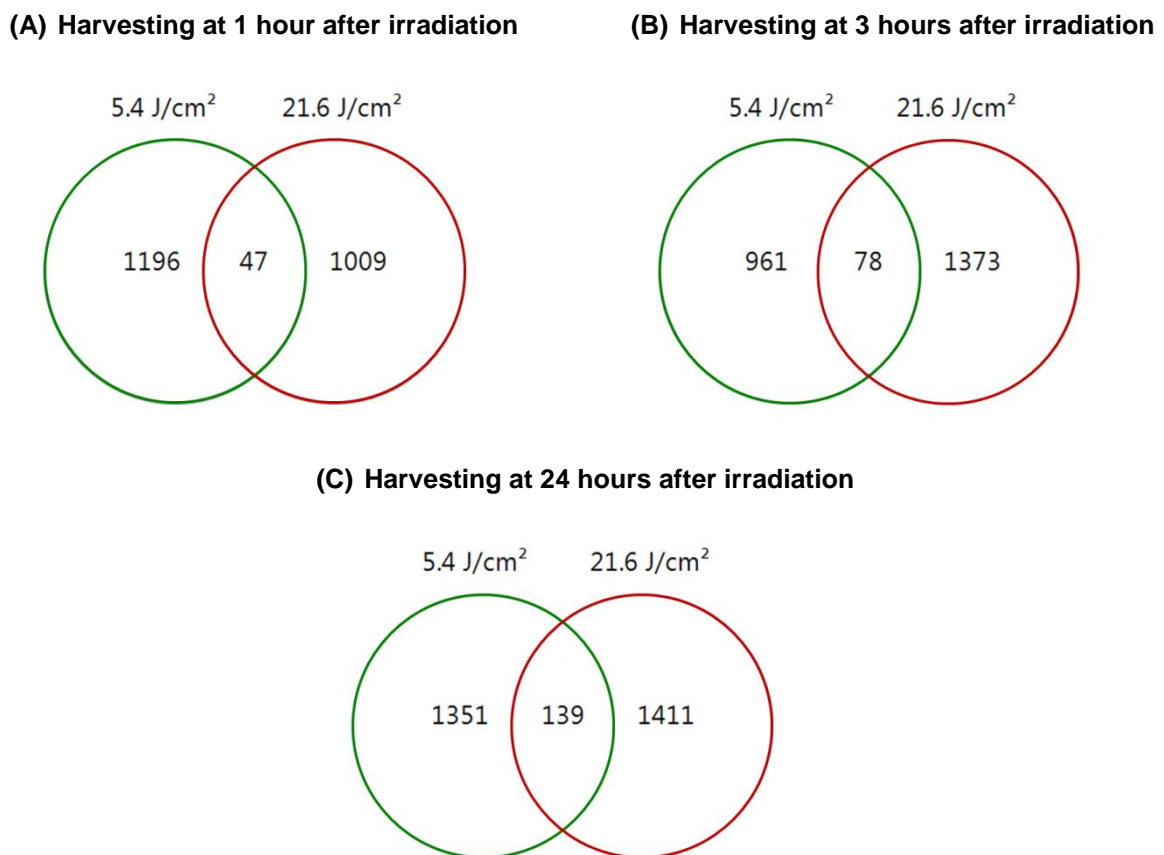


Figure 41: Venn diagrams showing the number of significantly (FDR < 0.05) commonly or differentially expressed genes in NHDF cells at (A) 1 hour, (B) 3 hours and (C) 24 hours following a single blue light treatment with either 5.4 J/cm² shown in green and 21.6 J/cm² displayed in red.

While the total amount of differentially expressed genes alternated for increasing harvesting times after 5.4 J/cm² of blue light, the number constantly accumulated for the higher dose of 21.6 J/cm². Nevertheless, for both blue light doses, the highest amount of de-regulated genes was given at 24 hours of cell harvesting (Figure 41). Table 10 lists the counts of significantly up- and down-regulated genes for each treatment group. At 1 hour following irradiation, the number of down-regulated genes prevailed for both irradiation doses, while the lower blue light dose of 5.4 J/cm² affected a higher number of genes. In the following, at 3 hours of harvesting, the opposite occurred, as 21.6 J/cm² of blue light affected more genes with the majority being up-regulated. In contrast, the overall number of differentially expressed genes was reduced for 5.4 J/cm² of blue light with a similar ratio of up- and down-regulated genes compared to 1 hour of harvesting. At 24 hours after irradiation, the number of up-regulated genes was nearly equal for both irradiation doses, while the data sets showed a difference of 57 significantly down-regulated genes (Table 10). However, differential changes induced by varying blue light doses rather emerged in the early phase after irradiation, which might lead to different cell fates in the long run.

Table 10: Number of significantly up- and down-regulated genes differentially expressed in NHDF cells at different harvesting time points following a single blue light treatment with either 5.4 J/cm² or 21.6 J/cm².

Treatment group		Significantly differentially expressed genes	
Dose [J/cm ²]	Time Point [h]	Up-regulated genes	Down-regulated genes
5.4	1	567	676
21.6	1	489	567
5.4	3	444	595
21.6	3	789	662
5.4	24	754	736
21.6	24	757	793

Using ranked lists of differentially expressed genes, GSEA was performed to identify differences in genes sets predefined by KEGG. Hence, higher (or lower) normalized enrichment scores (NES) indicate a shift of genes towards the top (or the bottom) of the ranked list representing up-regulated pathways with positive values (or down-regulated pathways with negative values). Table 11 lists the numbers of de-regulated KEGG pathways at different time points following single blue light treatments with either 5.4 J/cm² or 21.6 J/cm².

With 146 and 134 gene sets, the total number of up- and down-regulated pathways was comparable at 1 hour following irradiation with the lower blue light dose of 5.4 J/cm^2 , while 21 pathways containing mainly up-regulated genes were significantly enriched at a nominal p-value < 0.05 . In the further time course, respectively at 3 hours and 24 hours of harvesting, the counts of up- and down-regulated pathways were characterized by contrary trends. Whereas the amount of down-regulated pathways peaked at 3 hours with 183 gene sets in total (16 pathways at a nominal p-value < 0.05), the number of pathways prevailed by up-regulated genes reached its maximum at 24 hours with 165 gene sets (22 pathways at a nominal p-value < 0.05) (Table 11). Using 21.6 J/cm^2 of blue light, the total number of up- and down-regulated pathways remained nearly constant. The highest amount of up-regulated gene sets was given at 3 hours of cell harvesting with 117 sets in total, of which 14 pathways were significantly enriched at a nominal p-value < 0.05 . In contrast, down-regulated pathways emerged predominantly after 24 hours with 180 sets in total, while 38 of them were significantly enriched at a nominal p-value < 0.05 (Table 11).

Table 11: Number of differentially expressed KEGG pathways at different time points following a single blue light treatment of NHDF cells with either 5.4 J/cm^2 or 21.6 J/cm^2 . Starting from an overall gene set number of 280, total numbers of up-regulated and down-regulated pathways are shown. In addition, the number of significantly enriched pathways is listed for different significance levels: at a nominal p-value of < 0.05 , at a nominal p-value of < 0.01 and at an adjusted p-value (FDR) < 0.25 .

Time Point of Harvesting [h]	1		3		24	
Dose [J/cm^2]	5.4	21.6	5.4	21.6	5.4	21.6
De-regulated pathways in total	280	280	280	280	280	280
Up-regulated pathways in total	146	103	97	117	165	100
With nominal p-value < 0.05	21	1	5	14	22	10
With nominal p-value < 0.01	7	1	1	6	10	5
With adjusted p-value (FDR) < 0.25	11	0	1	5	19	6
Down-regulated pathways in total	134	177	183	163	115	180
With nominal p-value < 0.05	12	8	16	17	7	38
With nominal p-value < 0.01	1	2	6	9	1	15
With adjusted p-value (FDR) < 0.25	0	2	7	9	0	16

Comparing the number of up- and down-regulated gene sets, significantly enriched at a nominal p-value < 0.05 , between both light doses, they showed contrary counts, especially with respect to the time course of up-regulated pathways. For 5.4 J/cm^2 of blue light, a similar amount of about 20 pathways was given at 1 hour and 24 hours of harvesting, whereas the highest number arose at 3 hours after 21.6 J/cm^2 .

In contrast to alternating counts of down-regulated pathways after 5.4 J/cm² of blue light, their number constantly increased over time following a single treatment using the higher irradiation dose of 21.6 J/cm² (Figure 42).

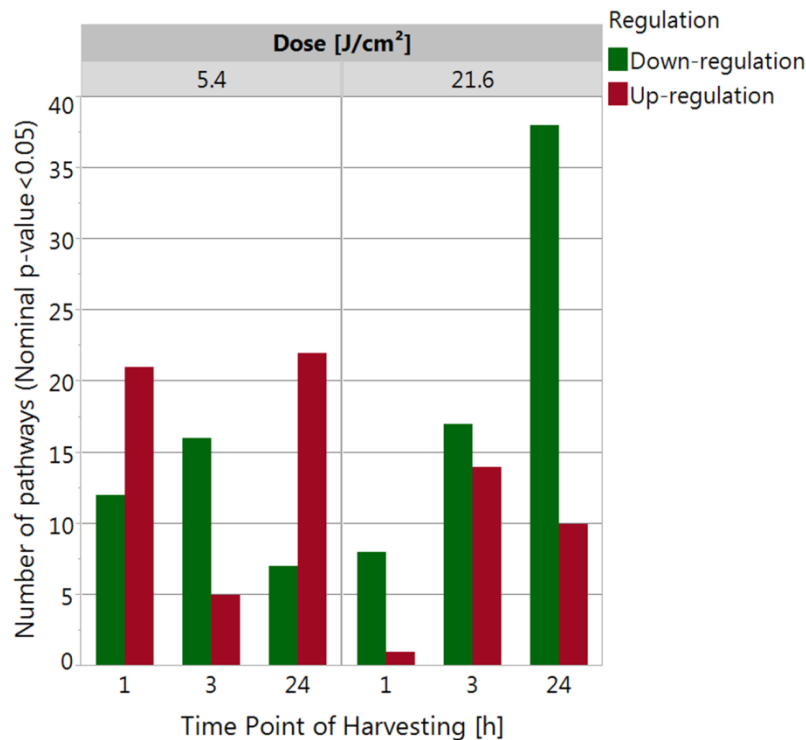


Figure 42: Total counts of up-regulated and down-regulated KEGG pathways, significantly enriched at a nominal p-value < 0.05, at different time points following a single blue light treatment of NHDF cells with either 5.4 J/cm² or 21.6 J/cm².

In order to assess which molecular interactions, reactions and networks were mainly affected when using two different irradiation doses, Figure 43 and Figure 44 illustrate the classification of significantly enriched pathways (nominal p-value < 0.05) into KEGG main categories. For 5.4 J/cm² of blue light, up-regulated pathways could be mainly assigned to the main category of metabolism with 11 de-regulated genes sets at 1 hour and 24 hours after irradiation. However, only 4 up-regulated gene sets were found to be in common between those time points, with 2 of them belonging to the main category of metabolism, galactose metabolism and oxidative phosphorylation. In contrast, down-regulated gene sets rather belonged to other main categories of genetic information processing, environmental information processing and cellular processes mainly involving protein processing, signal transduction as well as cellular community. The corresponding Venn diagrams for different harvesting time points hardly showed any commonly shared gene sets de-regulated over time. However, the lower dose of 5.4 J/cm² mainly affected metabolic processes (Figure 43).

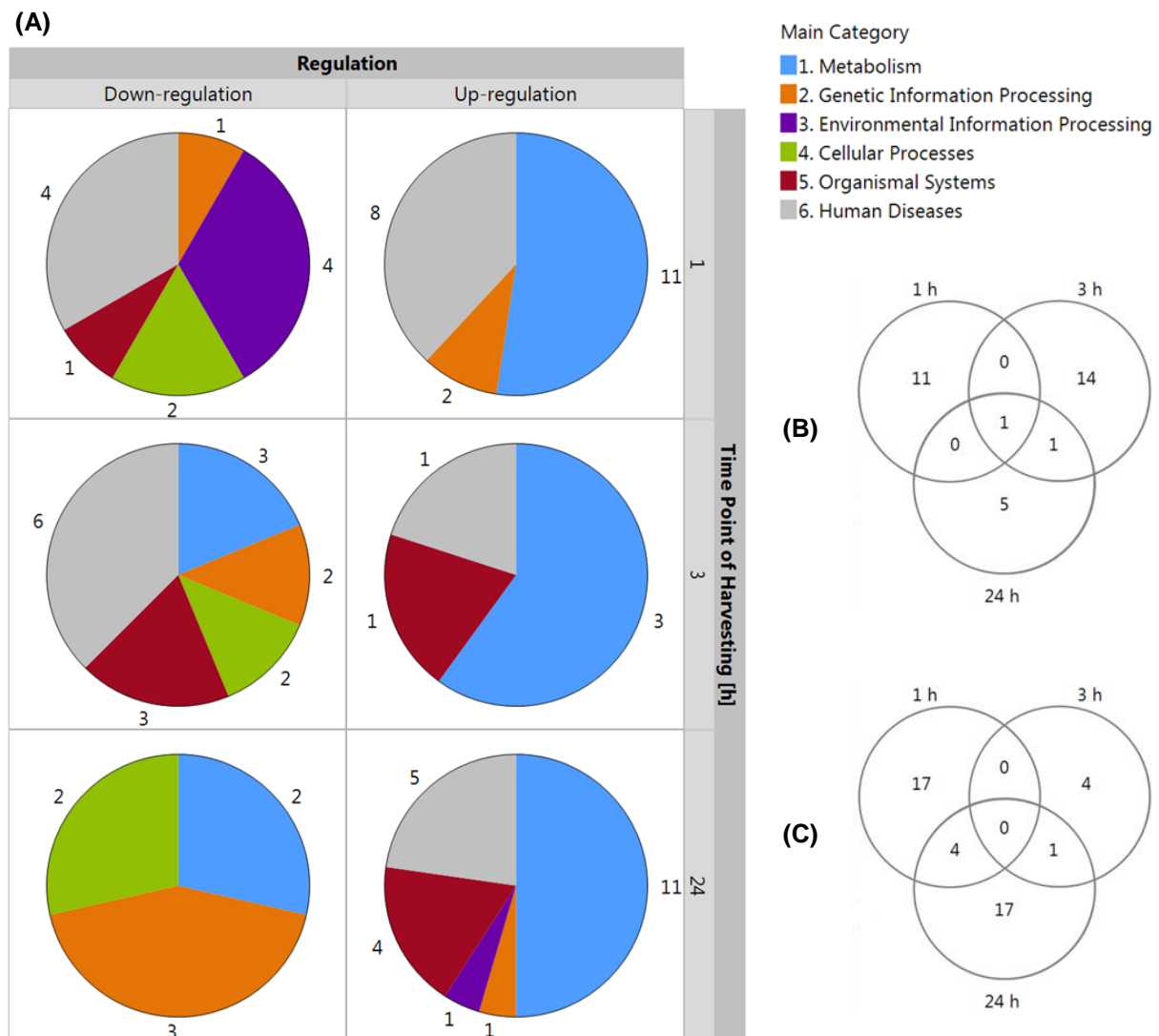


Figure 43: (A) Distribution of significantly enriched pathways (nominal p -value < 0.05), either up-regulated ($NES > 0$) or down-regulated ($NES < 0$), within the KEGG main categories and comparison of significant pathway lists with **(B)** $NES < 0$ and **(C)** $NES > 0$ at different harvesting time points following a single continuous blue light treatment of NHDF cells with 5.4 J/cm^2 .

Compared to 5.4 J/cm^2 , the higher blue light dose of 21.6 J/cm^2 yielded less changes in metabolic processes showing a constant number of significantly down-regulated pathways throughout the different harvesting time points. Moreover, from 3 hours after irradiation, down-regulated gene sets were found in all KEGG categories, with the highest number of significantly enriched pathways belonging to the main category of human diseases. Contrary to down-regulated gene sets, up-regulated pathways affected less categories, while they still revealed a greater variety compared to the lower light dose of 5.4 J/cm^2 (Figure 43). Corresponding Venn diagrams indicated only two significantly down-regulated gene sets shared in common at 3 hours and 24 hours after blue light irradiation, with one of them representing the ECM-receptor interaction of the main category 'environmental information processing' (Figure 44).

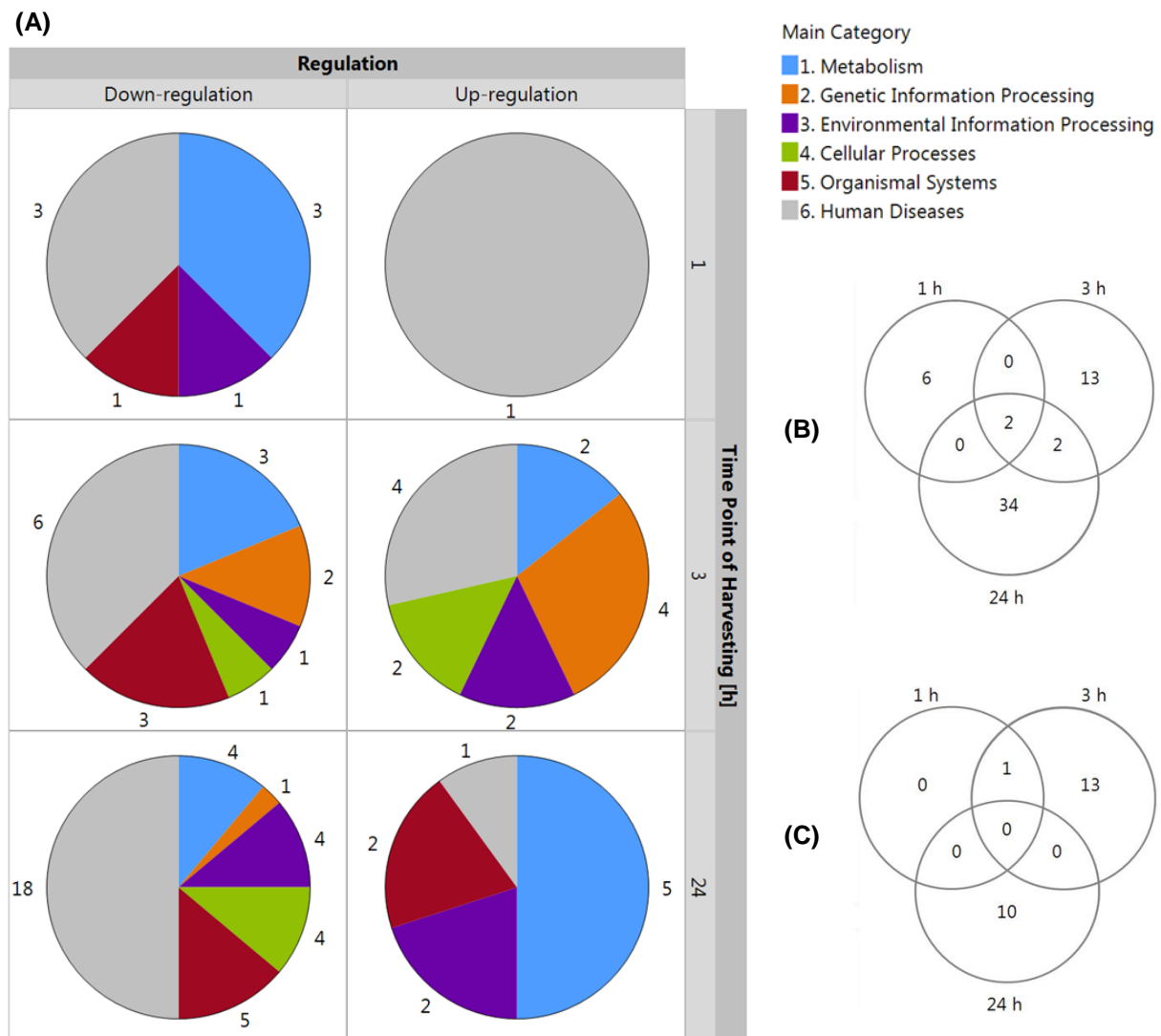


Figure 44: (A) Distribution of significantly enriched pathways (nominal p-value < 0.05), either up-regulated (NES > 0) or down-regulated (NES < 0), within the KEGG main categories and comparison of significant pathway lists with (B) NES < 0 and (C) NES > 0 at different harvesting time points following a single continuous blue light treatment of NHDF cells with 21.6 J/cm².

In addition, Venn diagrams were used in order to determine relations between both irradiation doses at each respective harvesting time. Thereby, de-regulated pathways equally modulated by both irradiation doses were found at 3 hours and 24 hours of harvesting. However, no commonly affected up- and down-regulated pathways were observed at 1 hour after blue light treatment. Significantly enriched gene sets shared in common are listed in Table 12 subdivided by the harvesting time point and the type of regulation.

Table 12: Up- and down-regulated pathways (nominal p-value < 0.05) commonly affected at different harvesting time points after continuous blue light treatment of NHDF cells with 5.4 J/cm² or 21.6 J/cm².

		Dose [J/cm ²]	5.4			21.6		
Time Point [h]		Pathway	NES	Nom. p-val	Adj. p-val.	NES	Nom. p-val	Adj. p-val.
3	↓	Alzheimer's disease	-1.46	0.018	0.418	-1.88	0.000	0.014
		Complement and coagulation cascades	-1.48	0.026	0.430	-1.37	0.026	0.445
		Huntington's disease	-1.72	0.000	0.091	-1.83	0.000	0.017
		Non-alcoholic fatty liver disease (NAFLD)	-1.36	0.020	0.614	-1.52	0.004	0.237
		Oxidative phosphorylation	-1.74	0.000	0.102	-2.10	0.000	0.001
		Parkinson's disease	-1.94	0.000	0.033	-2.10	0.000	0.001
		Ribosome	-1.84	0.000	0.065	-1.89	0.000	0.014
	↑	MicroRNAs in cancer	1.80	0.000	0.100	1.74	0.000	0.062
24	↓	Adherens junction	-1.34	0.049	0.733	-1.40	0.031	0.260
	↑	Arylhydrocarbon receptor (AhR) signaling pathway	1.81	0.002	0.041	1.80	0.000	0.057
		Chemical carcinogenesis	1.81	0.000	0.031	1.92	0.000	0.024
		Glycolysis/ Gluconeogenesis	1.67	0.000	0.118	1.49	0.018	0.311
		Metabolism of xenobiotics by cytochrome P450	2.04	0.000	0.006	1.72	0.002	0.086
		Ovarian steroidogenesis	1.50	0.035	0.206	1.44	0.047	0.347

At 3 hours after irradiation, several pathways belonging to the main category 'human diseases' like Alzheimer's disease, Parkinson's disease or Huntington's disease were down-regulated. Despite their link to certain diseases, all of these gene sets involve a mitochondrial pathway related to changes in ROS and ATP production as well as modulations of $\Delta\Psi_m$ indicating mitochondrial function. In this context, also oxidative phosphorylation was found to be down-regulated after treatment with both irradiation doses. In contrast, several up-regulated pathways were equally affected at 24 hours following irradiation including glycolysis/gluconeogenesis, ovarian steroidogenesis, chemical carcinogenesis, the arylhydrocarbon receptor (AhR) signaling pathway as well as the metabolism of xenobiotics by cytochrome P450. The last three signaling pathways involve a number of oxidative stress-dependent nuclear factor erythroid 2-related factor 2 (Nrf2)-transcribed genes encoding phase II detoxification enzymes, such as glutathione S-transferases (GST) and UDP-glucuronosyltransferases (UGT). Moreover, several genes encoding phase I xenobiotic-metabolizing enzymes (XMEs), for instance cytochrome P450 (CYP) monooxygenases, were up-regulated. Besides GST and UGT gene families, gene expression analyses performed for different harvesting time points after irradiation with either 5.4 J/cm² or 21.6 J/cm² revealed also other Nrf2-transcribed genes, which were significantly de-regulated (Figure 45). Besides *ALDH3A1* and *NQO1*, respectively encoding the phase II XMEs aldehyde dehydrogenase 3 family member A1 as well as NAD(P)H quinone dehydrogenase 1,

GCLC, *GCLM*, *HMOX1*, *TXNRD1*, *TXNRD2* and *SRXN1* represent important genes, which promote antioxidant defense, while the latter mainly detoxify peroxides like H_2O_2 . Whereas at 1 hour following blue light treatment with both doses, only a few genes were found significantly up-regulated, most of them showed an increased expression after 3 hours and 24 hours of harvesting. Especially after irradiation with $21.6 J/cm^2$, *ALDH3A1*, *NQO1*, *GCLM*, *HMOX1* and *TXNRD1* were highly expressed, whereas expression levels remained rather constant using $5.4 J/cm^2$ of blue light (Figure 45). Nonetheless, some of these genes were commonly affected (Figure 41).

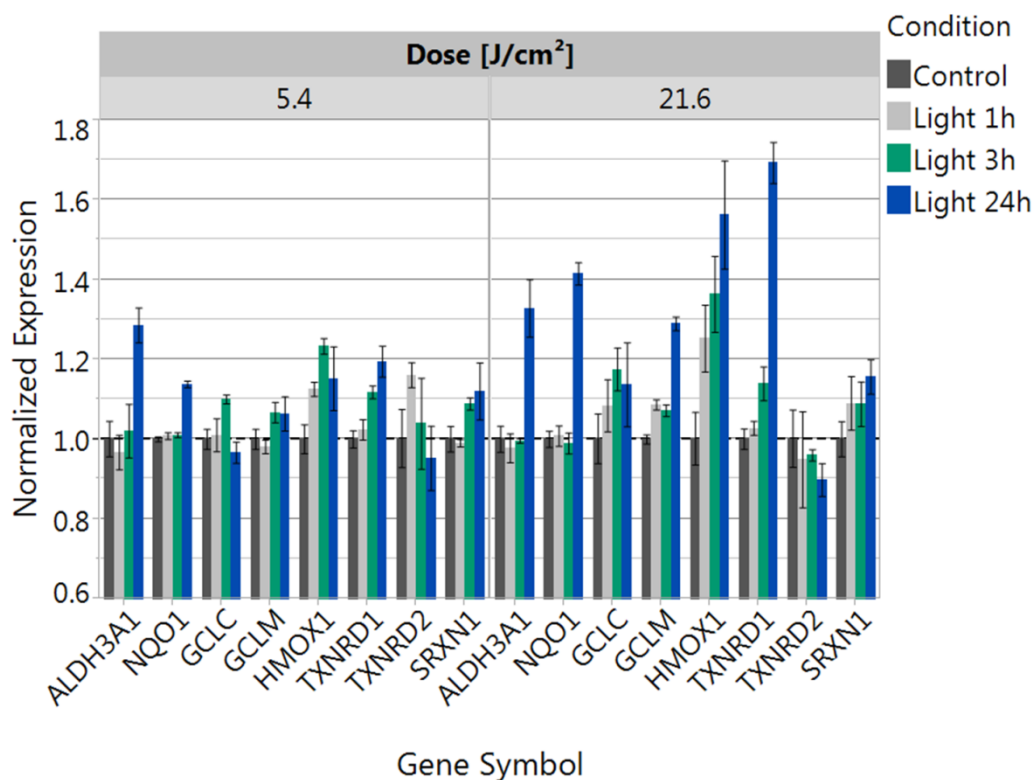


Figure 45: Expression changes of a selection of Nrf2-transcribed genes for different harvesting time points following a single continuous blue light treatment of NHDF cells with either $5.4 J/cm^2$ or $21.6 J/cm^2$.

Besides metabolic processes involving genes dedicated to detoxification and thus cell protection, many pathways belonging to the KEGG main category 'metabolism' were highly affected by light irradiation, especially at 1 hour and 24 hours following blue light treatment with $5.4 J/cm^2$ (Figure 43). With respect to KEGG subcategories, the metabolism of various molecules like carbohydrates, amino acids, glycans, lipids and terpenoids was modulated. However, the only significantly enriched gene set, which was continuously expressed at all harvesting time points following $5.4 J/cm^2$ of blue light was oxidative phosphorylation. Although it was enhanced at 1 hour and 24 hours following irradiation, it was down-regulated at 3 hours of cell harvesting.

Table 13 depicts metabolic pathways significantly enriched (nominal p-value < 0.05) at different time points after blue light treatment using (A) 5.4 J/cm² or (B) 21.6 J/cm².

Table 13: Significantly de-regulated KEGG pathways (nominal p-value < 0.05) of the main category 'metabolism' at different time points after continuous blue light treatment of NHDF cells with (A) 5.4 J/cm² or (B) 21.6 J/cm². Up-regulated pathways are indicated by NES > 0; down-regulated pathways show NES < 0.

(A)

Time Point [h]	Sub Category	Pathway	NES	Nom. p-val.	Adj. p-val.
1	1.8 Metabolism of cofactors and vitamins	Nicotinate and nicotinamide metabolism	1.83	0.006	0.116
1	1.9 Metabolism of terpenoids and polyketides	Terpenoid backbone biosynthesis	1.69	0.008	0.169
1	1.7 Glycan biosynthesis and metabolism	Glycosaminoglycan biosynthesis - HS/Hep	1.67	0.010	0.149
1	1.3 Lipid metabolism	Glycerophospholipid metabolism	1.60	0.002	0.190
1	1.7 Glycan biosynthesis and metabolism	Glycosylphosphatidylinositol(GPI)-anchor biosynthesis	1.58	0.024	0.171
1	1.5 Amino acid metabolism	Glycine, serine and threonine metabolism	1.56	0.023	0.185
1	1.1 Carbohydrate metabolism	Glyoxylate and dicarboxylate metabolism	1.55	0.031	0.183
1	1.1 Carbohydrate metabolism	Galactose metabolism	1.54	0.026	0.174
1	1.5 Amino acid metabolism	Alanine, aspartate and glutamate metabolism	1.44	0.037	0.313
1	1.7 Glycan biosynthesis and metabolism	N-Glycan biosynthesis	1.43	0.040	0.337
1	1.2 Energy metabolism	Oxidative phosphorylation	1.39	0.033	0.362
3	1.5 Amino acid metabolism	Arginine Biosynthesis	1.64	0.014	0.271
3	1.1 Carbohydrate metabolism	Propanoate metabolism	1.52	0.039	0.533
3	1.7 Glycan biosynthesis and metabolism	Glycosphingolipid biosynthesis - lacto and neolacto series	1.48	0.039	0.540
3	1.7 Glycan biosynthesis and metabolism	Mucin type O-Glycan biosynthesis	-1.53	0.034	0.352
3	1.7 Glycan biosynthesis and metabolism	Glycosaminoglycan biosynthesis - KS	-1.70	0.010	0.093
3	1.2 Energy metabolism	Oxidative phosphorylation	-1.74	0.000	0.102
24	1.11 Xenobiotics biodegradation and metabolism	Metabolism of xenobiotics by cytochrome P450	2.04	0.000	0.006
24	1.1 Carbohydrate metabolism	Galactose metabolism	1.98	0.000	0.007
24	1.11 Xenobiotics biodegradation and metabolism	Arylhydrocarbon receptor (AhR) signaling pathway	1.81	0.002	0.041
24	1.1 Carbohydrate metabolism	Glycolysis / Gluconeogenesis	1.67	0.000	0.118
24	1.5 Amino acid metabolism	Histidine metabolism	1.59	0.010	0.173
24	1.11 Xenobiotics biodegradation and metabolism	Drug metabolism - cytochrome P450	1.59	0.006	0.157
24	1.6 Metabolism of other amino acids	beta-Alanine metabolism	1.56	0.014	0.166
24	1.5 Amino acid metabolism	Phenylalanine metabolism	1.55	0.030	0.167
24	1.1 Carbohydrate metabolism	Fructose and mannose metabolism	1.49	0.041	0.203
24	1.1 Carbohydrate metabolism	Amino sugar and nucleotide sugar metabolism	1.46	0.022	0.211
24	1.2 Energy metabolism	Oxidative phosphorylation	1.33	0.040	0.423
24	1.7 Glycan biosynthesis and metabolism	Mucin type O-Glycan biosynthesis	-1.58	0.019	0.502
24	1.5 Amino acid metabolism	Valine, leucine and isoleucine degradation	-1.66	0.011	0.480

(B)

Time Point [h]	Sub Category	Pathway	NES	Nom. p-val.	Adj. p-val.
1	1.5 Amino acid metabolism	Tyrosine metabolism	-1.40	0.045	0.917
1	1.5 Amino acid metabolism	Valine, leucine and isoleucine degradation	-1.51	0.022	0.600
1	1.6 Metabolism of other amino acids	Selenocompound metabolism	-1.52	0.045	0.709
3	1.3 Lipid metabolism	Linoleic acid metabolism	1.68	0.010	0.088
3	1.3 Lipid metabolism	alpha-Linolenic acid metabolism	1.51	0.045	0.304
3	1.4 Nucleotide metabolism	Purine metabolism	-1.40	0.011	0.398
3	1.1 Carbohydrate metabolism	Galactose metabolism	-1.52	0.015	0.252
3	1.2 Energy metabolism	Oxidative phosphorylation	-2.10	0.000	0.001
24	1.11 Xenobiotics biodegradation and metabolism	Arylhydrocarbon receptor (AhR) signaling pathway	1.80	0.000	0.057
24	1.11 Xenobiotics biodegradation and metabolism	Metabolism of xenobiotics by cytochrome P450	1.72	0.002	0.086
24	1.9 Metabolism of terpenoids and polyketides	Terpenoid backbone biosynthesis	1.63	0.015	0.122
24	1.1 Carbohydrate metabolism	Glycolysis / Gluconeogenesis	1.49	0.018	0.311
24	1.6 Metabolism of other amino acids	Glutathione metabolism	1.48	0.031	0.284
24	1.7 Glycan biosynthesis and metabolism	N-Glycan biosynthesis	-1.49	0.028	0.291
24	1.7 Glycan biosynthesis and metabolism	Glycosaminoglycan degradation	-1.54	0.038	0.323
24	1.0 Global and overview maps	2-Oxocarboxylic acid metabolism	-1.84	0.004	0.051
24	1.7 Glycan biosynthesis and metabolism	Glycosaminoglycan biosynthesis - HS/Hep	-1.93	0.000	0.027

Whereas a remarkable number of metabolic pathways was differentially expressed by blue light, gene sets related to cell growth, replication, proliferation, cell survival and signal transduction were hardly found to be significantly enriched. However, with respect to the KEGG subcategory 2.4 involving replication and repair processes, the base excision repair pathway was continuously up-regulated following blue light irradiation with 5.4 J/cm², which was significant at 1 hour of harvesting. In contrast, homologous recombination was found to be significantly down-regulated at 1 hour after irradiation (Table 14, (A)). When using the higher blue light dose of 21.6 J/cm², two repair processes, homologous recombination and the Fanconi anemia pathway, showed constant up-regulation, with significant effects at 3 hours after blue light treatment (Table 14, (B)). Other DNA repair mechanisms such as mismatch and nucleotide excision repair were not significantly modulated by blue light.

Table 14: KEGG pathways belonging to the main category: 2. Genetic Information Processing, and subcategory: 2.4 Replication and repair de-regulated at different time points after continuous blue light treatment of NHDF cells with either (A) 5.4 J/cm² or (B) 21.6 J/cm². Significantly enriched pathways are indicated by a nominal p-value < 0.05.

(A) 5.4 J/cm² of blue light

Pathway	Time Point of Harvesting [h]								
	1			3			24		
	NES	Nom. p-val.	Adj. p-val.	NES	Nom. p-val.	Adj. p-val.	NES	Nom. p-val.	Adj. p-val.
DNA replication	0.73	0.860	1.000	-0.65	0.970	1.000	1.1	0.300	0.729
Mismatch repair	-0.75	0.832	1.000	0.68	0.907	1.000	-0.86	0.643	1.000
Base excision repair	1.6	0.020	0.170	0.71	0.907	1.000	1.05	0.396	0.761
Nucleotide excision repair	-0.88	0.678	1.000	0.77	0.829	1.000	-1.25	0.149	0.812
Homologous recombination	-1.52	0.034	1.000	0.67	0.925	1.000	-1.25	0.139	0.835
Fanconi anemia pathway	-1.11	0.275	1.000	1.18	0.206	1.000	-1.43	0.051	0.742

(B) 21.6 J/cm² of blue light

Pathway	Time Point of Harvesting [h]								
	1			3			24		
	NES	Nom. p-val.	Adj. p-val.	NES	Nom. p-val.	Adj. p-val.	NES	Nom. p-val.	Adj. p-val.
DNA replication	1.03	0.393	1.000	1.06	0.350	0.868	-0.86	0.685	0.909
Mismatch repair	-1.04	0.416	1.000	0.74	0.852	0.989	-0.75	0.834	0.980
Base excision repair	-0.95	0.531	1.000	-1.15	0.233	0.715	-1.03	0.409	0.728
Nucleotide excision repair	0.64	0.968	1.000	1.08	0.344	0.870	-0.66	0.967	0.993
Homologous recombination	1.18	0.233	1.000	1.49	0.038	0.330	0.84	0.728	1.000
Fanconi anemia pathway	1.12	0.277	1.000	1.81	0.000	0.040	1.22	0.141	0.633

In addition, contrary effects on DNA replication were noted at 24 hours of harvesting, with 5.4 J/cm² of blue light stimulating DNA replication, while the higher irradiation dose of 21.6 J/cm² blocked new DNA synthesis (Table 14). Dose-dependent blue light effects on cell growth and proliferation were further confirmed by the cell cycle pathway. While the lower dose of 5.4 J/cm² revealed a continuous but non-significant up-regulation of the cell cycle, the gene set was down-regulated for the higher dose of 21.6 J/cm², apart from 3 hours of cell harvesting showing significant up-regulation (Table 15). Apparently, the higher expression of the cell cycle pathway following 21.6 J/cm² of blue light was accompanied by a significantly up-regulated p53 signaling pathway, which was conversely found to be significantly down-regulated at 24 hours following blue light treatment with 5.4 J/cm². Furthermore, two apoptosis pathways were found up-regulated in most cases for both blue light doses, although statistical significance was hardly achieved. However, shortly after treating NHDF cells with 5.4 J/cm², the apoptosis pathway for mammals (multiple species) was significantly down-regulated at 3 hours of harvesting, rather involving genes linked to the intrinsic apoptosis pathway affecting mitochondria (Table 15, (A)).

Table 15: KEGG pathways belonging to the main category: 4. Cellular processes, and subcategory: 4.3 Cell growth and death de-regulated at different time points after continuous blue light treatment of NHDF cells with either (A) 5.4 J/cm² or (B) 21.6 J/cm². Significantly enriched pathways are indicated by a nominal p-value < 0.05.

(A) 5.4 J/cm² of blue light

Pathway	Time Point of Harvesting [h]								
	1			3			24		
	NES	Nom. p-val.	Adj. p-val.	NES	Nom. p-val.	Adj. p-val.	NES	Nom. p-val.	Adj. p-val.
Cell cycle	0.93	0.654	0.927	0.92	0.649	1.000	0.85	0.848	0.990
p53 signaling pathway	1.18	0.190	0.639	0.89	0.648	1.000	-1.4	0.039	0.780
Apoptosis	0.86	0.807	0.927	0.64	1.000	1.000	0.94	0.583	0.944
Apoptosis - multiple species	1.32	0.112	0.467	-1.46	0.043	0.453	0.82	0.765	1.000

(B) 21.6 J/cm² of blue light

Pathway	Time Point of Harvesting [h]								
	1			3			24		
	NES	Nom. p-val.	Adj. p-val.	NES	Nom. p-val.	Adj. p-val.	NES	Nom. p-val.	Adj. p-val.
Cell cycle	-0.78	0.924	1.000	1.43	0.011	0.359	-0.80	0.897	0.953
p53 signaling pathway	0.87	0.709	1.000	2.03	0.000	0.002	-1.00	0.434	0.735
Apoptosis	0.87	0.780	1.000	1.16	0.169	0.786	-1.21	0.118	0.448
Apoptosis - multiple species	1.01	0.431	1.000	1.12	0.309	0.845	1.00	0.440	0.998

In addition, the regulation of several signal transduction pathways such as the AMPK, MAPK, NF-kappa B (NF-κB), PI3K-Akt, TGF-β and the TNF signaling pathway, which are known to be involved in the regulation of cell metabolism, growth, proliferation, apoptosis, survival, immune cell recruitment and cell interactions, were compared for both blue light doses. Similar expression changes over time were observed for the FoxO and Jak-STAT signaling pathways showing alternating regulation as well as for the mTOR and PI3K-Akt signaling pathways, which were characterized by constant down-regulation. For the TGF-β signaling pathway, time-dependent changes were contrary for both blue light doses, 5.4 J/cm² and 21.6 J/cm² (Table 16). Furthermore, the NF-κB signaling pathway was activated directly after irradiation with both doses, with a significant up-regulation at 3 hours following continuous blue light treatment using 21.6 J/cm² (Table 16, (B)). However, in the following time course, at 24 hours of harvesting, the pathway was down-regulated for both irradiation doses. Moreover, the TNF signaling pathway was continuously up-regulated after irradiation with 5.4 J/cm². However, the latter was found significantly up-regulated at 24 hours after blue light treatment with 21.6 J/cm², whereas the Wnt signaling pathway was constantly down-regulated (Table 16).

Table 16: KEGG pathways belonging to the main category: 3. Environmental Information Processing, and subcategory: 3.2 Signal transduction de-regulated at different time points after continuous blue light treatment of NHDF cells with either (A) 5.4 J/cm² or (B) 21.6 J/cm². Significantly enriched pathways are indicated by a nominal p-value < 0.05.

(A) 5.4 J/cm² of blue light

Pathway	Time Point of Harvesting [h]								
	1			3			24		
	NES	Nom. p-val.	Adj. p-val.	NES	Nom. p-val.	Adj. p-val.	NES	Nom. p-val.	Adj. p-val.
AMPK signaling pathway	-1.28	0.056	0.676	-1.03	0.369	0.963	1.14	0.202	0.736
ErbB signaling pathway	-0.74	0.943	1.000	-0.98	0.490	0.967	1.19	0.173	0.641
FoxO signaling pathway	-0.99	0.462	1.000	0.92	0.641	1.000	-0.85	0.814	1.000
Jak-STAT signaling pathway	-0.75	0.968	1.000	0.84	0.830	1.000	-1.09	0.265	1.000
MAPK signaling pathway	0.83	0.907	0.962	-1.03	0.345	0.946	-0.85	0.905	1.000
mTOR signaling pathway	-1.51	0.021	1.000	-0.97	0.524	0.952	-0.81	0.823	1.000
NF-kappa B signaling pathway	0.96	0.535	0.901	1.19	0.153	1.000	-0.79	0.886	1.000
PI3K-Akt signaling pathway	-1.03	0.360	1.000	-0.93	0.733	1.000	-1.02	0.390	1.000
TGF-β signaling pathway	0.72	0.970	1.000	-1.21	0.137	0.798	0.85	0.801	0.984
TNF signaling pathway	1.09	0.292	0.673	0.86	0.751	1.000	1.11	0.231	0.749
VEGF signaling pathway	0.85	0.716	0.938	0.68	0.965	1.000	1.08	0.313	0.742
Wnt signaling pathway	0.93	0.614	0.921	-0.86	0.816	1.000	1.22	0.100	0.599

(B) 21.6 J/cm² of blue light

Pathway	Time Point of Harvesting [h]								
	1			3			24		
	NES	Nom. p-val.	Adj. p-val.	NES	Nom. p-val.	Adj. p-val.	NES	Nom. p-val.	Adj. p-val.
AMPK signaling pathway	0.74	0.971	1.000	-1.13	0.195	0.737	-0.96	0.545	0.784
ErbB signaling pathway	-0.96	0.526	1.000	1.33	0.065	0.478	-0.73	0.937	0.986
FoxO signaling pathway	-0.95	0.592	1.000	1.43	0.011	0.338	-0.90	0.698	0.857
Jak-STAT signaling pathway	-1.39	0.013	0.915	0.93	0.634	0.885	-1.06	0.306	0.680
MAPK signaling pathway	-1.01	0.417	1.000	0.98	0.499	0.833	-0.96	0.582	0.789
mTOR signaling pathway	-1.04	0.375	1.000	-1.18	0.177	0.640	-0.81	0.815	0.948
NF-kappa B signaling pathway	0.86	0.740	1.000	1.45	0.020	0.336	-0.90	0.647	0.851
PI3K-Akt signaling pathway	-1.06	0.270	1.000	-1.05	0.296	0.734	-1.47	0.000	0.237
TGF- β signaling pathway	-0.78	0.889	1.000	1.00	0.433	0.889	-0.94	0.545	0.799
TNF signaling pathway	-1.09	0.286	1.000	1.02	0.410	0.912	1.34	0.037	0.452
VEGF signaling pathway	-0.75	0.893	1.000	0.91	0.627	0.924	0.86	0.727	1.000
Wnt signaling pathway	-0.84	0.871	1.000	-1.19	0.101	0.633	-1.23	0.099	0.452

Although listed KEGG pathways hardly showed significant expression, especially with respect to signal transduction processes, trends in gene expression changes will be discussed with particular focus on metabolic control, proliferation, stress response and cell survival.

3.2 MEDILIGHT system

In April 2018, the first generation of prototypes was finalized and distributed to the consortium partners. To prove their efficacy and validate their use for subsequent *in vivo* studies, blue light effects on metabolic activity, found after irradiation with the BioLight LED Lamp, had to be confirmed. Since the system was still a first prototype, many issues were occurring, especially in the early period of testing, necessitating a few modifications and optimizations, in particular with respect to thermal properties.

3.2.1 Temperature measurements

As heat management represents an important issue for patient safety, temperature measurements were performed with integrated as well as external sensors using two different irradiance values. The latter were based on different blue light applications throughout single wound healing stages. Whereas an irradiance of 12 mW/cm² was intended to accelerate granulation and epidermization by promoting the activity of different skin cell types, 23 mW/cm² were identified to induce antibacterial effects. However, operating the flexible LED foil in continuous mode yielding 23 mW/cm² underneath the entire component stack resulted in a fast temperature rise on human skin, which finally induced thermal hyperalgesia. Thus, worst case scenarios were subsequently tested on a skin-like polymer from URGO RID (Chenôve, France).

The required irradiance values of 10 mW/cm² and 23 mW/cm², resulting underneath the entire component stack including back-reflector, diffusor and the wound dressing E2723, were given at DCs of 25% and 78%. With an irradiance of 10 mW/cm² the maximum temperature reached at the center of the flexible LED foil and external sensor #2 was approximately 39°C, while external sensor #1 showed a rise up to 41°C at the polymer surface. Whereas these values were close to the set threshold of 40°C, the higher irradiance of 23 mW/cm² resembled a maximum temperature of 52°C on the LED array and about 51°C at the polymer (Figure 46, (A)). Therefore, in order to prevent the risk of thermal hyperalgesia, irradiation had to be fractionated in cycles to enable the LED foil and consequently the patient's skin to cool down. By pausing irradiation with cycles of 1 minute at 10 mW/cm², temperature maxima of all sensors were reduced to a range between 35°C and 37°C (Figure 46, (B)).

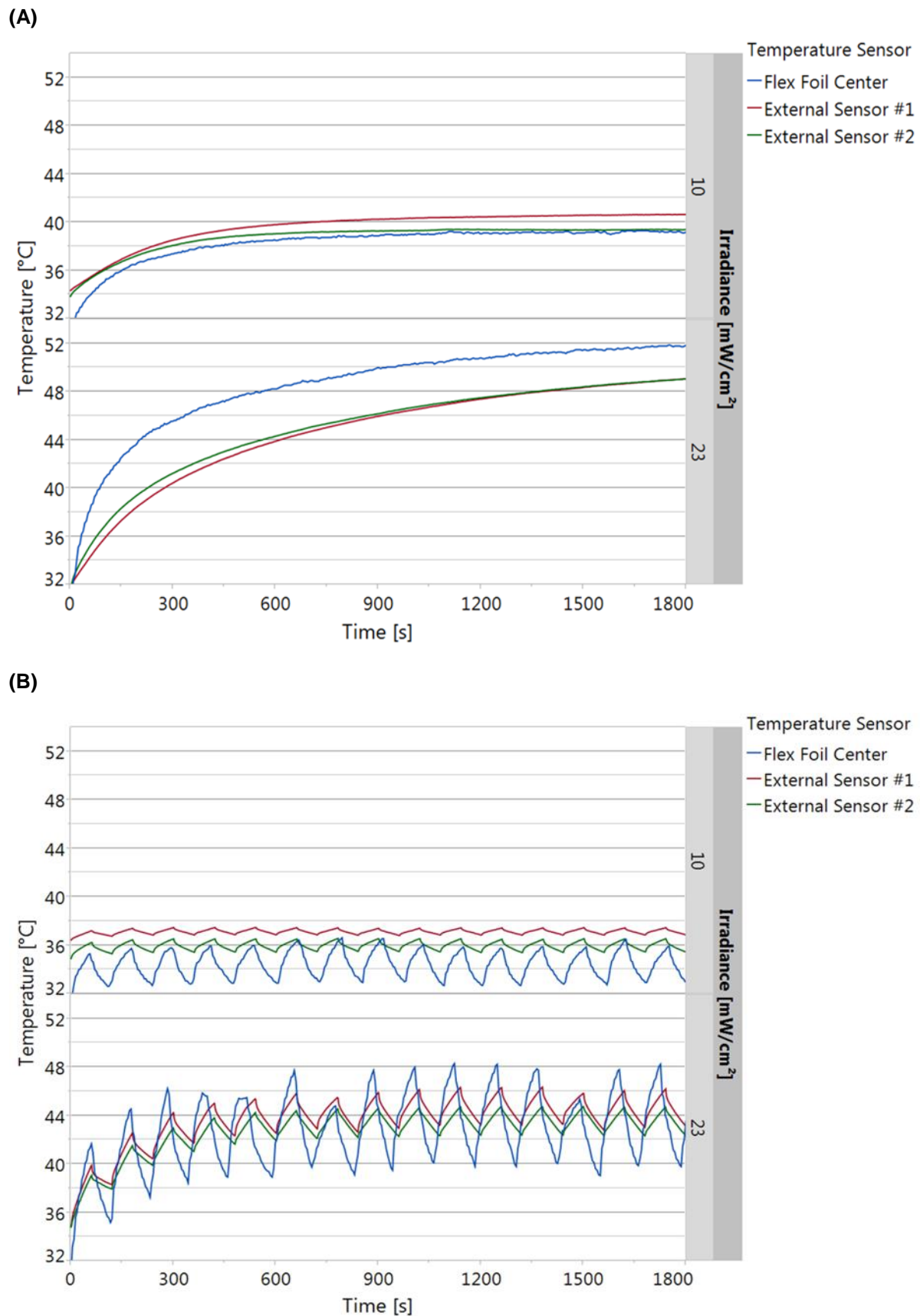


Figure 46: Temperature measurements using the flexible LED foil equipped with back-reflector on a skin-like polymer with $10 \text{ mW}/\text{cm}^2$ (25% DC) or $23 \text{ mW}/\text{cm}^2$ (78% DC) in (A) continuous or (B) cycled mode (cycles of 1 minute). Irradiances were adjusted underneath the complete stack involving the diffusor and the wound dressing E2723. In total, three sensors are shown: The safety temperature sensor integrated onto the LED array (Flex Foil Center) and two external sensors #1 and #2 placed underneath E2723 on the polymer surface.

With the higher irradiance of 23 mW/cm^2 , the safety temperature sensor on the LED foil showed a temperature increase up to 48°C , while both external sensors recorded approximately 46°C at maximum (Figure 46, (B)). Although cooling rates of the LED array and the polymer seemed to be fast, the recorded temperature maxima reached were still highly above the threshold set at 40°C . Moving to a more realistic set-up enabling heat transfer by blood circulation, temperature profiles at 23 mW/cm^2 were tested on porcine skin. In Figure 47, the maximum skin temperature measured by both external sensors was limited to 37°C leading to a temperature rise of 45°C on the LED array. While the sensors located at the periphery of the LED foil showed constant values of $32^\circ\text{C} - 34^\circ\text{C}$, the recordings of the central safety sensor revealed cycles of 30 seconds. The LED foil was still able to cool down fast (Figure 47).

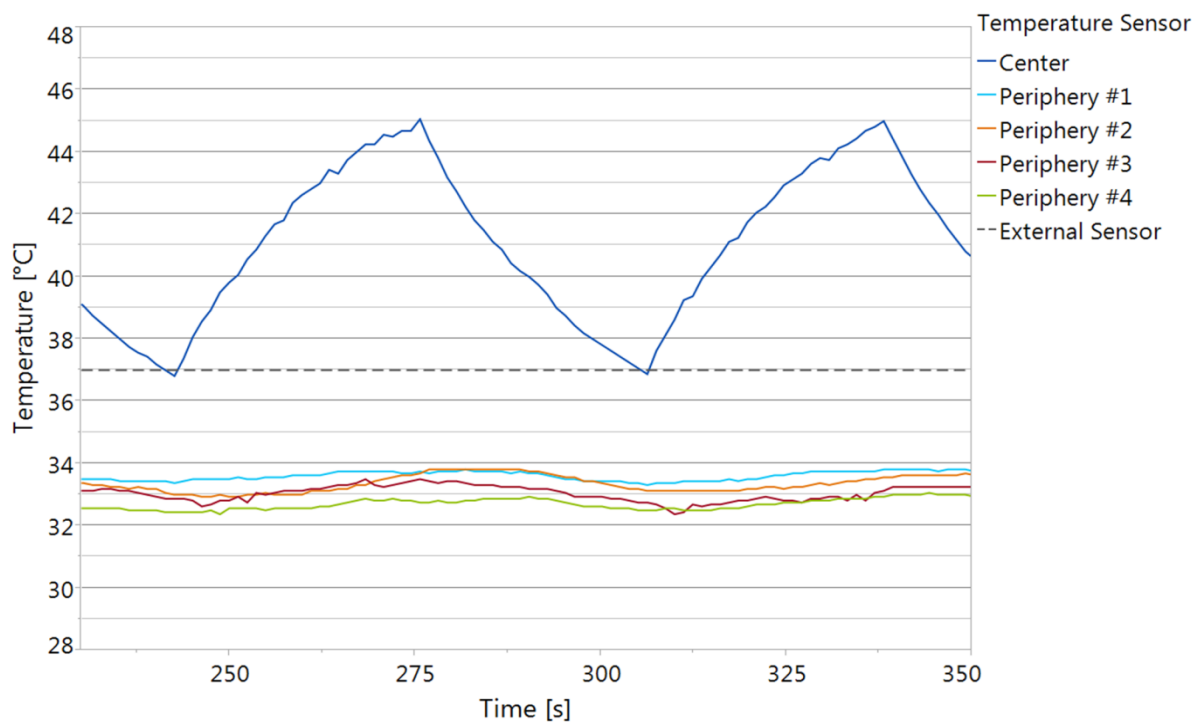


Figure 47: Temperature measurement using the flexible LED foil equipped with back-reflector on porcine skin with 23 mW/cm^2 (62% DC). Irradiance was adjusted underneath the complete stack involving the wound dressing E2723, but excluding the diffusor. Five different sensors are shown: One sensor in the center of the flexible LED foil (dark blue) and 4 different sensors at the borders of the foil (light blue, orange, red and green).

Coming back to *in vitro* validation tests, the irradiance underneath the complete stack was adjusted to 23 mW/cm^2 given at the plate surface. Due to light absorption by the set-up (black plate, lid, etc.), NHDF cells received about 12 mW/cm^2 (see 2.2.2.1). With a 68% DC and cycles of 30 seconds, the safety sensor on the LED foil showed a maximum temperature of 35°C measured at the plate surface, which stayed below the incubation temperature of 37°C . Thus, induction of heat stress could be excluded.

3.2.2 *In vitro* validation of prototypes

In order to validate the prototype's use for subsequent *in vivo* studies, several blue light doses with a maximum value of 43.2 J/cm^2 , previously applied with the BioLight LED Lamp, were investigated once again with the MEDILIGHT system. Similar to Figure 20, blue light effects on cell metabolism were evaluated at 24 hours after light treatment using the colorimetric XTT Cell Viability Kit. As described in 2.2.2.2, blue light irradiation was either performed through the wound dressing E2723 at 68% DC or the diffusor at 38% DC with 23 mW/cm^2 adjusted underneath each respective component stack. In comparison to Figure 20, Figure 48 depicts a less pronounced increase in metabolic activity following a single irradiation with 5.4 J/cm^2 of 450 nm blue light (2.50% ($p < 0.0001$) with diffusor and 1.95% ($p = 0.0032$) with E2723).

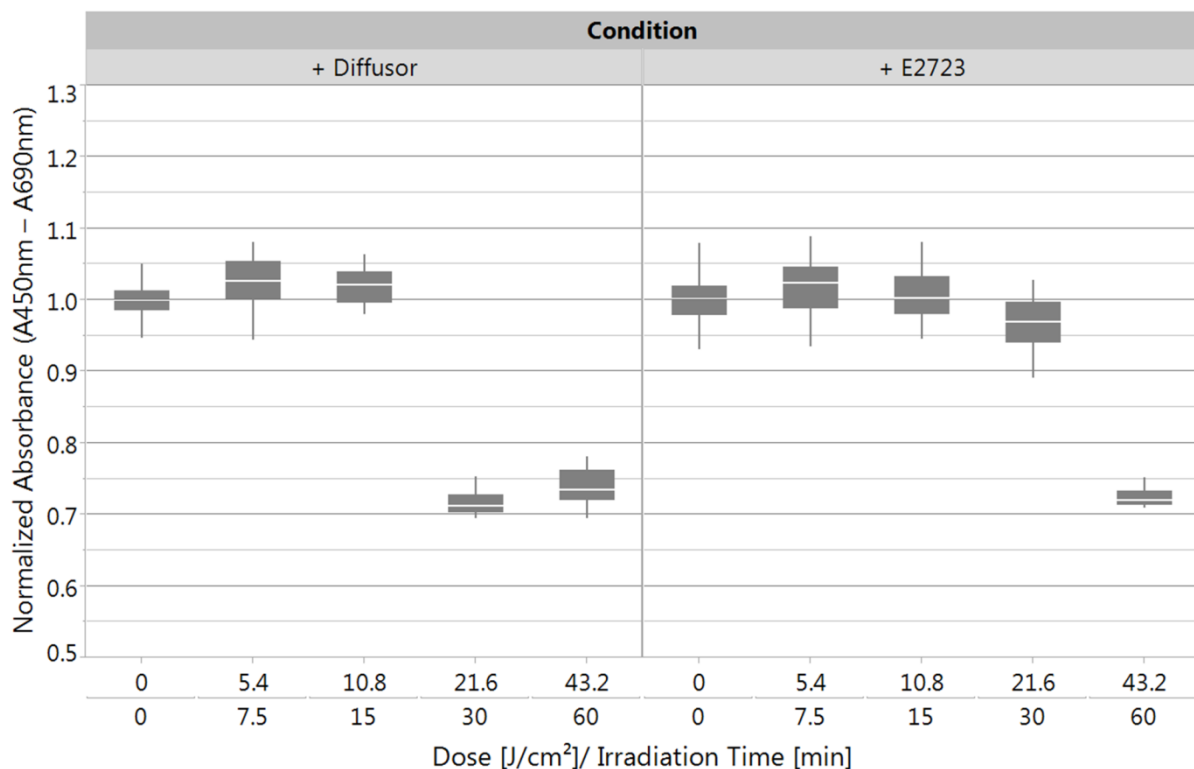


Figure 48: Changes in the metabolic activity of NHDF cells following different blue light doses with a constant time point of XTT testing at 24 hours after irradiation. Continuous irradiation using the silicone-encapsulated flexible LED foil was either performed through the diffusor or the wound dressing E2723 providing a homogenous illumination field. Irradiance was adjusted to 23 mW/cm^2 underneath the respective component stacks yielding a DC of 38% with the diffusor and 68% with E2723. Fold changes were evaluated versus time-matched, non-irradiated controls. Data are presented as mean \pm SD ($N = 3$ repetitions, 3 replicates). Corresponding statistics are summarized in Table 29 (Appendix).

Moreover, for both conditions, the mitochondrial activity of NHDF cells was hardly affected by 10.8 J/cm^2 of blue light, although this dose represented the inflection point from stimulatory to inhibitory effects in Figure 20. However, using an irradiation dose of 21.6 J/cm^2 , blue light treatment through the diffusor decreased the cellular metabolism by 28.21% ($p < 0.0001$), whereas through the dressing E2723 a reduction by 3.42% ($p = 0.0001$) was found compared to the non-irradiated control. Blue light irradiation with 43.2 J/cm^2 compensated the effect at around 70% – 75% ($p < 0.0001$) of cell activity being left after light treatment (Figure 48), which agrees to the outcome displayed in Figure 20. Thereby, the maximum temperature reached throughout blue light treatment through the diffusor was about 36°C . However, continuous irradiation through E2723 could no longer be performed since a predefined temperature safety threshold of 50°C was exceeded multiple times during operation resulting in a temporary shutdown of the LEDs. Moreover, NHDF cells were probably exposed to high temperatures ($> 37^\circ\text{C}$). In order to prevent temperature effects on cell activity and growth, defined irradiation schemes, derived from temperature profiles tested on the skin-like polymer and porcine skin (Figure 46, Figure 47), were evaluated *in vitro* using the XTT Cell Viability Kit.

Figure 49 depicts the XTT test results for NHDF cells, which were treated with the irradiation scheme specified in Figure 47, and a direct comparison to the outcomes, which had been obtained with the BioLight LED Lamp. However, it has to be noted that the light treatment with the BioLight LED Lamp was performed in continuous mode and without wound dressing, while the MEDILIGHT prototype was run in cycled mode (30-second cycles) irradiating the cells through E2723. Though, equal doses were applied by doubling the irradiation time for the latter. Moreover, the distance of the light sources to the surface of the 96-well plates was different. Nevertheless, both light sources provided an irradiance level of about 23 mW/cm^2 at the plate surface. Compared to continuous light treatment, cycled irradiation yielded stimulatory effects on cell metabolism at higher doses. Using the BioLight LED Lamp, the highest cell activity was given at a dose of 5.4 J/cm^2 (7.10%, $p < 0.0001$), whereas an increase of 4.71% ($p < 0.0001$) was found at 10.8 J/cm^2 with the MEDILIGHT prototype. Also, the stimulatory range was broadened from 3.6 J/cm^2 to 12.6 J/cm^2 . In the following, cell metabolism was reduced with a difference of about 10.0% ($p < 0.0001$) at 21.6 J/cm^2 of blue light, which was narrowed at higher doses of 32.4 J/cm^2 and 43.2 J/cm^2 .

With a maximum inhibition of mitochondrial activity by 25% – 30% ($p < 0.0001$), both curves showed a biphasic dose-response validating the functionality and efficacy of MEDILIGHT prototypes.

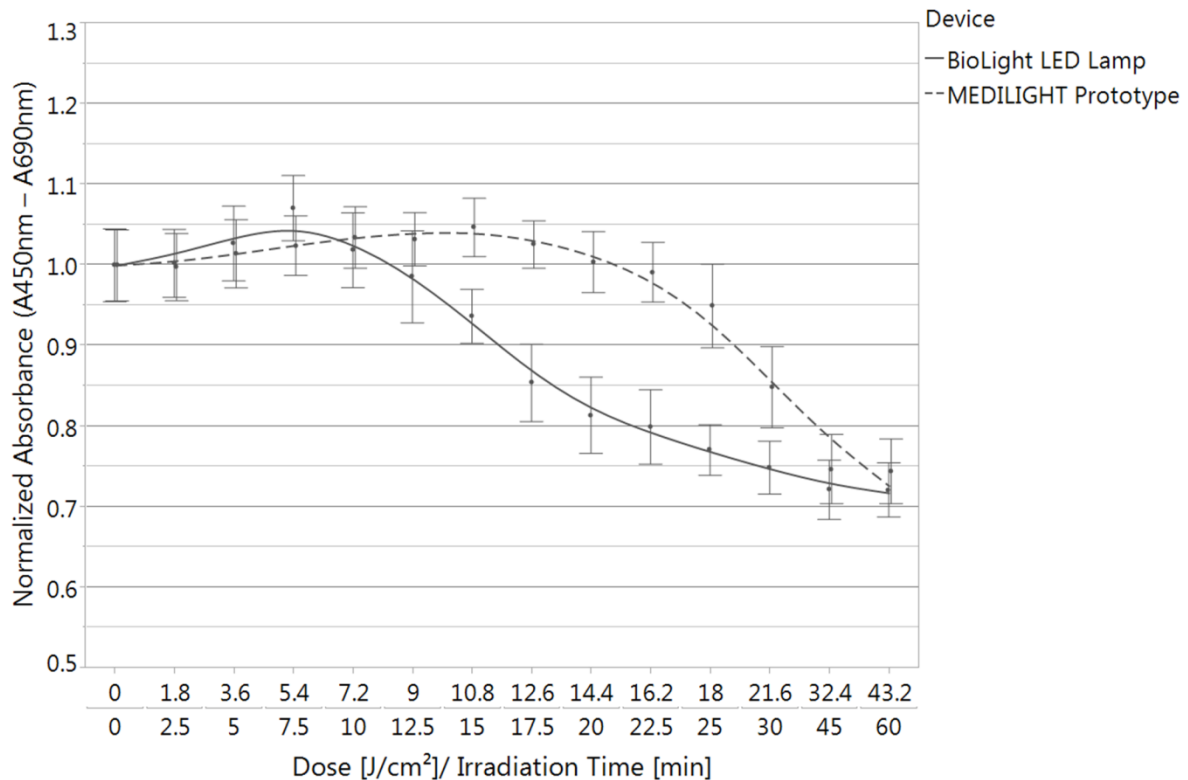


Figure 49: Changes in the metabolic activity of NHDF cells following different blue light doses with a constant time point of XTT testing at 24 hours after irradiation. Single blue light treatments were either performed with the BioLight LED Lamp (Philips Research, Eindhoven, Netherlands) in continuous mode or with the MEDILIGHT prototype through the wound dressing E2723 in cycled mode (cycles of 30 seconds). For the latter, the irradiance was adjusted to 23 mW/cm² underneath the respective component stack (68% DC), which complied with the irradiance value of the Philips device. Fold changes were evaluated versus time-matched, non-irradiated controls. Data are presented as mean \pm SD (N = 3 repetitions, 3 replicates for the BioLight LED Lamp; N = 2 repetitions, 3 replicates for the MEDILIGHT prototype). Corresponding statistics are summarized in Table 30 (Appendix).

3.2.3 Light distribution studies

A homogenous light distribution is indispensable to induce stable photobiological effects. In consequence, light, which is emitted by single LED spots, needs to be distributed uniformly. Using the *in vitro* model described in 2.2.2.2, light homogeneity was investigated based on the biological activity of NHDF cells tested with the XTT Cell Viability Kit. Adding only the diffuser between the illumination field of the MEDILIGHT prototype and the transparent 96-well plate, color coding of absorbance intensities clearly showed that the reduction in cell metabolism of NHDF cells was carried over to two adjacent columns and rows (Figure 50).

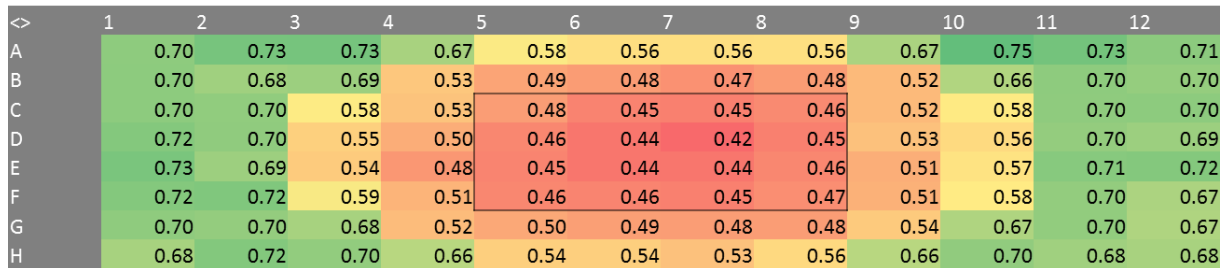


Figure 50: Changes in the metabolic activity of NHDF cells following continuous irradiation in transparent 96-well plates using a blue light dose of 21.6 J/cm² – Color coding of absorbance intensities. The black rectangle shows the area in which the irradiation took place through the diffusor.

Since the diffusor represents an additional layer in the component stack leading to an increase in DCs and the resulting energy input, it was tested whether only the wound dressing E2723 provided by URGO RID (Chenôve, France) could homogenize the light sufficiently. Absorbance intensities obtained following light treatment through E2723, either with or without the diffusor, did not indicate a clear difference in light distribution within the transparent plate. Moreover, the metabolic inhibition of NHDF cells induced by 21.6 J/cm² of blue light was still carried over to at least two adjacent columns and rows (Figure 51). Thus, the diffusor did not improve light distribution when using it with the dressing E2723. In addition, with respect to heat management, the exclusion of the diffusor could benefit to a DC reduction and thus to a decrease of temperature increases within the irradiation system.

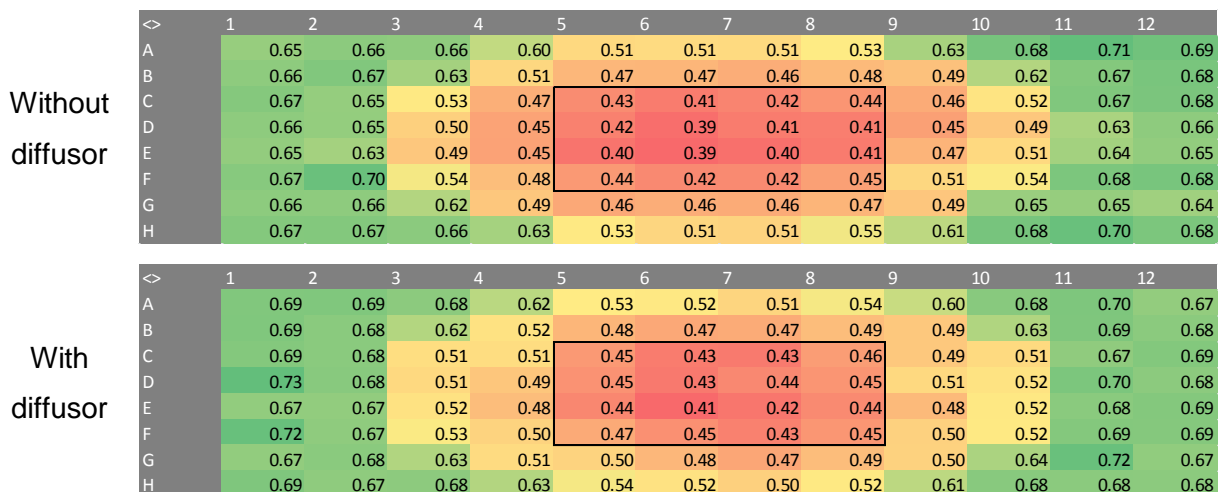


Figure 51: Changes in the metabolic activity of NHDF cells following continuous irradiation in transparent 96-well plates using a blue light dose of 21.6 J/cm² – Color coding of absorbance intensities. The black rectangle shows the area in which the irradiation took place through E2723. The addition of the diffusor was optional: (A) without diffusor, (B) with diffusor.

4 DISCUSSION

Throughout the past decade, PBM has gained more and more attention as a new treatment modality for a wide range of medical applications. Nevertheless, it is still considered as an alternative treatment approach due to a vast inconsistency of published outcomes and a lack of understanding the underlying molecular cascades triggered by irradiation. In contrast to red and (N)IR light, predominantly used in PBM studies, the application of blue light is rather connected to inhibitory effects and therefore only suitable for a few ailments. Thus, this study aimed at characterizing the response of primary human dermal fibroblasts to 453 nm light. Appropriate irradiation doses were inferred from XTT cell metabolism studies. Then, photobiomodulatory effects were investigated at different time points following light treatment monitoring short-term and long-term changes. In addition, the number of treatments was varied to set up a preliminary light schedule on cellular level for subsequent *in vivo* tests. Using various cell proliferation assays like cell cycle distribution studies, BrdU-ELISA and cell counting, it was tested whether metabolic changes are also reflected in altered proliferation rates. Furthermore, dose-dependent effects of blue light on mitochondria of NHDF cells were analyzed by measuring H₂O₂ concentrations and the mitochondrial membrane potential $\Delta\Psi_m$ at different time points after irradiation. Moreover, for safety reasons, cell viability was assessed after treating NHDF cells with high blue light doses. To elucidate which genes and signaling pathways were commonly or differentially expressed after different irradiation doses, comprehensive gene expression analyses were performed at several time points following blue light treatment. All results were contributed to the European project MEDILIGHT, which developed a medical device facilitating personalized light therapy for chronic wound patients. Examining the mitochondrial activity of NHDF cells following treatment with selected light doses, the efficacy of the MEDILIGHT prototype was compared to the BioLight LED Lamp and finally validated for upcoming *in vivo* tests.

A broad analysis of studies already published in the PBM research field showed that metabolic activity is one of the most common measures evaluated as an indicator of cell viability and proliferation. Since reports investigating blue light effects on a variety of fibroblast cell types showed different experimental outcomes using varying sets of irradiation parameters (Table 1), NHDF cells were at first exposed to different doses.

Therefore, the irradiation time was adjusted keeping a constant irradiance value of 12 mW/cm^2 at the plate surface (see 2.2.2.1, Table 7). Using the XTT Cell Viability Kit, changes in mitochondrial activity were investigated at 24 hours after irradiation. Over a range from 0.0 J/cm^2 to 86.4 J/cm^2 a biphasic dose-response curve was obtained with a maximum acceleration of cell metabolism by 7.10% using 5.4 J/cm^2 of blue light, while lower doses induced less significant effects. In contrast, higher irradiation doses suppressed the activity of mitochondrial enzymes to a maximum of about 30% (Figure 20). The phenomenon of dose-dependent effects has often been described in literature and is thus well-known in PBM research⁹⁹. These biphasic dose-response curves are frequently linked to a common model dating back to 1887, the Arndt-Schulz law^{100, 101}, which is nowadays defined by the term 'hormesis', first referenced by Stebbing in 1982¹⁰² and followed up by Calabrese^{103, 104}. The law specifies that a certain energy threshold has to be crossed to evoke stimulation reaching its maximum following even stronger stimuli; instead, applying too much energy results in inhibitory effects (Figure 52).

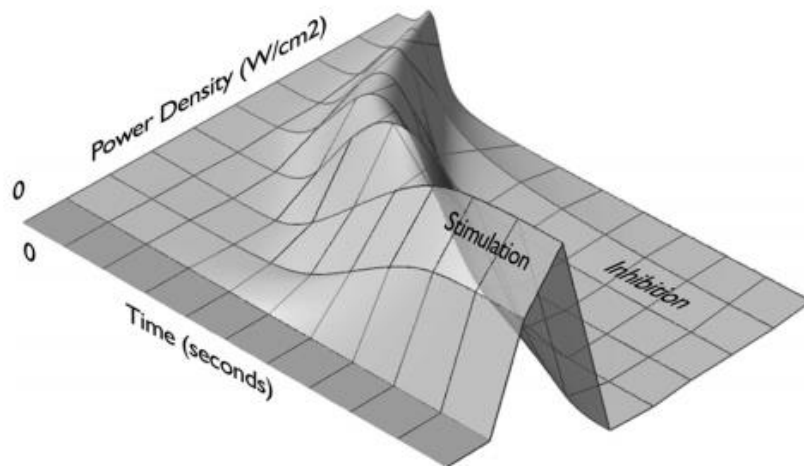


Figure 52: Three-dimensional surface plot illustrating the influence of an increasing irradiance [W/cm^2] or irradiation time [s] on dose-dependent PBM effects⁸.

In order to study both phases of the biphasic response curve, two irradiation doses were selected for subsequent experiments: 5.4 J/cm^2 corresponding to 7.5 minutes of blue light and 21.6 J/cm^2 resulting from an irradiation time of 30 minutes. In addition to the observed dose-dependency of metabolic activity, it was also shown to be time-dependent (Figure 21). Both, stimulatory and inhibitory effects were long-lasting up to 24 hours after a single treatment with respectively 5.4 J/cm^2 and 21.6 J/cm^2 of blue light, whereas at 48 hours and 72 hours the effects could not be maintained.

In a similar manner, Wataha et al.⁸⁸ measured the mitochondrial activity of different types of fibroblasts at 24-hour intervals for 72 hours following exposure to different blue light sources. Whereas aneuploid mouse lung fibroblasts (Balb/c) revealed a constant suppression of succinate dehydrogenase activity for 72 hours, slower-growing human gingival fibroblasts (HGF) and diploid human fibroblasts (WI-38) reacted differently. Blue light exposure of human gingival fibroblasts resulted in a transient suppression of succinate dehydrogenase activity by 30% at 24 hours, which was attenuated by 10% within the next 48 hours. Based on these cell type-specific responses, the authors claim that differential effects might depend on varying population doubling times and related energy consumption levels suggesting rapidly dividing cells to be more sensitive to irradiation⁸⁸. With a population doubling time of 43.3 hours, NHDF cells used in this study are rather classified as a slowly growing cell line reasoning the fast recovery of mitochondrial activity within 48 hours after irradiation (Figure 21), which is in line with the findings described by Wataha et al.⁸⁸.

Since a steady up- or down-regulation of cellular activity would benefit respectively the impaired healing process of chronic wounds or hypertrophic scarring, NHDF cells were treated once per day on two and three consecutive days. Hence, multiple light treatments were carried out in order to come up with a potential irradiation regimen for subsequent *in vivo* wound healing studies. In line with Oplander et al.⁸¹ and Taflinski et al.⁸⁴, consecutive exposures to 21.6 J/cm² of blue light revealed a further decrease in metabolic activity, while consecutive irradiations with 5.4 J/cm² did not enhance the stimulatory effect found after a single treatment (Figure 22). However, two irradiations per day using 5.4 J/cm² each with a 3-hour interval, accounting for a daily dosage of 10.8 J/cm², caused a higher increase in metabolic activity compared to only one or even three treatments per day (Figure 23). Similarly, Brondon et al.¹⁰⁵ evaluated the effect of different treatment frequencies on the metabolic activity and proliferative capacity of human HEP-2 carcinoma cells and murine L-929 fibroblasts. Using red light of 670 nm, cells were treated either once, twice or four times a day receiving 5.0 J/cm² per treatment. For both cell lines, the authors observed the highest stimulation with two irradiations per day, while four daily treatments led to reduced proliferation rates, which correlates to the results obtained for NHDF cells treated three times a day (Figure 23). Thus, besides determining favorable irradiation parameters, an appropriate light regimen has to be identified for each cell line.

To elucidate whether changed cellular activities are accompanied by a modulation of mitochondrial function and thus oxidative phosphorylation, overall differences in ATP concentration of untreated and light-treated cells were assessed. Whereas cellular ATP contents were diminished following irradiation with the higher blue light dose of 21.6 J/cm^2 , mitochondrial respiration was stimulated at 1 hour and 24 hours after light treatment using 5.4 J/cm^2 (Figure 24). Consequently, using indirect and direct assays examining the cellular energy status confirmed that blue light irradiation was capable of regulating mitochondrial respiration. In contrast to that, Liebmann et al.⁶³ reported opposing trends when comparing the metabolic activity and ATP synthesis rates of keratinocytes and endothelial cells irradiated with 453 nm light, which were traced back to the onset of cellular differentiation. However, differentiation markers such as Thy-1, encoding the CD90 surface antigen¹⁰⁶, and transforming growth factor beta (TGF- β), which is particularly related to an increased mitochondrial function¹⁰⁷, were not significantly expressed in this study.

Most notably, XTT and ATP assays, performed at matching time points following blue light treatment, showed correlating changes in the metabolic rate of NHDF cells when using different irradiation doses. However, since cell metabolism can be affected by a lot of different factors, its quantification cannot be directly translated into changes in cell proliferation¹⁰⁸. Using different test strategies, including the analysis of cell cycle distribution, determination of new DNA synthesis and cell counting, proliferation was studied after single and consecutive irradiations with either 5.4 J/cm^2 or 21.6 J/cm^2 . Flow cytometry analyses revealed a higher proportion of S-phase cells after a single and two consecutive light treatments with 5.4 J/cm^2 , which was accompanied by a lower cell fraction staying in G0/G1 (Figure 26). Hence, low doses of blue light seemed to result in a higher proliferative capacity, which was confirmed by an increased synthesis of cellular DNA (Figure 27) and elevated cell counts (Figure 28). However, three consecutive light treatments slightly reversed the stimulatory effect, which might be explained by a nearly confluent cell monolayer yielding contact inhibition and therefore limited proliferation. Although the seeded cell number was adjusted according to the respective experiment duration, it could not be further reduced since low plating densities favor differentiation into myofibroblasts¹⁰⁹. In addition, three irradiations delivering 5.4 J/cm^2 each (16.2 J/cm^2) seemed to evoke replication stress, indicated by a slightly higher amount of apoptotic cells (Figure 26).

The latter observation was even more enhanced with an increasing number of light treatments using 21.6 J/cm^2 each leading to deleterious effects. A single irradiation revealed a higher proportion of G0/G1-phase cells accompanied by a reduction in S-phase cells, which was exactly the opposite compared to the cell cycle distribution obtained after one treatment with 5.4 J/cm^2 . Two and three treatments rather resulted in a shift to increasing percentages of G2/M-phase cells (Figure 26). At 72 hours and 96 hours after exposure to 470 nm light, Ohara et al.¹¹⁰ observed similar effects in B16 melanoma cells, suggesting an inhibited G1/S transition as well as a prolonged M phase as possible reasons for slower cell growth. In accordance with Li et al.¹¹¹ the increased amount of G2/M-phase cells after multiple exposures might be explained by several bursts in H_2O_2 , since they had reported that H_2O_2 evoked G2 cell cycle arrest and therefore inhibited cell proliferation of murine and human osteoblasts. The continuous decline in S-phase cells was confirmed by BrdU-ELISA results, showing a persistent slow-down of DNA synthesis (Figure 27), and lower cell counts (Figure 28).

A delayed ability to enter mitosis from G2 might be also inferred from an increased size of cell nuclei, which was constantly enhanced following multiple exposures of NHDF cells to 21.6 J/cm^2 (Figure 29). According to Gregory et al.¹¹² and Cavalier-Smith et al.¹¹³ describing the 'nucleoskeletal theory', a larger nuclear size might be related to a higher DNA content as well as a lower extent of chromatin condensation giving rise to a larger cell volume. In contrast, several other studies propose different mechanisms affecting nuclear size and shape involving either the re-organization of the endoplasmic reticulum¹¹⁴ or the activation of nuclear lamina proteins¹¹⁵. However, cell nuclei staining following consecutive irradiations using 5.4 J/cm^2 revealed only slight, negligible changes in nuclear size (Figure 29).

Assuming that blue light mediates cellular processes to some extent via stimulation or inhibition of mitochondrial respiration, further tests were carried out investigating mitochondrial function following blue light exposure. Moreover, the latter were mainly justified by the fact that photosensitizers absorbing wavelengths of the visible blue range, namely porphyrin ring structures and flavins, are supposed to be concentrated in mitochondria. Upon blue light absorption, they are known to generate ROS, which represent key secondary messengers mediating downstream effects¹¹⁶. Therefore, ROS generation is another widely used test variable in PBM research (Table 1).

As a result of normal mitochondrial metabolism, ROS are produced in physiological concentrations acting as beneficial signaling molecules in metabolic control, cellular proliferation, stress responses, cell survival, death and inflammatory processes¹¹⁷. In contrast, high ROS levels or sustained ROS generation promote oxidative damage, particularly to DNA, proteins as well as lipids, finally leading to cell death, which characterizes ROS as so-called 'Janus-type' mediators⁹⁹. Since H₂O₂ represents a major component of ROS species in cells¹¹⁸ and is relatively stable¹¹⁹, its production was analyzed at different time points following single blue light exposures to either 5.4 J/cm² or 21.6 J/cm² (Figure 30). In line with the study performed by Zeng et al.¹²⁰, who assessed intracellular ROS generation in mouse dermal fibroblasts after UVB irradiation, the H₂O₂ concentration reached its maximum at 30 minutes and was normalized at 1 hour after irradiation. Thus, the well-known effect of increased ROS levels by blue light was confirmed^{77, 85, 89}. However, contrary to the assumption that higher irradiation doses correlate with elevated ROS levels¹²¹, a higher H₂O₂ peak was found directly after blue light treatment with the lower dose of 5.4 J/cm². Similar outcomes were reported by Huang et al.¹⁰, who observed a biphasic response of intracellular ROS levels in mouse embryonic fibroblasts, measured at 5 minutes following irradiation with different doses of 810 nm laser light. This observation might be connected to the higher metabolic activity found when using the lower blue light dose of 5.4 J/cm², generating even higher concentrations of mitochondrial ROS.

Since both blue light doses resulted in a rapid depolarization of $\Delta\Psi_m$, reflected by decreased TMRE fluorescence intensities (Figure 31, Figure 32), and a subsequent impairment of oxidative phosphorylation and therefore ATP synthesis at 3 hours after irradiation (Table 12, Figure 24), increased ROS levels were considered to induce oxidative stress. However, in contrast to Zeng et al.¹²⁰, who showed a progressive decline in $\Delta\Psi_m$ of mouse dermal fibroblasts after 4x 120 mJ/cm² of UVB irradiation, leading to premature senescence and apoptosis, $\Delta\Psi_m$ was found to recover within 6 hours (Figure 31). Besides highly increased ROS levels, also repair mechanisms were found significantly up-regulated shortly after irradiation with both doses, which reinforces the hypothesis of oxidative stress induction. For the lower blue light dose of 5.4 J/cm², the KEGG gene set 'base excision repair' was significantly enriched representing the predominant DNA repair pathway for small base lesions most likely induced by oxidative stress¹²² (Table 14, (A)).

In contrast, using 21.6 J/cm² of blue light revealed a significant up-regulation of homologous recombination as well as of the Fanconi anemia pathway (Table 14, (B)) probably indicating the occurrence of DNA double-strand breaks or interstrand cross-links, which are rather ascribed to high-energy X-ray radiation instead of VIS or even UV irradiation^{123, 124}. Moreover, this assumption is contrary to the findings of Taoufik et al.⁸⁵, who did not observe formation of DNA double-strand breaks following blue light treatment of primary human gingival fibroblasts, although they used even higher irradiation doses. Mignon et al.⁸⁰ even observed several repair pathways to be down-regulated after exposing primary reticular fibroblasts to 30 J/cm² of 450 nm light. However, a single blue light treatment using 21.6 J/cm² seemed to harm NHDF cells to a higher extent than the lower irradiation dose of 5.4 J/cm², although the H₂O₂ concentration, measured at 30 minutes after irradiation, was less (Figure 30). As suggested by Huang et al.⁹⁹, this observation might be explained by the generation of different kind of ROS species hypothesizing superoxides as good ROS, whereas hydroxyl radicals and peroxyxynitrite represent bad ROS showing a higher damaging potential. Consequently, apart from testing H₂O₂, additional studies examining other ROS species might be necessary to broaden the investigation of redox regulation.

However, single blue light treatments up to 172.8 J/cm² did not show any signs of cell death induction (Figure 39), which was similarly observed by Liebmann et al.⁶³ claiming cytotoxic effects on human keratinocytes and endothelial cells only for high doses of 453 nm light (> 500 J/cm²). In addition, cell viability tests performed by Masson-Meyers et al.⁷⁸ showed that doses < 110 J/cm² of 470 nm light were safe when irradiating human dermal fibroblasts.

Based on gene expression levels, KEGG pathways related to cell growth and death were not significantly regulated in most cases (Table 15). However, shortly after irradiation with 5.4 J/cm², *TP53* coding for p53 was slightly up-regulated inducing the expression of genes like *GADDA45A*, *CDKN1A* (p21), *BID* and *CASP3*, which indicates the onset of DNA repair and damage prevention by promoting cell cycle arrest and apoptosis¹²⁵. Chen et al.¹²⁶ have observed similar changes in H₂O₂-treated fetal lung fibroblasts, suggesting that oxidant exposure induces cell recovery via p53 activation. Accordingly, Smith et al.¹²⁷ figured out that mouse embryonic fibroblasts lacking *p53* or *GADD45* genes exhibited a higher sensitivity to DNA damage.

In the following time course, *TP53* transcription was suppressed by the activation of its antagonist *MDM2*, which encodes a nuclear-localized E3 ubiquitin ligase. This observation might reflect a decrease in cellular stress, which was accompanied by significantly down-regulated genes involved in the caspase cascade like *APAF-1*, *CASP8* and *CASP3*. In comparison, the higher blue light dose of 21.6 J/cm² induced a time-shifted up-regulation of stress response genes at 3 hours after irradiation accounting for statistical enrichment of the entire pathway (Table 15, (B)). However, at 24 hours of harvesting apoptotic genes were found down-regulated, whereas the activity of CCND1/CDK4 and CCNE1/CDK2 complexes were inhibited promoting G1 arrest¹²⁸, which was also reflected by time-matched cell cycle analyses (Figure 26).

Although apoptosis pathways were rather up-regulated following blue light treatment of NHDF cells with 5.4 J/cm² (Table 15, (A)), single gene expression indicated a continuous up-regulation of *BCL2* encoding a homonymous, anti-apoptotic protein, which antagonizes *BID* activity within the intrinsic apoptosis pathway. Thereby, Bak/Bax-mediated mitochondrial outer membrane permeabilization (MOMP) yielding cytochrome c release and subsequent caspase activation involving inter alia *CASP3*, *CASP7* and *CASP9* might be counteracted preventing the translation of stress responses into apoptosis. Also, Naik et al.¹²⁹ observed that overexpression of Bcl-2 in mouse embryonic fibroblasts promoted cell survival by the inhibition of apoptotic signaling thereby enhancing their resistance to UV radiation. Besides the intrinsic apoptosis pathway, genes encoding death ligands of the extrinsic pathway such as FASLG or TNFSF10 were found significantly up-regulated at 3 hours after blue light treatment; nevertheless, the caspase cascade executing programmed cell death still remained slightly down-regulated since respective adaptors were not significantly expressed. In contrast, when using the higher blue light dose of 21.6 J/cm², the interplay between *BCL2* and *BID* was reversed at 1 hour of cell harvesting, followed by a significant up-regulation of genes encoding extrinsic death receptors like FAS and TNFRSF10D as well as cytoplasmic proteins like APAF-1 promoting caspase activation at 3 hours after irradiation. Though, gene transcription levels of single caspases were not significantly modulated, which strongly correlated with the results of cell viability analyses using flow cytometry (Figure 39). Therefore, oxidative stress induced by blue light seemed to be reversible preventing the cells from undergoing persistent damage and death, particularly for 5.4 J/cm² of blue light.

This was also indicated by the fast alleviation of immediate H₂O₂ bursts shortly after irradiation (Figure 30). Since mitochondria represent the primary source of ROS contributing up to 95% of intracellular levels¹³⁰ and contain classical blue light photosensitizers⁶², the fast recovery to physiological ROS levels might be explained as a result of mitochondrial hormesis ('mitohormesis'). Under conditions of metabolic stress, inter alia indicated by a reduction of $\Delta\Psi_m$ directly after irradiation (Figure 31), unbalanced AMP/ATP ratios are likely to arise. In this context, several disease pathways like Alzheimer's disease, Parkinson's disease and Huntington's disease, in which mitochondria play a critical role, were found significantly down-regulated at 3 hours after blue light treatment with both irradiation doses (Table 12). In detail, the expression of genes like *NDUFA1*, *SDHB*, *CYC1*, *COX4I1* and *ATP5A1* encoding subunits of respiratory chain complexes I – V was significantly lower when compared to the control. Hence, the activity of mitochondrial complexes might be impaired, which leads to a compromised energy metabolism by blocking electron transfer within the respiratory chain. The latter was confirmed by an accompanying down-regulation of oxidative phosphorylation for both blue light doses (Table 12), which may result in a decreased susceptibility to apoptosis¹³¹. Moreover, *SLC25A4*, encoding the subunit of an ADP/ATP carrier across the mitochondrial membrane was found significantly down-regulated, favoring an unbalanced energy status.

Consequently, AMP-activated protein kinase (AMPK), an important cellular energy sensor, might be activated restoring ATP homeostasis by stimulating catabolic energy-releasing pathways and inhibiting anabolic energy-consuming processes¹³². This assumption was supported by gene expression profiles showing a significant up-regulation of *PRKAA1* at 1 hour and 3 hours after blue light treatment with 5.4 J/cm², coding for the catalytic subunit of AMPK. As a result, mitochondrial activity was increased, which was proven by XTT assays (Figure 21) as well as the significant up-regulation of oxidative phosphorylation at 1 hour and 24 hours following irradiation (Table 13), which coincided with elevated ATP concentrations at the respective time points (Figure 24). Inevitably, mitochondrial ROS levels were probably increased, which might also trigger AMPK activation leading to adaptive changes in cellular metabolism¹³³. In addition, several other metabolic pathways were significantly up-regulated, which provides further evidence of metabolic reprogramming (Figure 43, Table 13).

Thereupon, several redox-sensitive transcription factors might be activated, which translocate from the cytoplasm to the nucleus affecting gene transcription in a retrograde response^{134, 135}, mainly mediating cytoprotective responses to oxidative stress. Hence, recurrent and mild activations of defense mechanisms may contribute to the development of a long-term resistance against oxidative stress¹³⁶.

In contrast, at 1 hour and 24 hours following blue light treatment with 21.6 J/cm², *PRKAA1* was slightly down-regulated or left unaffected, explaining the emerging lack of metabolic and energy homeostasis in NHDF cells, which was represented by a continuous suppression of mitochondrial activity (Figure 21, Figure 24). Nonetheless, affirming the assumption of counteracting oxidative stress, the metabolism of xenobiotics by cytochrome P450 was significantly up-regulated at 24 hours after irradiation with both blue light doses involving several genes coding for XMEs (Table 12). Those, encoding phase II detoxification enzymes like GSTs and UGTs, belong to a group of stress-dependent genes activated by Nrf2. The latter represents a key transcription factor inducing cytoprotective responses to oxidative stress as well as a potential target of AMPK¹³⁷. Upon inactivation of kelch like ECH associating protein 1 (Keap1), Nrf2 translocates to the nucleus, binds to the antioxidant response element (ARE) and finally triggers the transcription of genes involved in xenobiotic metabolism and disposition, antioxidant defense and redox signaling^{138, 139}.

Moreover, at 1 hour after irradiation, both light doses resulted in an up-regulation of other Nrf2-transcribed genes¹⁴⁰, while in most cases their expression was enhanced over time, especially for 21.6 J/cm² of blue light (Figure 45). Similarly, Didier et al.¹⁴¹ as well as Meewes et al.¹⁴² proposed that UVA irradiation was found to increase superoxide dismutase (SOD) and thioredoxin (TRX) activity in human skin fibroblasts preventing phototoxicity mediated by oxidative stress. As a result, resistance against repeated ROS exposure might be induced by developing an adaptive antioxidant response, which is commonly known as 'preconditioning'. However, after consecutive exposures to 21.6 J/cm² of blue light, excessive ROS accumulation may not have been compensated by antioxidant defense mechanisms showing exhausted buffering capacity, which gave rise to long-term defects and finally cell death (Figure 26)¹⁴³.

Besides AMPK, the aryl hydrocarbon receptor (AhR) was suggested as a possible target of blue light irradiation activating downstream processes involved in antioxidant defense mechanisms. Becker et al.¹⁴⁴ reported that blue light irradiation of human keratinocytes for 7.5 minutes did not show significant changes in oxidative stress-dependent Nrf2-transcribed genes, while an exposure time of 30 minutes revealed a continuous up-regulation of phase I and II XMEs. In comparison, NHDF cells seemed to show a higher sensitivity in response to oxidative stress, since Nrf2 and its target genes were even up-regulated using the lower blue light dose. Moreover, at 24 hours after treating NHDF cells with both blue light doses, the AhR signaling pathway was found significantly up-regulated (Table 12). Consequently, the differential modulation of oxidative stress response genes shows cell-type specific changes, which might be explained by two possible reasons. First, the studies of Becker et al. were performed using immortalized human keratinocytes. Increasing evidence suggests that these cells are transcriptomically and functionally different from primary cells resulting in different sensitivity levels^{145, 146}. Second, fibroblasts are less amenable to blue light irradiation compared to keratinocytes, since they are located in deeper skin layers showing a higher sensitivity. Similar effects were reported by Marionnet et al.¹⁴⁷, who tested 24 markers involved in various antioxidant defense systems following UV radiation of a reconstructed skin model including keratinocytes and fibroblasts. In the latter, a higher number of genes was found to be significantly modulated shortly after UV treatment, which correlates with the results obtained for light-treated NHDF cells.

In addition, consistent with Tigges et al.'s observations¹⁴⁸, it was found that the AhR repressor gene *AHRR* was expressed twice as high in NHDF cells when compared to keratinocytes. This might be linked to a less pronounced up-regulation of *CYP1A1* and *CYP1B1*, coding for phase I detoxification enzymes, which was denied by Tigges et al. Though, in addition to xenobiotic metabolism, CYP enzymes are also reported to play a crucial role in steroid hormone biosynthesis¹⁴⁹, accounting for the anti-inflammatory effects found after blue light irradiation of human keratinocytes¹⁴⁴. Treating NHDF cells with both blue light doses showed no significant changes in the steroid hormone biosynthesis pathway, while the ovarian steroidogenesis was found to be significantly up-regulated at 24 hours following blue light treatment (Table 12). Nonetheless, in direct comparison to the effects described for human keratinocytes, blue light irradiation revealed less anti-inflammatory potential exerted in NHDF cells.

Inflammatory processes, stress-induced responses as well as cell survival can be also mediated via the nuclear factor kappa B (NF- κ B), a redox-sensitive transcription factor, which can be equally activated by AMPK and AhR, while it is still controversial for the latter^{16, 150, 151}. Known from a study performed by Liu et al.¹⁵⁰, activated AMPK facilitates the transcriptional activity of NF- κ B by enhancing the ubiquitination and therefore degradation of κ B inhibitors (I κ Bs). Thus, AMPK is capable of triggering the expression of anti-apoptotic genes via the canonical NF- κ B pathway, promoting cell survival. Shortly after irradiation, the NF- κ B signaling pathway was up-regulated for both irradiation doses reaching statistical significance at 3 hours following light treatment with 21.6 J/cm² (Table 16). Indeed, especially the latter condition showed many anti-apoptotic genes being up-regulated involving inter alia *BCL2*, *BCL2A1*, *BIRC2*, *XIAP* and *GADD45B*, which correlates to the findings made by Liu and colleagues¹⁵⁰. Moreover, inflammatory processes seemed to be enhanced, which matched with a nearly continuous up-regulation of the TNF signaling pathway defined by KEGG (Table 16). Although blue light is said to be anti-inflammatory^{29, 58}, genes encoding pro-inflammatory chemokines and cytokines were also significantly up-regulated favoring the recruitment and activation of various immune cells to the site of injury. With respect to acute and chronic wound healing by blue light treatment, this might be particularly helpful in accelerating the entire repairing process.

Moreover, the up-regulation of *PRKAA1* shortly after irradiation with 5.4 J/cm² of blue light might have led to the phosphorylation and thus activation of *FOXO1* encoding the forkhead box protein O1^{136, 152}, which represents an important transcription factor involved in cell cycle progression, stress tolerance and cell survival. At 1 hour of harvesting, *FOXO1* was significantly up-regulated inducing the transcription of genes encoding CDK inhibitors such as p15 (*CDKN2B*) and p21 (*CDKN1A*) as well as the growth arrest and DNA-damage-inducible protein GADDA45 alpha promoting cell cycle arrest. In addition, *FOXO1*-dependent transcription of antioxidant genes was increased, which matches to the modified expression of *TP53* and Nrf2-transcribed genes. Hence, cell cycle progression might be halted allowing cells to recover from oxidative stress and to repair potential damage before resuming normal proliferation. However, at 3 hours after irradiation, the regulation of FOXO-transcribed genes lost statistical significance turning to down-regulation at 24 hours following blue light treatment (Table 16, (A)).

In addition to AMPK, serine/threonine kinase 1 (AKT), encoded by *AKT1*, acts as a primary effector in response to metabolic stress, while their interplay is characterized by antagonistic roles. Thus, at 24 hours following irradiation using 5.4 J/cm² of blue light, *FOXO1* was significantly down-regulated by its inhibitor *AKT1*, which surpasses AMPK activation by phosphorylation¹⁵³. Therefore, genes enhancing growth arrest were significantly down-regulated favoring an unimpaired cell cycle progression of light-treated NHDF cells, which was shown by an increased accumulation of cells in the S phase (Figure 26) and higher DNA replication rates (Figure 27, Table 14 (A)). In line with a lower expression of *TP53*, cell cycle regulation turned from inhibition in the short-term to stimulation in the long-term. In contrast, with the higher blue light dose of 21.6 J/cm² *PRKAA1* was slightly up-regulated at 3 hours of harvesting, while *AKT1* was not significantly enriched. Consequently, *FOXO1* was equally up-regulated promoting cell growth arrest as well as oxidative stress resistance and DNA repair. In addition to an accompanying up-regulation of the p53 signaling pathway, correlating changes were followed within the significantly enriched NF-κB gene set, revealing higher expression levels of anti-apoptotic genes. Just like AMPK, AKT is also known to be involved in the regulation of NF-κB¹⁵⁴; however, this relation could not be inferred in this study. The differential expression of *AKT1* by both irradiation doses also indicated a divergent trend in the regulation of cell survival, showing significant down-regulation of the PI3K-Akt signaling pathway at 24 hours after 21.6 J/cm² of blue light (Table 16, (B)).

In addition to the FoxO signaling pathway, the antagonistic crosstalk between AMPK and AKT plays an important role in the mTOR signaling pathway¹⁵³. While AMPK stimulation inhibits the mechanistic target of rapamycin (mTOR), AKT is known to activate its expression leading to changes in protein synthesis, cellular growth and metabolism¹⁵⁵. In line with the significant up-regulation of *PRKAA1* at 1 hour and 3 hours following irradiation using 5.4 J/cm², *MTOR* was found down-regulated. The opposing regulation of cell metabolism and growth was also confirmed at 24 hours of harvesting, while *MTOR* got significantly up-regulated probably yielding an increased protein synthesis, which might enhance cell growth and therefore proliferation. In direct comparison, the higher light dose of 21.6 J/cm² showed a contrary regulation over time: Directly following irradiation *MTOR* was slightly up-regulated going along with an inhibition of *PRKAA1*, while their regulation was inversed at 24 hours.

Consequently, blue light irradiation with the lower dose of 5.4 J/cm² resulted in a higher growth capacity over time, which matched to the results of various proliferation assays (Figure 26 - Figure 28).

Time-dependent changes in cell proliferation after blue light irradiation could also be inferred from cell cycle-related genes. In addition to an early up-regulation of p21 at 1 hour after blue light treatment with 5.4 J/cm² promoting cell cycle arrest, *CDK9* was found significantly enriched maintaining cell cycle recovery and thus genome integrity in response to replication stress or spontaneous DNA damage¹⁵⁶. However, *CCND2* encoding cyclin D2 was highly expressed at 3 hours of harvesting promoting G1/S phase transition and thus cell cycle progression. At 24 hours after irradiation, *CDK2* was found significantly up-regulated encoding a cyclin-dependent serine/threonine protein kinase with maximum activity during S and G2 phase. Throughout cell cycle progression, CDK2, which interacts with cyclin A, B1, B3, D and E, phosphorylates retinoblastoma proteins and thereby releases the transcription factor E2F1. Upon activation, the latter promotes the expression of genes involved in G1/S transition, DNA replication and mitosis, such as *FOXM1*, which was highly expressed after 24 hours. Moreover, genes playing a crucial role in the formation of the anaphase promoting complex like *ANAPC1*, *ANAPC4* and *ANAPC5* were highly up-regulated, revealing an increased proliferative activity. In comparison to the lower blue light dose, which induced a continuous up-regulation of the cell cycle pathway, it was inhibited after irradiation with 21.6 J/cm² of blue light, apart from showing significant up-regulation at 3 hours of harvesting (Table 16). The latter might be explained by an increased expression of DNA-damage response genes, like *PRKDC* as well as *ATM*, without significantly affecting genes, which are responsible for cell cycle progression. *PRKDC* and *ATM* can be activated upon double-strand breaks¹⁵⁷ matching to the up-regulation of the repair mechanism 'homologous recombination' (Table 14, (B)). *ATM* can directly activate p53 by phosphorylation, with the respective pathway shown to be highly up-regulated at 3 hours of harvesting (Table 15, (B)), inducing the activation of DNA repair proteins and cell growth arrest. At 24 hours after irradiation, all CDKs were down-regulated indicating a slowed-down cell cycle progression. Moreover, the proliferation stop was confirmed by a significantly decreased expression of *PRKCA*, coding for protein kinase C (PKC), which was reported to promote irradiation-induced apoptosis in human lung fibroblasts by down-regulating anti-apoptotic markers¹⁵⁸.

However, coming back to the increasing proportion of G2/M-phase cells following consecutive light treatments with 21.6 J/cm^2 each (Figure 26), G2 cell cycle arrest was suggested as a possible explanation. Since the G2 phase provides time for proofreading and packaging of replicated DNA prior to cell division, its increasing prolongation might indicate an accumulation of replication errors, which retains NHDF cells at the G2/M checkpoint and thus prevents them from passing through the cell cycle¹⁵⁹. Though, the mismatch repair pathway, which is activated in response to replication errors¹²², was not significantly enriched. According to Lanzini et al.¹⁶⁰, another explanation for the growing emergence of G2/M-phase cells could be an excessive accumulation of cyclin B in cells arrested in the late cell cycle due to a lack of p53 signaling. Contrary to the expectation that a higher blue light dose, a potential stress signal, triggers an increase of p53, *TP53* was slightly down-regulated at 1 hour and 3 hours after irradiation reaching statistical significance at 24 hours. Moreover, at 24 hours of harvesting, a significant up-regulation of *CCNB1* encoding cyclin B arose indicating elevated cyclin B1 protein levels. Therefore, although *CDK1* encoding the associated kinase was slightly down-regulated, some cells might have shown a premature entry into mitosis due to an overaccumulation of cyclin B1. As suggested by Lanzini et al.¹⁶⁰, this could possibly lead to an abrogation of the G2/M checkpoint followed by mitotic catastrophe (MC), which often results in cell death. The latter finding correlates with the growing population of apoptotic cells induced by multiple irradiations with 21.6 J/cm^2 each on consecutive days (Figure 26), which in turn might also explain lower DNA synthesis rates and cell counts (Figure 27, Figure 28).

Due to uncontrolled temperature rises during continuous operation, irradiations with the MEDILIGHT system had to be performed in cycled mode (Figure 46, Figure 47). Compared to cell metabolism studies with the BioLight LED Lamp, a similar biphasic dose-response curve was obtained, although higher doses were required to induce comparable changes (Figure 49). A literature review revealed that the use of thermal cycling is quite known for heat management issues, whereas especially laser light treatments are rather performed in pulsed mode (light pulses of < 1 second, DIN EN 60079-28) avoiding tissue heating¹⁶¹. However, on the one hand, dose fractionation might have increased the threshold to induce stimulation, while on the other hand, less cytotoxic effects might have been induced by recurrent lower doses. Therefore, the stimulatory window was not only shifted to higher doses, but also broadened.

Consequently, with a sufficient light distribution through the wound dressing E2723, the MEDILIGHT prototype showed a comparable efficacy to the BioLight LED Lamp validating its use for subsequent *in vivo* tests. Nevertheless, in order to analyze the discrepancy of biological effects induced by different irradiation modes, further studies are needed to elucidate the underlying mechanisms of action.

In conclusion, it was shown that varying blue light doses, 5.4 J/cm^2 and 21.6 J/cm^2 , differentially impacted the metabolic activity, proliferation rates and the mitochondrial function of NHDF cells. Moreover, gene expression profiles suggested different levels of oxidative stress to occur after single treatments with both irradiation doses. In addition to antioxidant defense mechanisms, the balance between pro-survival and pro-apoptotic forces was affected, finally leading to contrary cell fates. Thereby, the lower blue light dose of 5.4 J/cm^2 seemed to allow a faster cell adaptation to acute light stress via redox homeostasis and metabolic reprogramming, which was crucial for maximizing cell survival and resistance to cell death. All in all, several routes of cytoprotection were found to be activated shortly after irradiation, including growth arrest, antioxidant defense and DNA repair mechanisms promoting cell recovery and even an enhanced proliferation activity in the long run. In contrast, following blue light treatment with 21.6 J/cm^2 , cytoprotective responses were activated at a later time point showing an increasing stimulation of antioxidant defense strategies up to 24 hours afterwards. Nonetheless, when exposing NHDF cells to consecutive blue light treatments with 21.6 J/cm^2 each, they probably failed to maintain redox balance leading to a sustained mitochondrial dysfunction and finally cell death, either induced by an accumulation of cell damage over time or MC.

However, it has to be noted that the study was performed with artificially cultured cells lacking physiological conditions of mammalian tissue, which involves the interaction of several cell types in the local milieu as well as other response factors induced by irradiation. Although suitable irradiation parameters were found for NHDF cells cultured under optimized conditions, further investigation needs to be performed using *in vitro* disease and animal models. Thereby, effective PBM regimens could be established, particularly with respect to the light treatment of non-healing chronic wounds characterized by an impaired activity of dividing cells, but also hypertrophic scars and keloids.

5 SUMMARY

Phototherapy, basically heliotherapy, has already been used for the last 3,000 years. However, major breakthroughs in modern clinical phototherapy were achieved since the beginning of the 20th century, including for instance the invention of lasers. From then on, the use of light as a therapeutic tool grew constantly, demonstrated by the development of new artificial light sources and an increasing number of published studies on a variety of medical, mostly cutaneous, disorders. But although the last decade has witnessed a rapid expansion of PBM, its scientific acceptance is still debated: first, due to inconsistent experimental outcomes, caused by highly variable study designs and irradiation parameters, and second, due to a lack of mechanistic insights into light-triggered signaling. The latter especially applies for blue light, which is, in comparison to red and N(IR) light, rather used for a limited range of medical cutaneous ailments, primarily necessitating inhibitory or even cytotoxic effects, like fibrotic skin diseases. However, also stimulatory effects of blue light have rarely been reported in wound healing studies. Hence, the biomodulatory potential of different blue light doses on cellular activity was examined using primary normal human dermal fibroblasts, NHDF cells, in particular with respect to metabolic processes, cell proliferation and transcriptome changes.

PBM using blue light revealed dose-dependent effects on the metabolism of NHDF cells, with low doses resulting in an increased activity, whereas higher irradiation doses induced a decreased and therefore inhibited cell metabolism. Based on the biphasic response, two irradiation doses, each leading to the maximum effect in the respective phase, were selected: 5.4 J/cm² and 21.6 J/cm². Cell metabolism assays performed at different time points after irradiation with either 5.4 J/cm² or 21.6 J/cm², revealed a fast response following the lower dose, while the higher one led to a delayed onset of metabolic inhibition. Nevertheless, both, stimulation and inhibition of cellular metabolism were long-lasting until 24 hours after light treatment. Subsequent studies with repeated irradiations on consecutive days, imitating a 'chronic' exposure model, showed an enhanced inhibition following multiple treatments using 21.6 J/cm² of blue light, whereas two daily treatments over several days were required for an increased stimulation by 5.4 J/cm² of blue light.

The contrary effects on cell metabolism observed for both irradiation doses, were translated into similar, but less pronounced effects in proliferation, which was studied with various assays testing cell cycle distribution, DNA synthesis and cell counts. Also gene expression profiles revealed contrary trends in DNA replication and cell cycle regulation affecting cyclins, CDKs as well as repair checkpoints. Mitochondrial function was assessed by measuring H_2O_2 concentrations and $\Delta\Psi_m$ at different time points following irradiation. Both blue light doses revealed a rapid increase of H_2O_2 levels, accompanied by fast decreases in $\Delta\Psi_m$ indicating metabolic stress; however, both effects returned towards control levels within 24 hours. Thus, to some extent, light effects were identified to rely on retrograde mitochondrial signaling altering the expression of several transcription factors like NF- κ B or Nrf2 via changes in $\Delta\Psi_m$ and the Janus-face mediator ROS. Moreover, *PRKAA1* and *AKT1* coding for primary effectors of metabolic stress, respectively AMPK and AKT, were found significantly expressed exerting antagonistic regulations of *FOXO1* and *MTOR*, which modulate oxidative stress resistance, cell survival and growth. In addition, genes involved in antioxidant defense mechanisms, inter alia transcribed by Nrf2 and AhR, were found up-regulated, showing a higher activation for 21.6 J/cm². Cytoprotection was further promoted by affecting the interplay between pro- and anti-apoptotic genes inducing stress resistance and even a higher proliferative capacity following 5.4 J/cm² of blue light. Prevention of apoptotic signaling was verified by cell viability studies negating cytotoxicity up to a single light dose of 172.8 J/cm². Though, reduced proliferation rates observed after consecutive irradiations with 21.6 J/cm² each were accompanied by a higher occurrence of apoptotic cells, possibly indicating mitotic catastrophe.

In conclusion, blue light seemed to be pro-oxidant in the short term, but anti-oxidant in the long term likely to induce stress resistance, at least following low and controlled amounts of oxidative stress. Driven by metabolic and redox homeostasis, various downstream processes were activated modifying antioxidant defense, survival and proliferation. Moreover, the results indicated that an optimal choice of irradiation parameters, particularly the dose, is important for the effectiveness of the treatment, since doses lower or higher than the optimum can lead to ineffective or even negative outcomes. Using cycled irradiation, the differential effect of blue light doses on NHDF cells might be exploited for novel concepts in advanced wound care, particularly for chronic wounds showing impaired activity of dividing cells and fibrotic skin diseases.

6 REFERENCES

1. Finsen, NR: *Nobel Lectures, Physiology or Medicine 1901-1921*, Amsterdam, Elsevier Publishing Company, 1967.
2. Schawlow, AL, Townes, CH: Infrared and Optical Masers. *Phys Rev*, 112: 1940-1949, 1958.
3. Mester, E, Szende, B, Gartner, P: The effect of laser beams on the growth of hair in mice. *Radiobiologia, Radiotherapia*, 9: 621-626, 1968.
4. Mester, E, Spiry, T, Szende, B, Tota, JG: Effect of laser rays on wound healing. *American Journal of Surgery*, 122: 532-535, 1971.
5. Mester, E, Nagylucskay, S, Doklen, A, Tisza, S: Laser stimulation of wound healing. *Acta Chirurgica Academiae Scientiarum Hungaricae*, 17: 49-55, 1976.
6. Anders, JJ, Lanzafame, RJ, Arany, PR: Low-level light/laser therapy versus photobiomodulation therapy. *Photomedicine and Laser Surgery*, 33: 183-184, 2015.
7. Arany, PR: Photobiomodulation: poised from the fringes. *Photomedicine and Laser Surgery*, 30: 507-509, 2012.
8. Chung, H, Dai, T, Sharma, SK, Huang, YY, Carroll, JD, Hamblin, MR: The nuts and bolts of low-level laser (light) therapy. *Annals of Biomedical Engineering*, 40: 516-533, 2012.
9. Parker, R: Putting the medicine in the lenses: The importance of blocking ultraviolet radiation and blue light. Updated edition from Jan 2016, Points de Vue, International Review of Ophthalmic Optics, Essilor International, 2014, pp 203-206.
10. Huang, YY, Chen, AC, Carroll, JD, Hamblin, MR: Biphasic dose response in low level light therapy. *Dose-Response*, 7: 358-383, 2009.
11. Bunsen, RW, Roscoe, HE: Photochemical researches - Part V. On the measurement of the chemical action of direct and diffuse sunlight. *Proc R Soc Lond*, 12: 306-312, 1862.
12. Karu, TI, Kolyakov, SF: Exact action spectra for cellular responses relevant to phototherapy. *Photomedicine and Laser Surgery*, 23: 355-361, 2005.
13. Lanzafame, RJ, Stadler, I, Kurtz, AF, Connelly, R, Peter, TA, Sr., Brondon, P, Olson, D: Reciprocity of exposure time and irradiance on energy density during photoradiation on wound healing in a murine pressure ulcer model. *Lasers in Surgery and Medicine*, 39: 534-542, 2007.
14. Jenkins, PA, Carroll, JD: How to report low-level laser therapy (LLLT)/photomedicine dose and beam parameters in clinical and laboratory studies. *Photomedicine and Laser Surgery*, 29: 785-787, 2011.
15. Sutherland, JC: Biological effects of polychromatic light. *Photochemistry and Photobiology*, 76: 164-170, 2002.
16. Chen, AC, Huang, YY, Arany, PR, Hamblin, MR: Role of reactive oxygen species in low level light therapy. *Proc of SPIE*, 7165: 716502-716503, 2009.
17. Karu, T: Primary and secondary mechanisms of action of visible to near-IR radiation on cells. *Journal of Photochemistry and Photobiology B: Biology*, 49: 1-17, 1999.
18. Svobodova, A, Walterova, D, Vostalova, J: Ultraviolet light induced alteration to the skin. *Biomedical Papers of the Medical Faculty of the University Palacky, Olomouc, Czechoslovakia*, 150: 25-38, 2006.

19. Mahmoud, BH, Hexsel, CL, Hamzavi, IH, Lim, HW: Effects of visible light on the skin. *Photochemistry and Photobiology*, 84: 450-462, 2008.
20. Juzeniene, A, Brekke, P, Dahlback, A: Solar radiation and human health. *Rep Prog Phys*, 74: 1-56, 2011.
21. Karu, TI: Molecular mechanism of the therapeutic effect of low-intensity laser radiation. *Lasers Life Sci*, 2: 53-74, 1988.
22. Letokhov, VS: Effects of transient local heating of spatially and spectrally heterogeneous biotissue by short laser pulses. *Il Nuovo Cimento D*, 13: 939-948, 1991.
23. Mailer, K: Superoxide radical as electron donor for oxidative phosphorylation of ADP. *Biochemical and Biophysical Research Communications*, 170: 59-64, 1990.
24. Spikes, JD: *Photosensitization*, New York, The Science of Photobiology, 1989.
25. Afonso, SG, Enriquez de Salamanca, R, Battle, AM: The photodynamic and non-photodynamic actions of porphyrins. *Brazilian Journal of Medical and Biological Research*, 32: 255-266, 1999.
26. Eichler, M, Lavi, R, Shainberg, A, Lubart, R: Flavins are source of visible-light-induced free radical formation in cells. *Lasers in Surgery and Medicine*, 37: 314-319, 2005.
27. Enwemeka, CS, Williams, D, Enwemeka, SK, Hollosi, S, Yens, D: Blue 470-nm light kills methicillin-resistant *Staphylococcus aureus* (MRSA) in vitro. *Photomedicine and Laser Surgery*, 27: 221-226, 2009.
28. Avci, P, Gupta, A, Sadasivam, M, Vecchio, D, Pam, Z, Pam, N, Hamblin, MR: Low-level laser (light) therapy (LLLT) in skin: stimulating, healing, restoring. *Seminars in Cutaneous Medicine and Surgery*, 32: 41-52, 2013.
29. Hamblin, MR: Mechanisms and applications of the anti-inflammatory effects of photobiomodulation. *AIMS Biophys*, 4: 337-361, 2017.
30. Held, L, Metzler, G, Schaller, M: Histologische Strukturen der normalen Haut. In: *Histopathologie der Haut*. 2nd ed. edited by CERRONI, L., GARBE, C., METZE, D., KUTZNER, H., KERL, H., Berlin; Heidelberg, Springer Reference Medizin, 2016, pp 61-76.
31. Kanitakis, J: Anatomy, histology and immunohistochemistry of normal human skin. *European Journal of Dermatology*, 12: 390-399, 2002.
32. Charkoudian, N: Skin blood flow in adult human thermoregulation: how it works, when it does not, and why. *Mayo Clinic Proceedings*, 78: 603-612, 2003.
33. Rawlings, AV, Harding, CR: Moisturization and skin barrier function. *Dermatologic Therapy*, 17: 43-48, 2004.
34. MacNeil, S: Progress and opportunities for tissue-engineered skin. *Nature*, 445: 874-880, 2007.
35. Freinkel, RK, Woodley, DT: *The biology of skin*, New York, Parthenon Publishing, 2001.
36. Fore, J: A review of skin and the effects of aging on skin structure and function. *Ostomy/Wound Management*, 52: 24-35, 2006.
37. Winslow, T: *Skin Anatomy*. Terese Winslow LLC Medical Illustration, 2008.
38. Chu, DH: Overview of biology, development, and structure of skin. In: *Fitzpatrick's dermatology in general medicine*. 7th ed. edited by WOLFF, K., GOLDSMITH, L. A., KATZ, S. I., GILCHREST, B. A., PALLER, A. S., LEFFEL, D. J., New York McGraw-Hill Medical, 2008, pp 57-73.
39. Ross, MH, Pawlina, W: *Histology: a text and atlas*, Philadelphia, Lippincott Williams & Wilkins, 2010.

40. Sorrell, JM, Caplan, AI: Fibroblast heterogeneity: more than skin deep. *Journal of Cell Science*, 117: 667-675, 2004.
41. Janson, DG, Saintigny, G, van Adrichem, A, Mahe, C, El Ghalbzouri, A: Different gene expression patterns in human papillary and reticular fibroblasts. *Journal of Investigative Dermatology*, 132: 2565-2572, 2012.
42. Korosec, A, Frech, S, Gesslbauer, B, Vierhapper, M, Radtke, C, Petzelbauer, P, Lichtenberger, BM: Lineage Identity and Location within the Dermis Determine the Function of Papillary and Reticular Fibroblasts in Human Skin. *Journal of Investigative Dermatology*, 139: 342-351, 2019.
43. Driskell, RR, Lichtenberger, BM, Hoste, E, Kretzschmar, K, Simons, BD, Charalambous, M, Ferron, SR, Herault, Y, Pavlovic, G, Ferguson-Smith, AC, Watt, FM: Distinct fibroblast lineages determine dermal architecture in skin development and repair. *Nature*, 504: 277-281, 2013.
44. Cole, MA, Quan, T, Voorhees, JJ, Fisher, GJ: Extracellular matrix regulation of fibroblast function: redefining our perspective on skin aging. *J Cell Commun Signal*, 12: 35-43, 2018.
45. Tomasek, JJ, Gabbiani, G, Hinz, B, Chaponnier, C, Brown, RA: Myofibroblasts and mechano-regulation of connective tissue remodelling. *Nature Reviews: Molecular Cell Biology*, 3: 349-363, 2002.
46. Tracy, LE, Minasian, RA, Caterson, EJ: Extracellular Matrix and Dermal Fibroblast Function in the Healing Wound. *Adv Wound Care (New Rochelle)*, 5: 119-136, 2016.
47. Enoch, S, Leaper, DJ: Basic science of wound healing. *Surgery*, 26: 31-37, 2008.
48. Werner, S, Krieg, T, Smola, H: Keratinocyte-fibroblast interactions in wound healing. *Journal of Investigative Dermatology*, 127: 998-1008, 2007.
49. Sowa, P, Rutkowska-Talipska, J, Rutkowski, K, Kosztyla-Hojna, B, Rutkowski, R: Optical radiation in modern medicine. *Postepy Dermatol Alergol*, 30: 246-251, 2013.
50. Bashkatov, AN, Genina, EA, Kochubey, VI, Tuchin, VV: Optical properties of human skin, subcutaneous and mucous tissues in the wavelength range from 400 to 2000 nm. *J Phys D: Appl Phys*, 38: 2543-2555, 2005.
51. Barolet, D: Light-emitting diodes (LEDs) in dermatology. *Seminars in Cutaneous Medicine and Surgery*, 27: 227-238, 2008.
52. Winkler, BS, Boulton, ME, Gottsch, JD, Sternberg, P: Oxidative damage and age-related macular degeneration. *Molecular Vision*, 5: 24-35, 1999.
53. Zhao, ZC, Zhou, Y, Tan, G, Li, J: Research progress about the effect and prevention of blue light on eyes. *Int J Ophthalmol*, 11: 1999-2003, 2018.
54. Lipovsky, A, Nitzan, Y, Gedanken, A, Lubart, R: Visible light-induced killing of bacteria as a function of wavelength: implication for wound healing. *Lasers in Surgery and Medicine*, 42: 467-472, 2010.
55. Maclean, M, MacGregor, SJ, Anderson, JG, Woolsey, G: Inactivation of bacterial pathogens following exposure to light from a 405-nanometer light-emitting diode array. *Applied and Environmental Microbiology*, 75: 1932-1937, 2009.
56. Guffey, JS, Wilborn, J: In vitro bactericidal effects of 405-nm and 470-nm blue light. *Photomedicine and Laser Surgery*, 24: 684-688, 2006.
57. Dai, T, Gupta, A, Murray, CK, Vrahas, MS, Tegos, GP, Hamblin, MR: Blue light for infectious diseases: Propionibacterium acnes, Helicobacter pylori, and beyond? *Drug Resist Updat*, 15: 223-236, 2012.
58. Shnitkind, E, Yaping, E, Geen, S, Shalita, AR, Lee, WL: Anti-inflammatory properties of narrow-band blue light. *J Drugs Dermatol*, 5: 605-610, 2006.

59. Pfaff, S, Liebmann, J, Born, M, Merk, HF, von Felbert, V: Prospective Randomized Long-Term Study on the Efficacy and Safety of UV-Free Blue Light for Treating Mild Psoriasis Vulgaris. *Dermatology*, 231: 24-34, 2015.
60. Pei, S, Inamadar, AC, Adya, KA, Tsoukas, MM: Light-based therapies in acne treatment. *Indian Dermatol Online J*, 6: 145-157, 2015.
61. Kumar, P, Chawla, D, Deorari, A: Light-emitting diode phototherapy for unconjugated hyperbilirubinaemia in neonates. *Cochrane Database of Systematic Reviews*: Cd007969, 2011.
62. Lewis, JB, Wataha, JC, Messer, RL, Caughman, GB, Yamamoto, T, Hsu, SD: Blue light differentially alters cellular redox properties. *Journal of Biomedical Materials Research: Part B, Applied Biomaterials*, 72: 223-229, 2005.
63. Liebmann, J, Born, M, Kolb-Bachofen, V: Blue-light irradiation regulates proliferation and differentiation in human skin cells. *Journal of Investigative Dermatology*, 130: 259-269, 2010.
64. Regazzetti, C, Sormani, L, Debayle, D, Bernerd, F, Tulic, MK, De Donatis, GM, Chignon-Sicard, B, Rocchi, S, Passeron, T: Melanocytes Sense Blue Light and Regulate Pigmentation through Opsin-3. *Journal of Investigative Dermatology*, 138: 171-178, 2018.
65. Yuan, Y, Yan, G, Gong, R, Zhang, L, Liu, T, Feng, C, Du, W, Wang, Y, Yang, F, Li, Y, Guo, S, Ding, F, Ma, W, Idiatullina, E, Pavlov, V, Han, Z, Cai, B, Yang, L: Effects of Blue Light Emitting Diode Irradiation On the Proliferation, Apoptosis and Differentiation of Bone Marrow-Derived Mesenchymal Stem Cells. *Cellular Physiology and Biochemistry*, 43: 237-246, 2017.
66. Pagin, MT, de Oliveira, FA, Oliveira, RC, Sant'Ana, AC, de Rezende, ML, Greggi, SL, Damante, CA: Laser and light-emitting diode effects on pre-osteoblast growth and differentiation. *Lasers in Medical Science*, 29: 55-59, 2014.
67. Volpato, LE, de Oliveira, RC, Espinosa, MM, Bagnato, VS, Machado, MA: Viability of fibroblasts cultured under nutritional stress irradiated with red laser, infrared laser, and red light-emitting diode. *Journal of Biomedical Optics*, 16: 1-6, 2011.
68. Vinck, EM, Cagnie, BJ, Cornelissen, MJ, Declercq, HA, Cambier, DC: Increased fibroblast proliferation induced by light emitting diode and low power laser irradiation. *Lasers in Medical Science*, 18: 95-99, 2003.
69. Akiyama, M, Okano, K, Fukada, Y, Okano, T: Macrophage inhibitory cytokine MIC-1 is upregulated by short-wavelength light in cultured normal human dermal fibroblasts. *FEBS Letters*, 583: 933-937, 2009.
70. Bonatti, S, Hochman, B, Tucci-Viegas, VM, Furtado, F, Pinfieldi, CE, Pedro, AC, Ferreira, LM: In vitro effect of 470 nm LED (Light Emitting Diode) in keloid fibroblasts. *Acta Cirurgica Brasileira*, 26: 25-30, 2011.
71. Fushimi, T, Inui, S, Nakajima, T, Ogasawara, M, Hosokawa, K, Itami, S: Green light emitting diodes accelerate wound healing: characterization of the effect and its molecular basis in vitro and in vivo. *Wound Repair and Regeneration*, 20: 226-235, 2012.
72. Hwang, IY, Son, YO, Kim, JH, Jeon, YM, Kim, JG, Lee, CB, Park, JS, Lee, JC: Plasma-arc generated light inhibits proliferation and induces apoptosis of human gingival fibroblasts in a dose-dependent manner. *Dental Materials*, 24: 1036-1042, 2008.
73. Krassovka, J, Borgschulze, A, Sahlender, B, Logters, T, Windolf, J, Grotheer, V: Blue light irradiation and its beneficial effect on Dupuytren's fibroblasts. *PLoS One*, 14: e0209833, 2019.

74. Kushibiki, T, Hirasawa, T, Okawa, S, Ishihara, M: Blue laser irradiation generates intracellular reactive oxygen species in various types of cells. *Photomedicine and Laser Surgery*, 31: 95-104, 2013.
75. Lee, HS, Jung, SE, Kim, SK, Kim, YS, Sohn, S, Kim, YC: Low-Level Light Therapy with 410 nm Light Emitting Diode Suppresses Collagen Synthesis in Human Keloid Fibroblasts: An In Vitro Study. *Ann Dermatol*, 29: 149-155, 2017.
76. Malcic, AI, Pavicic, I, Trosic, I, Simeon, P, Katanec, D, Krmek, SJ: The effects of bluephase LED light on fibroblasts. *Eur J Dent*, 6: 311-317, 2012.
77. Mamalis, A, Garcha, M, Jagdeo, J: Light emitting diode-generated blue light modulates fibrosis characteristics: fibroblast proliferation, migration speed, and reactive oxygen species generation. *Lasers in Surgery and Medicine*, 47: 210-215, 2015.
78. Masson-Meyers, DS, Bumah, VV, Enwemeka, CS: A comparison of four methods for determining viability in human dermal fibroblasts irradiated with blue light. *Journal of Pharmacological and Toxicological Methods*, 79: 15-22, 2016.
79. Masson-Meyers, DS, Bumah, VV, Enwemeka, CS: Blue light does not impair wound healing in vitro. *Journal of Photochemistry and Photobiology B: Biology*, 160: 53-60, 2016.
80. Mignon, C, Uzunbajakava, NE, Castellano-Pellicena, I, Botchkareva, NV, Tobin, DJ: Differential response of human dermal fibroblast subpopulations to visible and near-infrared light: Potential of photobiomodulation for addressing cutaneous conditions. *Lasers in Surgery and Medicine*, 50: 859-882, 2018.
81. Oplander, C, Hidding, S, Werners, FB, Born, M, Pallua, N, Suschek, CV: Effects of blue light irradiation on human dermal fibroblasts. *Journal of Photochemistry and Photobiology B: Biology*, 103: 118-125, 2011.
82. Rotenberg, S, Lewis, JB, Lockwood, PE, Tseng, WY, Messer, RL, Hsu, SD, Omata, Y, Wataha, JC: Extracellular environment as one mediator of blue light-induced mitochondrial suppression. *Dental Materials*, 22: 759-764, 2006.
83. Seo, YK, Park, JK, Song, C, Kwon, SY: Comparison of light-emitting diode wavelength on activity and migration of rabbit ACL cells. *Lasers in Medical Science*, 29: 245-255, 2014.
84. Taflinski, L, Demir, E, Kauczok, J, Fuchs, PC, Born, M, Suschek, CV, Oplander, C: Blue light inhibits transforming growth factor-beta1-induced myofibroblast differentiation of human dermal fibroblasts. *Experimental Dermatology*, 23: 240-246, 2014.
85. Taoufik, K, Mavrogonatou, E, Eliades, T, Papagiannoulis, L, Eliades, G, Kletsas, D: Effect of blue light on the proliferation of human gingival fibroblasts. *Dental Materials*, 24: 895-900, 2008.
86. Teuschl, A, Balmayor, ER, Redl, H, van Griensven, M, Dungel, P: Phototherapy with LED light modulates healing processes in an in vitro scratch-wound model using 3 different cell types. *Dermatologic Surgery*, 41: 261-268, 2015.
87. Wataha, JC, Lockwood, PE, Lewis, JB, Rueggeberg, FA, Messer, RL: Biological effects of blue light from dental curing units. *Dental Materials*, 20: 150-157, 2004.
88. Wataha, JC, Lewis, JB, Lockwood, PE, Hsu, S, Messer, RL, Rueggeberg, FA, Bouillaguet, S: Blue light differentially modulates cell survival and growth. *Journal of Dental Research*, 83: 104-108, 2004.

89. Yoshida, A, Yoshino, F, Makita, T, Maehata, Y, Higashi, K, Miyamoto, C, Wada-Takahashi, S, Takahashi, SS, Takahashi, O, Lee, MC: Reactive oxygen species production in mitochondria of human gingival fibroblast induced by blue light irradiation. *Journal of Photochemistry and Photobiology B: Biology*, 129: 1-5, 2013.
90. Järbrink, K, Ni, G, Sönnnergren, H, Schmidtchen, A, Pang, C, Bajpai, R, Car, J: The humanistic and economic burden of chronic wounds: a protocol for a systematic review. *Syst Rev*, 6: 1-7, 2017.
91. Levinson, H: A Paradigm of Fibroblast Activation and Dermal Wound Contraction to Guide the Development of Therapies for Chronic Wounds and Pathologic Scars. *Adv Wound Care (New Rochelle)*, 2: 149-159, 2013.
92. Werdin, F, Tennenhaus, M, Schaller, HE, Rennekampff, HO: Evidence-based management strategies for treatment of chronic wounds. *Eplasty*, 9: e19, 2009.
93. Wound Healing Society: *Chronic wound care guidelines*. 2006. Online: <http://woundheal.org/Publications/WHS-Wound-Care-Guidelines.cgi>, Stand: 27.04.2019.
94. Martinengo, L, Olsson, M, Bajpai, R, Soljak, M, Upton, Z, Schmidtchen, A, Car, J, Jarbrink, K: Prevalence of chronic wounds in the general population: systematic review and meta-analysis of observational studies. *Annals of Epidemiology*, 29: 8-15, 2019.
95. Klapczynski, A, Kuch, N, Gretz, N: Report and guide line for the software development of improved light exposure schemes: on/off cycles, intensities. Unpublished report for MEDILIGHT - Miniaturized smart system for light stimulation and monitoring of wound healing, European Union's Horizon 2020 research and innovation program, Grant Agreement No. 644267, University of Heidelberg, 2018, pp 1-71.
96. Mu, Y, Kuch, N, Klapczynski, A, Gretz, N: Quantified effects of light exposure schemes on bacteria cultures and derivation of refined light exposure schemes for antibacterial effects. Unpublished report for MEDILIGHT - Miniaturized smart system for light stimulation and monitoring of wound healing, European Union's Horizon 2020 research and innovation program, Grant Agreement No. 644267, University of Heidelberg, 2018, pp 1-30.
97. Dai, M, Wang, P, Boyd, AD, Kostov, G, Athey, B, Jones, EG, Bunney, WE, Myers, RM, Speed, TP, Akil, H, Watson, SJ, Meng, F: Evolving gene/transcript definitions significantly alter the interpretation of GeneChip data. *Nucleic Acids Research*, 33: e175, 2005.
98. Subramanian, A, Tamayo, P, Mootha, VK, Mukherjee, S, Ebert, BL, Gillette, MA, Paulovich, A, Pomeroy, SL, Golub, TR, Lander, ES, Mesirov, JP: Gene set enrichment analysis: a knowledge-based approach for interpreting genome-wide expression profiles. *Proc Natl Acad Sci USA*, 102: 15545-15550, 2005.
99. Huang, YY, Sharma, SK, Carroll, J, Hamblin, MR: Biphasic dose response in low level light therapy - an update. *Dose-Response*, 9: 602-618, 2011.
100. Schulz, H: *Über die Theorie der Arzneimittelwirkung*, Virchows Archiv, 1877.
101. Schulz, H: *Über Hefegiste*, Pflügers Archiv Gesamte Physiologie, 1888.
102. Stebbing, AR: Hormesis--the stimulation of growth by low levels of inhibitors. *Science of the Total Environment*, 22: 213-234, 1982.
103. Calabrese, EJ: Hormesis: changing view of the dose-response, a personal account of the history and current status. *Mutation Research*, 511: 181-189, 2002.

104. Calabrese, EJ: Hormesis: a revolution in toxicology, risk assessment and medicine. *EMBO Rep*, 5: S37-40, 2004.
105. Brondon, P, Stadler, I, Lanzafame, RJ: A study of the effects of phototherapy dose interval on photobiomodulation of cell cultures. *Lasers in Surgery and Medicine*, 36: 409-413, 2005.
106. Schmidt, M, Gutknecht, D, Simon, JC, Schulz, JN, Eckes, B, Anderegg, U, Saalbach, A: Controlling the Balance of Fibroblast Proliferation and Differentiation: Impact of Thy-1. *Journal of Investigative Dermatology*, 135: 1893-1902, 2015.
107. Negmadjanov, U, Godic, Z, Rizvi, F, Emelyanova, L, Ross, G, Richards, J, Holmuhamedov, EL, Jahangir, A: TGF- β 1-mediated differentiation of fibroblasts is associated with increased mitochondrial content and cellular respiration. *PloS One*, 10: e0123046, 2015.
108. Quent, VM, Loessner, D, Friis, T, Reichert, JC, Hutmacher, DW: Discrepancies between metabolic activity and DNA content as tool to assess cell proliferation in cancer research. *Journal of Cellular and Molecular Medicine*, 14: 1003-1013, 2010.
109. Masur, SK, Dewal, HS, Dinh, TT, Erenburg, I, Petridou, S: Myofibroblasts differentiate from fibroblasts when plated at low density. *Proc Natl Acad Sci USA*, 93: 4219-4223, 1996.
110. Ohara, M, Kawashima, Y, Katoh, O, Watanabe, H: Blue light inhibits the growth of B16 melanoma cells. *Japanese Journal of Cancer Research*, 93: 551-558, 2002.
111. Li, M, Zhao, L, Liu, J, Liu, AL, Zeng, WS, Luo, SQ, Bai, XC: Hydrogen peroxide induces G2 cell cycle arrest and inhibits cell proliferation in osteoblasts. *Anat Rec (Hoboken)*, 292: 1107-1113, 2009.
112. Gregory, TR: Genome Size Evolution in Animals. In: *The Evolution of the Genome* edited by GREGORY, T. R., London, Elsevier Academic Press, 2005, pp 3-87.
113. Cavalier-Smith, T: Economy, speed and size matter: evolutionary forces driving nuclear genome miniaturization and expansion. *Ann Bot*, 95: 147-175, 2005.
114. Anderson, DJ, Hetzer, MW: Nuclear envelope formation by chromatin-mediated reorganization of the endoplasmic reticulum. *Nature Cell Biology*, 9: 1160-1166, 2007.
115. Brandt, A, Papagiannouli, F, Wagner, N, Wilsch-Brauninger, M, Braun, M, Furlong, EE, Loserth, S, Wenzl, C, Pilot, F, Vogt, N, Lecuit, T, Krohne, G, Grosshans, J: Developmental control of nuclear size and shape by Kugelkern and Kurzkern. *Current Biology*, 16: 543-552, 2006.
116. Gao, X, Xing, D: Molecular mechanisms of cell proliferation induced by low power laser irradiation. *Journal of Biomedical Science*, 16: 1-16, 2009.
117. Mittler, R: ROS Are Good. *Trends Plant Sci*, 22: 11-19, 2017.
118. Rhee, SG: Redox signaling: hydrogen peroxide as intracellular messenger. *Experimental and Molecular Medicine*, 31: 53-59, 1999.
119. Phaniendra, A, Jestadi, DB, Periyasamy, L: Free radicals: properties, sources, targets, and their implication in various diseases. *Indian Journal of Clinical Biochemistry*, 30: 11-26, 2015.
120. Zeng, JP, Bi, B, Chen, L, Yang, P, Guo, Y, Zhou, YQ, Liu, TY: Repeated exposure of mouse dermal fibroblasts at a sub-cytotoxic dose of UVB leads to premature senescence: a robust model of cellular photoaging. *Journal of Dermatological Science*, 73: 49-56, 2014.

121. Lubart, R, Eichler, M, Lavi, R, Friedman, H, Shainberg, A: Low-energy laser irradiation promotes cellular redox activity. *Photomedicine and Laser Surgery*, 23: 3-9, 2005.
122. Maynard, S, Schurman, SH, Harboe, C, de Souza-Pinto, NC, Bohr, VA: Base excision repair of oxidative DNA damage and association with cancer and aging. *Carcinogenesis*, 30: 2-10, 2009.
123. Osipov, AN, Grekhova, A, Pustovalova, M, Ozerov, IV, Eremin, P, Vorobyeva, N, Lazareva, N, Pulin, A, Zhavoronkov, A, Roumiantsev, S, Klokov, D, Eremin, I: Activation of homologous recombination DNA repair in human skin fibroblasts continuously exposed to X-ray radiation. *Oncotarget*, 6: 26876-26885, 2015.
124. Rizzo, JL, Dunn, J, Rees, A, Runger, TM: No formation of DNA double-strand breaks and no activation of recombination repair with UVA. *Journal of Investigative Dermatology*, 131: 1139-1148, 2011.
125. He, G, Siddik, ZH, Huang, Z, Wang, R, Koomen, J, Kobayashi, R, Khokhar, AR, Kuang, J: Induction of p21 by p53 following DNA damage inhibits both Cdk4 and Cdk2 activities. *Oncogene*, 24: 2929-2943, 2005.
126. Chen, QM, Bartholomew, JC, Campisi, J, Acosta, M, Reagan, JD, Ames, BN: Molecular analysis of H₂O₂-induced senescent-like growth arrest in normal human fibroblasts: p53 and Rb control G1 arrest but not cell replication. *Biochemical Journal*, 332 (Pt 1): 43-50, 1998.
127. Smith, ML, Ford, JM, Hollander, MC, Bortnick, RA, Amundson, SA, Seo, YR, Deng, CX, Hanawalt, PC, Fornace, AJ, Jr.: p53-mediated DNA repair responses to UV radiation: studies of mouse cells lacking p53, p21, and/or gadd45 genes. *Molecular and Cellular Biology*, 20: 3705-3714, 2000.
128. Gulappa, T, Reddy, RS, Suman, S, Nyakeriga, AM, Damodaran, C: Molecular interplay between cdk4 and p21 dictates G0/G1 cell cycle arrest in prostate cancer cells. *Cancer Letters*, 337: 177-183, 2013.
129. Naik, E, Michalak, EM, Villunger, A, Adams, JM, Strasser, A: Ultraviolet radiation triggers apoptosis of fibroblasts and skin keratinocytes mainly via the BH3-only protein Noxa. *Journal of Cell Biology*, 176: 415-424, 2007.
130. Vakifahmetoglu-Norberg, H, Ouchida, AT, Norberg, E: The role of mitochondria in metabolism and cell death. *Biochemical and Biophysical Research Communications*, 482: 426-431, 2017.
131. Dey, R, Moraes, CT: Lack of oxidative phosphorylation and low mitochondrial membrane potential decrease susceptibility to apoptosis and do not modulate the protective effect of Bcl-x(L) in osteosarcoma cells. *Journal of Biological Chemistry*, 275: 7087-7094, 2000.
132. Zhang, J, Wang, Y, Liu, X, Dagda, RK, Zhang, Y: How AMPK and PKA Interplay to Regulate Mitochondrial Function and Survival in Models of Ischemia and Diabetes. *Oxidative Medicine and Cellular Longevity*, 2017: 1-12, 2017.
133. Han, Y, Wang, Q, Song, P, Zhu, Y, Zou, MH: Redox regulation of the AMP-activated protein kinase. *PloS One*, 5: e15420, 2010.
134. Sena, LA, Chandel, NS: Physiological roles of mitochondrial reactive oxygen species. *Molecular Cell*, 48: 158-167, 2012.
135. Yun, J, Finkel, T: Mitohormesis. *Cell Metabolism*, 19: 757-766, 2014.
136. Ristow, M: Unraveling the truth about antioxidants: mitohormesis explains ROS-induced health benefits. *Nature Medicine*, 20: 709-711, 2014.

137. Zimmermann, K, Baldinger, J, Mayerhofer, B, Atanasov, AG, Dirsch, VM, Heiss, EH: Activated AMPK boosts the Nrf2/HO-1 signaling axis--A role for the unfolded protein response. *Free Radical Biology and Medicine*, 88: 417-426, 2015.
138. Kansanen, E, Kuosmanen, SM, Leinonen, H, Levonen, AL: The Keap1-Nrf2 pathway: Mechanisms of activation and dysregulation in cancer. *Redox Biol*, 1: 45-49, 2013.
139. Kobayashi, A, Ohta, T, Yamamoto, M: Unique function of the Nrf2-Keap1 pathway in the inducible expression of antioxidant and detoxifying enzymes. *Methods in Enzymology*, 378: 273-286, 2004.
140. Ma, Q: Role of nrf2 in oxidative stress and toxicity. *Annual Review of Pharmacology and Toxicology*, 53: 401-426, 2013.
141. Didier, C, Kerblat, I, Drouet, C, Favier, A, Beani, JC, Richard, MJ: Induction of thioredoxin by ultraviolet-A radiation prevents oxidative-mediated cell death in human skin fibroblasts. *Free Radical Biology and Medicine*, 31: 585-598, 2001.
142. Meewes, C, Brenneisen, P, Wenk, J, Kuhr, L, Ma, W, Alikoski, J, Poswig, A, Krieg, T, Scharffetter-Kochanek, K: Adaptive antioxidant response protects dermal fibroblasts from UVA-induced phototoxicity. *Free Radical Biology and Medicine*, 30: 238-247, 2001.
143. Masgras, I, Carrera, S, de Verdier, PJ, Brennan, P, Majid, A, Makhtar, W, Tulchinsky, E, Jones, GD, Roninson, IB, Macip, S: Reactive oxygen species and mitochondrial sensitivity to oxidative stress determine induction of cancer cell death by p21. *Journal of Biological Chemistry*, 287: 9845-9854, 2012.
144. Becker, A, Klapczynski, A, Kuch, N, Arpino, F, Simon-Keller, K, De La Torre, C, Sticht, C, van Abeelen, FA, Oversluizen, G, Gretz, N: Gene expression profiling reveals aryl hydrocarbon receptor as a possible target for photobiomodulation when using blue light. *Scientific Reports*, 6: 1-11, 2016.
145. Katayama, S, Skoog, T, Jouhilahti, EM, Siitonen, HA, Nuutila, K, Tervaniemi, MH, Vuola, J, Johnsson, A, Lonnerberg, P, Linnarsson, S, Elomaa, O, Kankuri, E, Kere, J: Gene expression analysis of skin grafts and cultured keratinocytes using synthetic RNA normalization reveals insights into differentiation and growth control. *BMC Genomics*, 16: 1-14, 2015.
146. Olschlager, V, Schrader, A, Hockertz, S: Comparison of primary human fibroblasts and keratinocytes with immortalized cell lines regarding their sensitivity to sodium dodecyl sulfate in a neutral red uptake cytotoxicity assay. *Arzneimittel-Forschung*, 59: 146-152, 2009.
147. Marionnet, C, Pierrard, C, Lejeune, F, Sok, J, Thomas, M, Bernerd, F: Different oxidative stress response in keratinocytes and fibroblasts of reconstructed skin exposed to non extreme daily-ultraviolet radiation. *PLoS One*, 5: e12059, 2010.
148. Tigges, J, Weighardt, H, Wolff, S, Gotz, C, Forster, I, Kohne, Z, Huebenthal, U, Merk, HF, Abel, J, Haarmann-Stemmann, T, Krutmann, J, Fritsche, E: Aryl hydrocarbon receptor repressor (AhRR) function revisited: repression of CYP1 activity in human skin fibroblasts is not related to AhRR expression. *Journal of Investigative Dermatology*, 133: 87-96, 2013.
149. Slominski, A, Zbytek, B, Nikolakis, G, Manna, PR, Skobowiat, C, Zmijewski, M, Li, W, Janjetovic, Z, Postlethwaite, A, Zouboulis, CC, Tuckey, RC: Steroidogenesis in the skin: implications for local immune functions. *Journal of Steroid Biochemistry and Molecular Biology*, 137: 107-123, 2013.

150. Liu, C, Liang, B, Wang, Q, Wu, J, Zou, MH: Activation of AMP-activated protein kinase α 1 alleviates endothelial cell apoptosis by increasing the expression of anti-apoptotic proteins Bcl-2 and survivin. *Journal of Biological Chemistry*, 285: 15346-15355, 2010.
151. Ovrevik, J, Lag, M, Lecureur, V, Gilot, D, Lagadic-Gossmann, D, Refsnes, M, Schwarze, PE, Skuland, T, Becher, R, Holme, JA: AhR and Arnt differentially regulate NF-kappaB signaling and chemokine responses in human bronchial epithelial cells. *Cell Commun Signal*, 12: 1-17, 2014.
152. Yun, H, Park, S, Kim, MJ, Yang, WK, Im, DU, Yang, KR, Hong, J, Choe, W, Kang, I, Kim, SS, Ha, J: AMP-activated protein kinase mediates the antioxidant effects of resveratrol through regulation of the transcription factor FoxO1. *Febs j*, 281: 4421-4438, 2014.
153. Zhao, Y, Hu, X, Liu, Y, Dong, S, Wen, Z, He, W, Zhang, S, Huang, Q, Shi, M: ROS signaling under metabolic stress: cross-talk between AMPK and AKT pathway. *Molecular Cancer*, 16: 1-12, 2017.
154. Dan, HC, Cooper, MJ, Cogswell, PC, Duncan, JA, Ting, JP, Baldwin, AS: Akt-dependent regulation of NF- κ B is controlled by mTOR and Raptor in association with IKK. *Genes and Development*, 22: 1490-1500, 2008.
155. Mihaylova, MM, Shaw, RJ: The AMPK signalling pathway coordinates cell growth, autophagy and metabolism. *Nature Cell Biology*, 13: 1016-1023, 2011.
156. Yu, DS, Cortez, D: A role for CDK9-cyclin K in maintaining genome integrity. *Cell Cycle*, 10: 28-32, 2011.
157. Hartlerode, AJ, Morgan, MJ, Wu, Y, Buis, J, Ferguson, DO: Recruitment and activation of the ATM kinase in the absence of DNA-damage sensors. *Nature Structural & Molecular Biology*, 22: 736-743, 2015.
158. Bluwstein, A, Kumar, N, Leger, K, Traenkle, J, Oostrum, J, Rehrauer, H, Baudis, M, Hottiger, MO: PKC signaling prevents irradiation-induced apoptosis of primary human fibroblasts. *Cell Death & Disease*, 4: e498, 2013.
159. Abrahamse, H: Stimulation of cellular proliferation and migration: Is it a viable measure of photobiomodulation? *Photomedicine and Laser Surgery*, 33: 1-2, 2015.
160. Ianzini, F, Bertoldo, A, Kosmacek, EA, Phillips, SL, Mackey, MA: Lack of p53 function promotes radiation-induced mitotic catastrophe in mouse embryonic fibroblast cells. *Cancer Cell International*, 6: 1-8, 2006.
161. Hashmi, JT, Huang, YY, Sharma, SK, Kurup, DB, De Taboada, L, Carroll, JD, Hamblin, MR: Effect of pulsing in low-level light therapy. *Lasers in Surgery and Medicine*, 42: 450-466, 2010.

7 APPENDIX

Table 17: Statistics for Figure 20. Using the Wilcoxon method, nonparametric comparisons were performed for each pair. Statistically significant differences from the untreated control are indicated by a nominal p-value < 0.05.

- Level	0	0	0	0	0	0	0	0	0	0	0	0	0	0	0
Level	1.8	3.6	5.4	7.2	9.0	10.8	12.6	14.4	16.2	18	21.6	32.4	43.2	64.8	86.4
p-Value	0.5094	<.0001	<.0001	<.0001	0.0003	<.0001	<.0001	<.0001	<.0001	<.0001	<.0001	<.0001	<.0001	<.0001	<.0001

Table 18: Statistics for Figure 21. Using the Wilcoxon method, nonparametric comparisons were performed for each pair. Statistically significant differences from the untreated control are indicated by a nominal p-value < 0.05.

Dose [J/cm ²]	5.4							21.6							
- Level	0	0	0	0	0	0	0	0	0	0	0	0	0	0	0
Level	1	3	6	12	24	48	72	1	3	6	12	24	48	72	
p-Value	<.0001	<.0001	0.5560	0.2366	<.0001	<.0001	0.4001	0.3525	0.0611	<.0001	<.0001	<.0001	0.2172	<.0001	

Table 19: Statistics for Figure 22. Using the Student's t-test (Wilcoxon method), (nonparametric) comparisons were performed for each pair. Statistically significant differences for each pair are indicated by a nominal p-value < 0.05.

Dose [J/cm ²]	5.4 (Wilcoxon method)						21.6 (Student's t-test)					
- Level	0	0	0	5.4	5.4	10.8	0	0	0	21.6	21.6	43.2
Level	5.4	10.8	16.2	10.8	16.2	16.2	21.6	43.2	64.8	43.2	64.8	64.8
p-Value	<.0001	<.0001	<.0001	0.5359	<.0001	<.0001	<.0001	<.0001	<.0001	<.0001	<.0001	0.9727

Table 20: Statistics for Figure 23. Using the Student's t-test (Wilcoxon method), (nonparametric) comparisons were performed for each pair. Statistically significant differences from the untreated control are indicated by a nominal p-value < 0.05.

Irradiation No. per Day	1x (Wilcoxon method)			2x (Student's t-test)			3x (Student's t-test)		
	- Level	0	0	0	0	0	0	0	0
Level	5.4/10.8/16.2	10.8/21.6/32.4	16.2/32.4/48.6	5.4/10.8/16.2	10.8/21.6/32.4	16.2/32.4/48.6	5.4/10.8/16.2	10.8/21.6/32.4	16.2/32.4/48.6
p-Value	<.0001	<.0001	<.0001	<.0001	<.0001	<.0001	<.0001	<.0001	<.0001

Table 21: Statistics for Figure 24. Using the Wilcoxon method, nonparametric comparisons were performed for each pair. Statistically significant differences from the untreated control are indicated by a nominal p-value < 0.05.

Dose [J/cm ²]	5.4					21.6				
	- Level	0	0	0	0	0	0	0	0	0
Level	0.5	1	3	6	24	0.5	1	3	6	24
p-Value	0.0169	<.0001	<.0001	<.0001	<.0001	<.0001	<.0001	<.0001	<.0001	<.0001

Table 22: Statistics for Figure 26. Using the Student's t-test, comparisons were performed for each pair of respective cell cycle phases. Statistically significant differences from the untreated control are indicated by a nominal p-value < 0.05.

Dose [J/cm ²]	5.4			21.6		
	- Level	0	0	0	0	0
Level	5.4	10.8	16.2	21.6	43.2	64.8
p-Value (Sub-G0/G1)	0.3848	0.5733	<.0001	0.4519	0.0124	<.0001
p-Value (G0/G1)	<.0001	<.0001	<.0001	<.0001	0.0002	0.0246
p-Value (S)	0.0017	<.0001	0.0076	0.0002	<.0001	<.0001
p-Value (G2/M)	0.0468	0.0003	<.0001	0.0510	<.0001	<.0001

Table 23: Statistics for Figure 27. Using the Student's t-test, comparisons were performed for each pair. Statistically significant differences for each pair are indicated by a nominal p-value < 0.05.

Dose [J/cm^2]	5.4						21.6					
- Level	0	0	0	5.4	5.4	10.8	0	0	0	21.6	21.6	43.2
Level	5.4	10.8	16.2	10.8	16.2	16.2	21.6	43.2	64.8	43.2	64.8	64.8
p-Value	0.0007	<.0001	0.0073	0.0992	<.0001	<.0001	<.0001	<.0001	<.0001	0.0197	<.0001	<.0001

Table 24: Statistics for Figure 28. Using the Student's t-test, comparisons were performed for each pair. Statistically significant differences for each pair are indicated by a nominal p-value < 0.05.

Dose [J/cm^2]	5.4						21.6					
- Level	0	0	0	5.4	5.4	10.8	0	0	0	21.6	21.6	43.2
Level	5.4	10.8	16.2	10.8	16.2	16.2	21.6	43.2	64.8	43.2	64.8	64.8
p-Value	<.0001	<.0001	<.0001	<.0001	<.0001	<.0001	<.0001	<.0001	<.0001	<.0001	<.0001	<.0001

Table 25: Statistics for Figure 29. Using the Student's t-test, comparisons were performed for each pair. Statistically significant differences for each pair are indicated by a nominal p-value < 0.05.

Dose [J/cm^2]	5.4						21.6					
- Level	0	0	0	5.4	5.4	10.8	0	0	0	21.6	21.6	43.2
Level	5.4	10.8	16.2	10.8	16.2	16.2	21.6	43.2	64.8	43.2	64.8	64.8
p-Value	0.6240	0.0005	0.0047	0.0128	0.0067	<.0001	<.0001	<.0001	<.0001	0.0520	<.0001	<.0001

Table 26: Statistics for Figure 30. Using the Student's t-test, comparisons were performed for each pair. Statistically significant differences from the untreated control are indicated by a nominal p-value < 0.05.

Dose [J/cm^2]	5.4					21.6				
- Level	0	0	0	0	0	0	0	0	0	0
Level	0.5	1	3	6	24	0.5	1	3	6	24
p-Value	<.0001	<.0001	0.0005	0.1302	<.0001	<.0001	<.0001	<.0001	<.0001	<.0001

Table 27: Statistics for Figure 31. Using the Wilcoxon method, nonparametric comparisons were performed for each pair. Statistically significant differences from the untreated control are indicated by a nominal p-value < 0.05.

Dose [J/cm^2]	5.4					21.6				
- Level	0	0	0	0	0	0	0	0	0	0
Level	0.5	1	3	6	24	0.5	1	3	6	24
p-Value	<.0001	0.2283	0.1715	0.6994	0.1211	<.0001	<.0001	<.0001	0.3604	0.1222

Table 28: Statistics for Figure 39. Using the Student's t-test, comparisons were performed for each pair. Statistically significant differences for each pair are indicated by a nominal p-value < 0.05.

Quadrants	Living cells			Dead cells		
- Level	Untreated	Untreated	Treated	Untreated	Untreated	Treated
Level	Treated	Positive control	Positive control	Treated	Positive control	Positive control
p-Value ($5.4 \text{ J}/\text{cm}^2$)	0.7869	0.0003	0.0003	0.7869	0.0003	0.0003
p-Value ($21.6 \text{ J}/\text{cm}^2$)	0.6255	<.0001	<.0001	0.6255	<.0001	<.0001
p-Value ($43.2 \text{ J}/\text{cm}^2$)	0.2729	0.0001	0.0002	0.2729	0.0001	0.0002
p-Value ($86.4 \text{ J}/\text{cm}^2$)	0.2318	<.0001	<.0001	0.2318	<.0001	<.0001
p-Value ($172.8 \text{ J}/\text{cm}^2$)	0.0160	<.0001	<.0001	0.0160	<.0001	<.0001

Table 29: Statistics for Figure 48. Using the Student's t-test (Wilcoxon method), (nonparametric) comparisons were performed for each pair. Statistically significant differences from the untreated control are indicated by a nominal p-value < 0.05.

Condition	+ Diffusor (Wilcoxon method)				+ Wound dressing E2723 (Student's t-test)			
- Level	0	0	0	0	0	0	0	0
Level	5.4	10.8	21.6	43.2	5.4	10.8	21.6	43.2
p-Value	<.0001	0.0049	<.0001	<.0001	0.0032	0.3755	0.0001	<.0001

Table 30: Statistics for Figure 49. Using the Wilcoxon method, nonparametric comparisons were performed for each pair. Statistically significant differences from the untreated control are indicated by a nominal p-value < 0.05.

Light source	- Level	0	0	0	0	0	0	0	0	0	0	0	0	0
	Level	1.8	3.6	5.4	7.2	9.0	10.8	12.6	14.4	16.2	18	21.6	32.4	43.2
BioLight LED Lamp	p-Value	0.5094	<.0001	<.0001	<.0001	0.0003	<.0001	<.0001	<.0001	<.0001	<.0001	<.0001	<.0001	<.0001
MEDILIGHT Prototype	p-Value	0.4076	0.0005	<.0001	<.0001	<.0001	<.0001	<.0001	0.5254	0.1207	<.0001	<.0001	<.0001	<.0001

8 CURRICULUM VITAE AND PUBLICATIONS

PERSONALIEN

Name und Vorname: Anna Sophie Klapczynski
Geburtsdatum: 12.12.1990
Geburtsort: 67346 Speyer, Deutschland
Familienstand: Ledig
Vater: Henry Stefan Klapczynski
Mutter: Dorothee Emma Klapczynski

SCHULISCHER WERDEGANG

2001 – 2010 Werner-Heisenberg-Gymnasium, Bad Dürkheim
20.03.2010 Hochschulreife, Abschlussnote: 2,0

UNIVERSITÄRER WERDEGANG

09/2010 – 02/2014 **Bachelor of Science**
Studienfach: Biologische Chemie (Biotechnologie)
Hochschule Mannheim, Deutschland
Abschlussnote: 1,8 (08.04.2014)

09/2012 – 02/2013

- Praktisches Studiensemester
Titel: „Innovative Methoden in der Strukturaufklärung“
Agrarzentrum der BASF SE, Limburgerhof, Deutschland
Global Product Safety & Registration
Betreuer: Dr. Reinhard Dötzer, Dr. Markus Radzom

10/2013

- Praktische Studienarbeit
Titel: „Entwicklung von Immunoassays zur Bestimmung von humanem Albumin in Urin“
Hochschule Mannheim, Deutschland
Institut für Biochemie
Betreuerin: Prof. Roswitha Stenzel

11/2013 – 04/2014

- Bachelorarbeit
Titel: „Entwicklung und Validierung einer pH-Gradienten Plattform Ionenaustauschchromatographie-Methode zur Trennung der Ladungsvarianten monoklonaler Antikörper“
AbbVie Deutschland GmbH&Co.KG, Ludwigshafen am Rhein
NBE Analytical R&D
Betreuer: Alexander Feick
Note: 1,0

03/2014 – 08/2015

Master of Science

Studienfach: Biomedical Science and Technology
(Biotechnology)
Hochschule Mannheim, Deutschland
Abschlussnote: 1,3 (17.08.2015)

02/2015 – 08/2015

- Masterarbeit

Titel: "Effects of blue light irradiation on human dermal fibroblasts"
Zentrum für Medizinische Forschung (ZMF)
Medizinische Fakultät Mannheim
Ruprecht-Karls-Universität Heidelberg, Deutschland
Betreuer: Prof. Norbert Gretz
Note: 1,0

10/2015 – Jetzt

Promotion, Dr. sc. hum. (scientiarum humanarum)

Titel: "Influence of photobiomodulation with blue light on the metabolism, proliferation and gene expression of human fibroblasts"
Zentrum für Medizinische Forschung (ZMF)
Medizinische Fakultät Mannheim
Ruprecht-Karls-Universität Heidelberg, Deutschland
Doktorvater: Prof. Norbert Gretz

PUBLICATIONS

- Becker, A, Distler, E, **Klapczynski, A**, Arpino, F, Kuch, N, Simon-Keller, K, Sticht, C, van Abeelen, FA, Gretz, N, Oversluizen, G: Blue light inhibits proliferation of melanoma cells. In: SPIE (Ed.) *SPIE BiOS*, San Francisco, International Society for Optics and Photonics, 2016, pp 969503-969513.
- Becker, A, **Klapczynski, A**, Kuch, N, Arpino, F, Simon-Keller, K, De La Torre, C, Sticht, C, van Abeelen, FA, Oversluizen, G, Gretz, N: Gene expression profiling reveals aryl hydrocarbon receptor as a possible target for photobiomodulation when using blue light. *Sci Rep*, 6: 33847, 2016.

PATENTS

- Patent in collaboration with URGO RID on the proliferative effect of 7.5 min blue light found in human keratinocytes and human fibroblasts: "Flexible device for the irradiation of chronic wounds inducing wound healing by accelerated proliferation of fibroblasts and keratinocytes (LEDs (wavelength 450-490 nm))"; EP16181721.8 (EU), PCT/EP2017/068951 (USA)
- Patent in collaboration with URGO RID and the University of Heidelberg on the antibacterial effect of blue light: "Flexible photobiomodulation device that is able to emit blue light at 450 nm and is suitable at least to be bacteriostatic and preferably to reduce proliferative effect of bacteria"; EP18305067 (EU)

9 ACKNOWLEDGEMENTS

First of all, I sincerely thank my supervisor Prof. Norbert Gretz for giving me the opportunity to work on this interesting and future-based project. I am very thankful for all his valuable advices, suggestions as well as comments and moreover his constant support throughout the whole period of research and writing.

Furthermore, I am very grateful for all the experiences I gained as a member of the European MEDILIGHT consortium introducing me to the challenges of international project work. It was a pleasure to work with all the partners involved, but a special thanks goes to URGO RID, providing the financial support for the last period of my PhD. I would like to take this opportunity to thank Dr. Marielle Bouschbacher for always thriving new ideas. Besides MEDILIGHT, I would like to thank Prof. Gretz for my participation in the Doctoral Program 'Cooperative Research Training Group – Tissue Analytics for Stem Cell based Diagnostics and Therapy (TASCDT)'. I am very thankful for all the helpful courses I could attend throughout this program.

Moreover, I thank Cathleen Fichtner for her excellent assistance in the lab and all the countless hours of help in upcoming questions and problems. I also thank Elisabeth Seelinger, Jasmin Baumgartl and Maria Muciek for their technical support. A special thanks goes to Dr. Carolina De La Torre and Dr. Carsten Sticht for helping me in gene expression analyses and statistics. In addition, I deeply thank Dr. Katja Simon-Keller for supporting me in new experimental set-ups. Thanks to all my ZMF colleagues for sharing knowledge, frustrations and success. A special thanks goes to Natalia Kuch, Fabiola Arpino and my former colleague Anja Becker, who had introduced me to the cell culture lab. Moreover, I would like to thank Sina Schwalm and Edda Eustachi for their support in administrative concerns as well as all the encouraging conversations.

My greatest and deepest thanks goes to my dearest parents, sisters and my beloved boyfriend, for always believing in me and being at my side during this long journey of ups and downs. This work would not have been possible without your efforts, support and patience. You are part of who I am today. All my successes are also yours.